

TRANSPORT OF A HIGHLY LIPOPHILIC WEAK ACID MOLECULE
(CAPRIC ACID) ACROSS A LIPOPHILIC MEMBRANE BETWEEN
TWO AQUEOUS PHASES IN THE PRESENCE
OF A CARRIER (CYCLODEXTRINS)

by

Richard Val Hymas

A dissertation submitted to the faculty of
The University of Utah
in partial fulfillment of the requirements for the degree of

Doctor of Philosophy

Department of Pharmaceutics and Pharmaceutical Chemistry

University of Utah

May 2010

UMI Number: 3405683

All rights reserved

INFORMATION TO ALL USERS

The quality of this reproduction is dependent upon the quality of the copy submitted.

In the unlikely event that the author did not send a complete manuscript and there are missing pages, these will be noted. Also, if material had to be removed, a note will indicate the deletion.



UMI 3405683

Copyright 2010 by ProQuest LLC.

All rights reserved. This edition of the work is protected against unauthorized copying under Title 17, United States Code.



ProQuest LLC
789 East Eisenhower Parkway
P.O. Box 1346
Ann Arbor, MI 48106-1346

Copyright © Richard Val Hymas 2010

All Rights Reserved

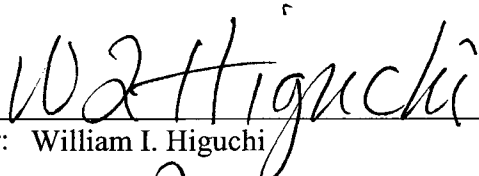
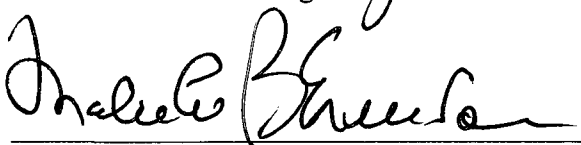
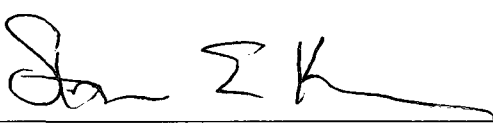
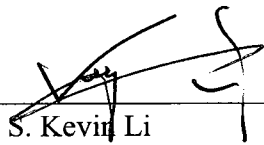
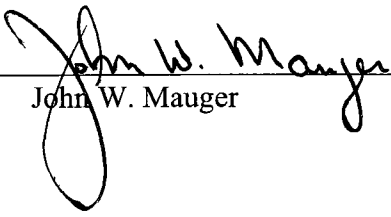
THE UNIVERSITY OF UTAH GRADUATE SCHOOL

SUPERVISORY COMMITTEE APPROVAL

of a dissertation submitted by

Richard Val Hymas

This dissertation has been read by each member of the following supervisory committee and by majority vote has been found to be satisfactory.

| | |
|------------------|--|
| <u>3/26/2010</u> |  Chair: William I. Higuchi |
| <u>3/26/2010</u> |  Malcolm M. Berenson |
| <u>3/26/2010</u> |  Steven E. Kern |
| <u>3/26/2010</u> |  S. Kevin Li |
| <u>3/26/2010</u> |  John W. Mauger |

THE UNIVERSITY OF UTAH GRADUATE SCHOOL

FINAL READING APPROVAL

To the Graduate Council of the University of Utah:

I have read the dissertation of Richard Val Hymas in its final form and have found that (1) its format, citations, and bibliographic style are consistent and acceptable; (2) its illustrative materials including figures, tables, and charts are in place; and (3) the final manuscript is satisfactory to the supervisory committee and is ready for submission to The Graduate School.

1/6/10
Date

William I. Higuchi
William I. Higuchi
Chair: Supervisory Committee

Approved for the Major Department

David W. Grainger
David W. Grainger
Chair/Dean

Approved for the Graduate Council

Charles A. Wight
Charles A. Wight
Dean of The Graduate School

ABSTRACT

There has been a continuing need for a better quantitative understanding of the gastrointestinal absorption of highly lipophilic drugs. With this aim in mind, the present study describes a physical model approach applicable to understanding the transport of lipophilic, ionizable drugs across a lipophilic membrane. In Chapter 3, model predictions were compared to experimental results of capric acid (HA) transport across a silicone polymer membrane in the presence and in the absence of 2-hydroxypropyl- β -cyclodextrin (HPB). Model predictions and experimental results were generally in agreement over the entire studied ranges of pH and HPB concentrations. In Chapter 4, the physical model approach was then applied to the in situ single pass perfusion system involving the rat ileum to obtain a more detailed understanding about cyclodextrin as an intestinal drug absorption enhancer through its role as a carrier. Model predictions were found to be generally in good agreement with experimental results. We also extended this model to account for the villus structure of the small intestine, resulting in equally good agreement. Both models demonstrated that HPB was able to reduce the capric acid concentration gradient across the aqueous boundary layer and increase the effective intestinal membrane surface area utilized for permeant absorption due to deeper penetration of the permeant into the villus crypts, accounting for the HPB-enhanced permeant flux.

In an exploratory investigation (Chapter 5), the in situ single pass perfusion technique was then used to examine the ability of two well known chemical permeation

enhancers of hydrophilic drug molecules, sodium caprate (HA) and sodium chenodeoxycholate (CDC), to enhance mannitol transport in the rat ileum in the presence and absence of different cyclodextrin carriers. Analysis of the experimental results with the villus model (VM) support the interpretation that an appropriate enhancer/carrier combination may 1) be able to increase the fraction of ileum surface area that is enhanced and, because of this, that 2) local toxicity effects of the enhancer might be avoided or reduced for any given mannitol permeability enhancement, while 3) at the same time provide increased enhancer duration of action.

TABLE OF CONTENTS

| | |
|--|------|
| ABSTRACT..... | iv |
| LIST OF TABLES..... | ix |
| LIST OF FIGURES | xi |
| ACKNOWLEDGMENTS | xiii |
| Chapter | |
| 1. INTRODUCTION..... | 1 |
| 1.1 Anatomical and Physiological Features of the Gastrointestinal Tract Relevant to Oral Drug Delivery | 2 |
| 1.2 Experimental Systems and Models for Determining the Absorption Rate of Drugs | 3 |
| 1.3 Barriers to Drug Absorption | 4 |
| 1.3.1 The aqueous boundary layer | 4 |
| 1.3.2 The epithelial membrane..... | 5 |
| 1.4 The Biopharmaceutical Classification System (BCS) | 6 |
| 1.5 Approaches for Overcoming Solubility and Permeability Limitations..... | 7 |
| 1.5.1 Drug carriers for improving solubility | 7 |
| 1.5.2 Chemical enhancers for improving membrane permeability..... | 9 |
| 1.6 References | 11 |
| 2. STATEMENT OF THE PROBLEM | 20 |
| 3. TRANSPORT OF A LIPOPHILIC IONIZABLE PERMEANT (CAPRIC ACID) ACROSS A LIPOPHILIC MEMBRANE (SILICONE POLYMER MEMBRANE) FROM AQUEOUS BUFFERED SOLUTIONS IN THE PRESENCE OF HYDROXYPROPYL- β -CYCLODEXTRIN..... | 22 |
| 3.1 Introduction | 22 |
| 3.2 The Model and Equations Used in the Analysis of Experimental Data..... | 24 |
| 3.3 Strategy | 28 |
| 3.4 Experimental | 30 |
| 3.4.1 Chemicals and reagents..... | 30 |
| 3.4.2 Methods..... | 31 |

| | |
|---|-----|
| 3.5 Results | 39 |
| 3.5.1 Key parameters associated with the capric acid transport across the silicone membrane | 39 |
| 3.5.2 Capric acid transport experiments with the silicone membrane plus six Millipore membranes (SM-MM) system..... | 54 |
| 3.5.3 Transport experiments with silicone membrane alone (SM)..... | 58 |
| 3.5.4 Radiochemical impurity corrections for capric acid transport and for the transport parameter values..... | 60 |
| 3.6 Discussion..... | 61 |
| 3.6.1 Flux of drug X across SM-MM at unit thermodynamic activity (saturated solutions)..... | 61 |
| 3.6.2 Flux of drug X across the rat ileum at unit thermodynamic activity | 65 |
| 3.7 Appendix A. Radiochemical Impurity Corrections for Capric Acid Transport Parameter Values..... | 68 |
| 3.8 Appendix B. Equilibrium Reactions, Species Concentrations and Fractions.. | 77 |
| 3.9 Glossary | 81 |
| 3.10 References..... | 85 |
| | |
| 4. CAPRIC ACID ABSORPTION IN THE PRESENCE OF HYDROXYPROPYL- β -CYCLODEXTRIN IN THE RAT ILEUM USING THE IN SITU SINGLE PASS PERFUSION TECHNIQUE | 88 |
| 4.1 Introduction..... | 88 |
| 4.2 Strategy | 90 |
| 4.2.1 The experimental method and the estimation of key FSM parameters..... | 90 |
| 4.2.2 Flat surface versus villus surfaces..... | 94 |
| 4.3 Materials and Methods..... | 102 |
| 4.3.1 Chemicals and reagents..... | 102 |
| 4.3.2 In situ single pass perfusion experiments | 102 |
| 4.3.3 Villus model simulations | 106 |
| 4.3.4 Treatment of experimental data using the FSM..... | 108 |
| 4.4 Results and Discussion..... | 112 |
| 4.4.1 Intestinal absorption..... | 112 |
| 4.4.2 Analysis of the experimental P_T data with the flat surface model (FSM)..... | 115 |
| 4.4.3 Analysis of the experimental results with the villus model (VM) | 123 |
| 4.4.4 A comparison of the villus model (VM) to the flat surface model (FSM)..... | 136 |
| 4.5 Significance..... | 137 |
| 4.6 Appendix A..... | 138 |
| 4.6.1 Analysis of the P_T results based on Eq 4.15 | 138 |
| 4.7 Appendix B | 142 |

| | |
|---|-----|
| 4.7.1 Calculation permitting the comparison of capric acid absorption data in the ileum with the jejunum data from Ho et al..... | 142 |
| 4.8 Glossary..... | 146 |
| 4.9 References..... | 149 |
| | |
| 5. EXPLORATORY STUDY OF THE ROLE OF CYCLODEXTRINS IN PRESENTING CHEMICAL ENHANCERS TO THE SURFACE OF THE RAT ILEUM USING THE IN SITU SINGLE PASS PERFUSION TECHNIQUE | 152 |
| 5.1 Introduction..... | 152 |
| 5.2 Overview..... | 155 |
| 5.3 Materials and Methods..... | 156 |
| 5.3.1 Chemicals and reagents..... | 156 |
| 5.3.2 Intestinal and mesenteric cannulation..... | 157 |
| 5.3.3 Intestinal perfusion..... | 157 |
| 5.4 Results and Discussion..... | 159 |
| 5.4.1 Enhancement of mannitol transport in the CDC/SBE system..... | 159 |
| 5.4.2 HA/HPB enhancer-carrier system for the enhancement of mannitol transport..... | 170 |
| 5.4.3 HA/HPG enhancer-carrier system for the enhancement of mannitol transport..... | 177 |
| 5.4.4 Insights obtained from examining the capric acid experimental results using the villus model..... | 180 |
| 5.5 Implications..... | 185 |
| 5.6 References..... | 188 |
| | |
| 6. SUMMARY | 193 |

LIST OF TABLES

| <u>Table</u> | <u>Page</u> |
|---|-------------|
| 1.1 The Biopharmaceutics Classification System (BCS)..... | 8 |
| 3.1 Key parameters associated with the transport of capric acid across the silicone polymer membrane..... | 40 |
| 3.2 The capric acid/HPB binding constant (K^u) as..... | 43 |
| 3.3 Diffusion coefficients or effective diffusion coefficients (all at 30°C) for..... | 45 |
| 3.4 Diffusion coefficients of the complexes calculated from the effective..... | 46 |
| 3.5 Total permeability coefficient (P_T) for transport of mannitol..... | 52 |
| 3.6 A comparison of parameters and P_T results before and after..... | 76 |
| 4.1 Parameter values used in model calculations. Diffusion coefficients, binding constants, and pK_a | 92 |
| 4.2 Parameters of the villus model..... | 97 |
| 4.3 Definition of boundary conditions for Fig 4.2..... | 99 |
| 4.4 Maximal surface area contributions in the VM of the rat ileum..... | 101 |
| 4.5 Experimentally determined flux (J_b) and total permeability coefficient..... | 118 |
| 4.6 Flat surface model (FSM) analysis of the influence of hydroxypropyl- β -cyclodextrin on the absorption of capric acid in..... | 119 |
| 4.7 VM analysis of the influence of HPB upon the absorption of capric acid in the rat ileum at pH 7.4..... | 126 |
| 4.8 Analysis of P_T results calculated from Eq 4.15..... | 139 |
| 4.9 Geometric villus parameters of the ileum and the jejunum..... | 144 |

| | | |
|------|--|-----|
| 4.10 | Intrinsic surface area (cm^2) per cm^2 of intestine | 144 |
| 5.1 | Experimental results for chenodeoxycholate (CDC) alone and CDC plus sulfobutyl ether- β -cyclodextrin | 160 |
| 5.2 | Experimental results for capric acid (HA) alone, capric acid plus hydroxypropyl- β -cyclodextrin (HA/HPB), and..... | 161 |
| 5.3 | Relative half-life in rat ileum for capric acid (HA) | 172 |
| 5.4 | Increase in accessibility (Acc) compared to the capric acid (HA) alone case. HPB and HPG concentrations are 30 mM | 183 |
| 5.5 | A comparison of capric acid (HA) flux and mannitol enhancement factor | 186 |

LIST OF FIGURES

| <u>Figure</u> | | <u>Page</u> |
|---------------|--|-------------|
| 3.1 | The apparent partition coefficient ($k_{p,app}$) for capric acid..... | 41 |
| 3.2 | Relative buffer viscosity as a function of the hydroxypropyl- β - | 48 |
| 3.3 | Total permeability coefficient (P_T) for capric acid transport across the | 50 |
| 3.4 | Total permeability coefficient (P_T) for capric acid transport across the | 55 |
| 3.5 | Total permeability coefficient (P_T) for capric acid transport across the | 59 |
| 3.6 | The influences of the HPB concentration and pH upon the flux | 64 |
| 3.7 | The influences of the HPB concentration and pH upon the flux | 67 |
| 3.8 | Experimental and predicted percent radiochemical impurity in the receiver..... | 69 |
| 3.9 | The results presented here (both the experimental and the model-..... | 72 |
| 3.10 | The results presented here (both the experimental and the model-..... | 73 |
| 4.1 | Schematic representation of the villus model (VM). Parameter values are listed in Table 4.2..... | 96 |
| 4.2 | Boundary conditions for the COMSOL finite-element villus model simulations,..... | 98 |
| 4.3 | Schematics of the open-ended perfusion of rat intestinal segment from an infinite drug solution reservoir and..... | 109 |
| 4.4 | Representative plots of the fraction of caprate remaining in the intestinal..... | 113 |
| 4.5 | Representative plots of cumulative caprate appearance in blood as a function ... | 114 |
| 4.6 | Intestinal perfusate flow rate of ^{14}C -caprate solution and blood flow rate out ... | 116 |
| 4.7 | Representative plot of periodic determination of the osmolarity (mOsm/kg) | 117 |

| | | |
|------|--|-----|
| 4.8 | Comparison of experimental P_T values with FSM predictions. The solid curve | 120 |
| 4.9 | Relative concentration of total capric acid, expressed as a fraction of the luminal | 124 |
| 4.10 | Log plot of experimentally determined permeability coefficients (P_T) for | 127 |
| 4.11 | Fraction of total capric acid concentration versus distance across ABL and | 128 |
| 4.12 | Iso-concentration profiles of caprate in the aqueous boundary layer and | 130 |
| 4.13 | Iso-concentrations profiles of caprate in the aqueous boundary layer and | 131 |
| 4.14 | Fraction of total caprate concentration versus distance across the ABL and in the | 135 |
| 5.1 | Mannitol permeability coefficients (P_T) for the rat ileum as a function of | 163 |
| 5.2 | Mannitol permeability coefficients (P_T) for the rat ileum as a function of free | 166 |
| 5.3 | Mannitol permeability coefficients (P_T) for the rat ileum as a function of sodium | 167 |
| 5.4 | Sodium chenodeoxycholate (CDC) flux across the rat ileum as a function of | 169 |
| 5.5 | Mannitol permeability coefficients (P_T) for the rat ileum as a function of total | 173 |
| 5.6 | Mannitol permeability coefficients (P_T) for the rat ileum as a function of | 174 |
| 5.7 | Capric acid (HA) flux across the rat ileum as a function of free capric acid | 176 |
| 5.8 | Free total capric acid (HA) concentration profiles for the three cases: 8 mM HA | 181 |
| 5.9 | Mannitol permeability coefficients (P_T) for the rat ileum as a function of capric | 184 |

ACKNOWLEDGMENTS

I wish to acknowledge the contributions of all those who made the completion of this dissertation possible. It has been my privilege to work under the direction and guidance of Dr. William I. Higuchi. His dedication to science and drive for excellence has pushed me to achieve my maximum potential. I wish to thank Dr. Norman F. H. Ho for his selfless contribution to this project. His expertise and insight was invaluable. I would like to thank Dr. S. Kevin Li for his contribution to my research and training. I am truly grateful for the time and effort put forth by each of my committee members. Dr. Berenson, Dr. Kern, Dr. Li, Dr. Mauger, and Dr. Higuchi all contributed to the success of this dissertation and to my training.

I have received continual support from every member of my family. My parents, parents-in-law, and children have all sacrificed much in my behalf. Most of all, I would like to thank my wife, Lynnae, for her endless sacrifices, and for staying by my side every step of the way.

Finally, I acknowledge with much thanks the generous financial support provided by Lipocine, Inc. that has made this study possible.

CHAPTER 1

INTRODUCTION

This is an introduction and review of the literature relevant to oral drug absorption, with emphasis placed on details relating to the study of intestinal membrane permeability and the design of formulations intended to improve permeant bioavailability. Relevant intestinal anatomy, experimental methods for studying intestinal absorption, barriers to drug absorption, the BCS classification system, and common approaches for overcoming solubility and permeability limitations are reviewed herein.

Oral dosage forms (i.e., tablets, capsules, suspensions, emulsions etc.) are the preferred method for administering drugs due to the safe, convenient, economical nature of oral dosing, and high patient compliance. Of the 50 most sold pharmaceutical products in the US and Europe, 42 are administered orally.¹ Despite its popularity and numerous advantages over other dosing methods, oral dosing is not without significant limitations. Currently, many compounds and therapeutic chemical entities are not formulated for oral delivery due to poor drug solubility and/or low membrane permeability. Recent efforts to overcome solubility and permeability limitations have resulted in significant progress from the standpoint of practical formulation development; however, relatively little progress has been made from the standpoint of quantitatively understanding the

underlying mechanisms by which bioavailability enhancing formulations increase permeant flux. Therefore, an examination of appropriate models, both theoretically and experimentally, is necessary to advance the cause of more rational approaches to drug delivery formulation of low solubility and low permeability drug molecules.

1.1 Anatomical and Physiological Features of the Gastrointestinal Tract Relevant to Oral Drug Delivery

For oral dosage forms, the majority of drugs are absorbed primarily in the small intestine. The primary barrier to intestinal drug absorption is the innermost layer of the mucosa which consists of a 20 μm thick monolayer of simple columnar epithelium. Most permeants that traverse the epithelial monolayer are freely absorbed into the circulatory system via capillaries that reside just below the mucous epithelium.

The small intestine contains several anatomical features which improve absorption by increasing the absorptive surface area. One feature that is present in humans, but largely absent in the rat is the plicae circulares, or folds of Kerckring, which increase the intestinal surface area by approximately a factor of three.² The surface of the small intestine, including the folds of Kerckring, is covered with tiny fingerlike projections known as villi. These projections are present in both man and in the rat, and exist along the entire length of the small intestine, with the villus height, density, and diameter varying among species. In general, the villi are taller and thinner in the upper small intestine, becoming gradually shorter and wider towards the lower small intestine. The surface of the epithelial cells comprising the villi are covered with tiny hairlike structures called microvilli,. These microvilli, also present in both man and rat, further

amplify the absorptive surface area by 20-30 fold.² Taken together, the folds of Kerckring, villi, and microvilli are reported to increase the surface area of the small intestine by up to 600 times compared with the surface area taken as a smooth, hollow, circular cylinder.²

Although the small intestine has a surface area several hundred fold larger than its macroscopic surface area, this surface area is not used equally. It has been demonstrated that the effective surface area available for absorption is much less than the anatomical surface area of the mucosal membrane,³ and that the effective surface area utilized for absorption varies with the compound being absorbed.⁴⁻⁶ For highly permeable compounds, absorption occurs mainly at the tips of the villi, however low permeability compounds are able to penetrate more deeply into the villus crypts, taking greater advantage of the available surface area.⁴⁻⁶

The pH of the gastrointestinal tract ranges from 1-2 in the stomach to 8-9 in the colon.^{2,7,8} The pH is controlled by enzymes and buffers secreted into the lumen at various locations in the gastrointestinal tract. This pH gradient down the intestinal tract influences the location at which weak acids and weak bases are most likely to be absorbed.

1.2 Experimental Systems and Models for Determining

the Absorption Rate of Drugs

A large number and variety of experimental and computational methods are used to study, analyze, and predict passive intestinal absorption. These methods include theoretical models which predict absorption based solely on the properties of the

molecule of interest, artificial membrane experimental transport models, cell monolayer permeability models (i.e., Caco-2, PAMPA, etc.), excised tissue models (i.e., everted sac, Ussing chamber, etc.), in situ perfusion models, and in vivo models. Both animal and human models are available. No one method gives all the desired absorption rate information, and discrepancies both among and between experimental models is prevalent.⁹ Each method has its own advantages and disadvantages. Generally speaking, in vitro experiments provide opportunities for isolated examination of transport characteristics under simplified membrane transport conditions. These experiments do not, however, always correlate well with actual human results. In situ and in vivo experiments are generally more expensive, time consuming, and complex; however, the results may correlate more closely to actual human results. Smyth reviews in detail the methods of studying intestinal absorption.⁹

1.3 Barriers to Drug Absorption

1.3.1 The aqueous boundary layer

The transport resistance due to the aqueous boundary layer (ABL) is well established, and should be considered in the analysis of transport across biological membranes.¹⁰⁻¹³ The effective thickness of the ABL is flow-rate dependent and the contribution of the ABL to the overall transport resistance is often dependent upon many parameters. Komiya et al.¹⁴ and Tsutsumi et al.¹⁵ used intestinal perfusion techniques in rat jejunum and ileum, respectively, to demonstrate that the overall transport rate of a series of steroids increased initially with increasing lipophilicity, reaching a plateau for the more lipophilic steroids. This plateau was shown to be due to the ABL, with the

transport of the highly lipophilic steroids being entirely ABL controlled. Yuasa et al.¹⁶ used a single pass perfusion technique with the rat jejunum to demonstrate that the effective ABL thickness was greater in anesthetized rats (785 μm) than in un-anesthetized rats (319 μm) for a 0.16 ml/min flow rate. They also demonstrated that even at higher flow rates (2.95 ml/min) the ABL still accounted for 85% of the total transport resistance of D-glucose. This demonstrated that although conscious animals have increased villus motility and decreased ABL thickness as compared to anesthetized animals, the ABL cannot be neglected.

1.3.2 The epithelial membrane

1.3.2.1 Transcellular transport

Transcellular simple diffusion is the preferred route of transport for lipophilic molecules and for very small molecules in general.¹⁷ Some very small hydrophilic molecules (e.g., H_2O) are thought to diffuse freely through transcellular pores, whereas larger lipophilic molecules partition into the lipid bilayer and are thought to diffuse laterally along the plasma membrane toward the basal membrane.¹⁹ For lipophilic molecules, the transcellular membrane permeability coefficient has been shown to be related to permeant lipophilicity.²⁰

1.3.2.2 Paracellular transport

Epithelial cells making up the intestinal transport barrier are joined to each other at intercellular junctions by a junctional complex. Adherence points include gap junctions, spot desmosomes, intermediate junctions, and zonula occludens (also known as

tight junctions).¹⁷ These junctions hold the cells making up the epithelial monolayer together. The tight junction is the apical-most junction and is generally considered the rate limiting junction with regards to the diffusion of molecules through the paracellular pathway. The tight junction also forms a “fence” between the apical and lateral plasma membrane domains, which prevents the random diffusion of membrane lipids and proteins between these two compartments which maintains cell surface polarity and prevents lipid molecules from diffusing between epithelial cells.²¹ The pores formed between the cells are the paracellular transport pathway, and the pore diameters are regulated by the tight junctions. This pore pathway is thought to be the principle transport pathway for molecules too polar to partition into the phospholipid bilayer. Any molecule small enough to diffuse through the aqueous pore formed by the tight junction can be transported via the paracellular pathway. Several transmembrane proteins have been identified as associating with tight junctions, and some chemical permeation enhancers are thought to act either directly or indirectly on the function of these proteins to increase the tight junction pore size. Although relatively little is known about how these proteins regulate the tight junction pore size and interact with chemical permeation enhancers,²² there has been a significant amount of work done to identify mechanisms and interactions involved in tight junction modulation.²³⁻²⁶

1.4 The Biopharmaceutical Classification System (BCS)

An increasing number of biologically active compounds discovered using high throughput screening have low inherent oral bioavailability because they are either large and polar, resulting in low permeability, or they are very lipophilic, resulting in low

aqueous solubility. Potential candidates for oral drug delivery are classified based on their solubility and permeability characteristics. Table 1.1 presents a recommended method accepted by the FDA for classifying potential permeant molecules into four categories based on solubility and permeability.²⁷

This classification of potential drug candidates identifies the rate limiting step(s) for oral drug delivery. Poor solubility and/or low permeability characteristics may cause otherwise active therapeutic agents to be dropped in the early stages of product development due to the difficulty of developing a formulation with adequate bioavailability.

1.5 Approaches for Overcoming Solubility and Permeability Limitations

1.5.1 Drug carriers for improving solubility

Many biologically active compounds have inadequate bioavailability for successful oral dosing because of poor membrane permeability, water solubility, and/or stability characteristics. One category of drug molecules that has been receiving much attention recently is that class of compounds which are both highly lipophilic and poorly water soluble (BCS classification class II).²⁸ For drug molecules in this category, an approach often taken to improve bioavailability is the inclusion of a solubilizing agent in the formulation to increase the drug solubility and to effect a greater maximum flux of drug into the blood stream.²⁹⁻³⁶

In recent years, cyclodextrins (CD) have received extensive attention as solubilizing agents in aqueous media because of their ability to form inclusion complexes with lipophilic drugs. Specifically, 2-hydroxypropyl- β -cyclodextrin (HPB) has been

Table 1.1 The Biopharmaceutics Classification System (BCS)

| | | |
|---------|-------------------|-----------------|
| Class 1 | High permeability | High solubility |
| Class 2 | High permeability | Low solubility |
| Class 3 | Low permeability | High solubility |
| Class 4 | Low permeability | Low solubility |

studied as a potential excipient in drug formulations because of its ability to improve the drug delivery characteristics for a large number of molecules.³⁷⁻⁴⁶

One concern about using cyclodextrins in oral formulations is that of safety. As with any potential excipient, questions arise concerning possible adverse side effects. While un-substituted cyclodextrins and cyclodextrins with lipophilic substitutions have been shown to cause damage to erythrocytes and biological membranes,^{47,48} the safety of HPB in oral formulations has been well documented.⁴⁹⁻⁵⁴ It has been demonstrated that HPB concentrations up to 100 mM do not extract lipids from biological membranes or otherwise disrupt the integrity of epithelial cells.⁵⁵⁻⁵⁷ In addition to HPB being well tolerated, it is highly soluble and not significantly absorbed in the gastrointestinal tract.^{58,59} These characteristics make HPB a good candidate as a potential solubilizing agent in oral dosage forms. Accordingly, the FDA has included HPB in its list of Inactive Pharmaceutical Ingredients.³⁷ In fact, HPB has already been used in approved and marketed drug formulations in Europe, Japan, and the United States, with several more formulations in clinical trials.⁶⁰

1.5.2 Chemical enhancers for improving membrane permeability

Effective gastrointestinal absorption of highly polar molecules is frequently limited by poor intestinal permeability. Because high solubility low permeability (BCS class III) molecules generally have low bioavailability, oral dosing formulations are not only inefficient, but generally have much higher inter- and intra-subject variability.⁶¹⁻⁶³ Recent efforts to improve intestinal permeability, and therefore bioavailability, of BCS class III compounds has included, among other approaches, the use of membrane

penetration-enhancing excipients. Compounds that have been studied for their membrane penetration-enhancing effects include ionic and non-ionic surfactants,⁶⁴⁻⁷³ bile salts,⁷³⁻⁸⁴ fatty acids,⁸⁵⁻⁹³ glycerides,⁹⁴⁻¹⁰⁰ and others.^{64-67,101-103} Intestinal membrane penetration enhancers consist of a wide range of molecules with a variety of molecular structures and mechanisms of action. Aungst et al.¹⁰⁴ believe that the three most important issues that need to be considered for evaluating absorption enhancers are: (1) how effective the absorption enhancer is for the drug of interest, (2) the potential to cause toxicity, and (3) the mechanisms by which absorption is enhanced. Frequently, the toxicity of the enhancers themselves is the limiting factor in successful application of the permeability enhancer.^{66,105,106} Additionally, enhancers are generally rapidly absorbed, and have a short half-life in the intestinal tract, which limits the duration of action of the enhancer. An ideal enhancer formulation would minimize enhancer toxicity and increase the duration of action. An approach that could incorporate these characteristics into an enhancer formulation would certainly increase the likelihood that a formulation could become a marketable product.

1.6 References

1. Lennernas H 2007. Modeling gastrointestinal drug absorption requires more in vivo biopharmaceutical data: experience from in vivo dissolution and permeability studies in humans. *Curr Drug Metab* 8(7):645-657.
2. DeSesso JM, Jacobson CF 2001. Anatomical and physiological parameters affecting gastrointestinal absorption in humans and rats. *Food Chem Toxicol.* 39(3):209-228.
3. Wilson FA, Dietschy JM 1974. The intestinal unstirred layer: its surface area and effect on active transport kinetics. *Biochim Biophys Acta* 363(1):112-126.
4. Oliver RE, Jones AF, Rowland M 1998. What surface of the intestinal epithelium is effectively available to permeating drugs? *J Pharm Sci* 87(5):634-639.
5. Winne D 1978. The permeability coefficient of the wall of a villous membrane. *J Math Biol* 6(1):95-108.
6. Winne D 1989. Effect of villosity and distension on the absorptive and secretory flux in the small intestine. *J Theor Biol* 139(2):155-186.
7. De Vito SC 2000, Absorption through cellular membranes: R.S. Boethling, D. Mackay (Eds.), *Handbook of Property Estimation Methods for Chemicals*, CRC Press, Boca Raton, 2000, p. 261-278.
8. Rubinstein A, *Gastrointestinal anatomy, physiology and permeation pathways*: Elka Touitou, Brian W. Barry (Eds.), *Enhancement in Drug Delivery*, CRC Press, Boca Raton, 2006, p. 3-35.
9. Smyth DH 1974. Methods of studying intestinal absorption. *Biomembranes* 4A(0):241-283.
10. Dainty J, House CR 1966. Unstirred layers in frog skin. *J Physiol* 182(1):66-78.
11. Diamond JM 1966. A rapid method for determining voltage-concentration relations across membranes. *J Physiol* 183(1):83-100.
12. Cuthbert AW, Dunant Y 1970. Diffusion of drugs through stationary water layers as the rate limiting process in their action at membrane receptors. *Br J Pharmacol* 40(3):508-521.
13. Barry PH, Diamond JM 1984. Effects of unstirred layers on membrane phenomena. *Physiol Rev* 64(3):763-872.

14. Komiya I, Park JY, Kamani A, Ho NFH, Higuchi WI 1980. Quantitative mechanistic studies in simultaneous fluid flow and intestinal absorption using steroids as model solutes. *Int J Pharm* 4(3):249-262.
15. Tsutsumi K, Li SK, Ghanem AH, Ho NF, Higuchi WI 2003. A systematic examination of the in vitro Ussing chamber and the in situ single-pass perfusion model systems in rat ileum permeation of model solutes. *J Pharm Sci* 92(2):344-359.
16. Yuasa H, Iga T, Hanano M, Watanabe J 1988. Comparative assessment of the resistance of the unstirred water layer to solute transport between two different intestinal perfusion systems. *Biochim Biophys Acta* 938(2):189-198.
17. Narawane L, Lee VHL. 1994. Absorption barriers. In de Boer ABG, editor *Drug Absorption Enhancement*, London: Harwood Academic Publishers. p 9-10.
18. Hamilton I, Rothwell J, Archer D, Axon AT 1987. Permeability of the rat small intestine to carbohydrate probe molecules. *Clin Sci (Lond)* 73(2):189-196.
19. Schwenk M 1987. Drug transport in intestine, liver and kidney. *Arch Toxicol* 60(1-3):37-42.
20. Ho NFH, Park JY, Ni PF, Higuchi WI. 1983. Advancing Quantitative and Mechanistic Approaches in Interfacing Gastrointestinal Drug Absorption Studies in Animals and Humans. In Crouthamel W, Sarapu AC, editors. *Animal Models for Oral Drug Delivery in Man*, Washington D.C.: American Pharmaceutical Association Academy of Pharmaceutical Sciences.
21. van Meer G, Simons K 1986. The function of tight junctions in maintaining differences in lipid composition between the apical and the basolateral cell surface domains of MDCK cells. *EMBO J* 5(7):1455-1464.
22. Bamforth SD, Kniesel U, Wolburg H, Engelhardt B, Risau W 1999. A dominant mutant of occludin disrupts tight junction structure and function. *J Cell Sci* 112 (Pt 12):1879-1888.
23. Ward PD, Ouyang H, Thakker DR 2003. Role of phospholipase C-beta in the modulation of epithelial tight junction permeability. *J Pharmacol Exp Ther* 304(2):689-698.
24. Ward PD, Klein RR, Troutman MD, Desai S, Thakker DR 2002. Phospholipase C-gamma modulates epithelial tight junction permeability through hyperphosphorylation of tight junction proteins. *J Biol Chem* 277(38):35760-35765.
25. Ward PD, Tippin TK, Thakker DR 2000. Enhancing paracellular permeability by modulating epithelial tight junctions. *Pharm Sci Technol Today* 3(10):346-358.

26. Gan LS, Yanni S, Thakker DR 1998. Modulation of the tight junctions of the Caco-2 cell monolayers by H2-antagonists. *Pharm Res* 15(1):53-57.
27. Amidon GL, Lennernas H, Shah VP, Crison JR 1995. A theoretical basis for a biopharmaceutic drug classification: the correlation of in vitro drug product dissolution and in vivo bioavailability. *Pharm Res* 12(3):413-420.
28. Loftsson T 2002. Cyclodextrins and the biopharmaceutics classification system of drugs. *J Incl Phenom Macroc Chem* 44(1-4):63-67.
29. Amidon GE, Higuchi WI, Ho NF 1982. Theoretical and experimental studies of transport of micelle-solubilized solutes. *J Pharm Sci* 71(1):77-84.
30. Lukyanov AN, Torchilin VP 2004. Micelles from lipid derivatives of water-soluble polymers as delivery systems for poorly soluble drugs. *Adv Drug Deliv Rev* 56(9):1273-1289.
31. Torchilin VP 2005. Recent advances with liposomes as pharmaceutical carriers. *Nat Rev Drug Discov* 4(2):145-160.
32. Higuchi WI 1964. Effects of interacting colloids on transport rates. *J Pharm Sci* 53(5):532-535.
33. Gupta S, Moulik SP 2008. *Biocompatible microemulsions and their prospective uses in drug delivery*. *J Pharm Sci* 97(1):22-45.
34. Cheng Y, Xu Z, Ma M, Xu T 2008. Dendrimers as drug carriers: applications in different routes of drug administration. *J Pharm Sci* 97(1):123-143.
35. Tillman Lloyd G, Geary Richard S, Hardee Gregory E 2008. Oral delivery of antisense oligonucleotides in man. *J Pharm Sci* 97(1):225-236.
36. Tsutsumi K, Li SK, Hymas Richard V, Teng C-L, Tillman Lloyd G, Hardee Gregory E, Higuchi William I, Ho Norman FH 2008. Systematic studies on the paracellular permeation of model permeants and oligonucleotides in the rat small intestine with chenodeoxycholate as enhancer. *J Pharm Sci* 97(1):350-367.
37. Brewster ME, Loftsson T 2007. Cyclodextrins as pharmaceutical solubilizers. *Adv Drug Deliv Rev* 59(7):645-666.
38. Rao VM, Stella VJ 2003. When can cyclodextrins be considered for solubilization purposes? *J Pharm Sci* 92(5):927-932.

39. Shaker DS, Ghanem AH, Li SK, Warner KS, Hashem FM, Higuchi WI 2003. Mechanistic studies of the effect of hydroxypropyl- β -cyclodextrin on in vitro transdermal permeation of corticosterone through hairless mouse skin. *Int J Pharm* 253(1-2):1-11.
40. Uekama K 2004. Design and evaluation of cyclodextrin-based drug formulation. *Chem Pharm Bull (Tokyo)* 52(8):900-915.
41. Redenti E, Szente L, Szejtli J 2001. Cyclodextrin complexes of salts of acidic drugs. Thermodynamic properties, structural features, and pharmaceutical applications. *J Pharm Sci* 90(8):979-986.
42. Stella VJ, Rajewski RA 1997. Cyclodextrins: their future in drug formulation and delivery. *Pharm Res* 14(5):556-567.
43. Kis GL, Schoch C, Szejtli J. 2003. Quaternary ammonium cyclodextrins as pharmaceutical penetration enhancers. ed., Application: WO (Novartis A.-G., Switz.; Novartis Pharma G.m.b.H.). p 35 pp.
44. Loftsson T, Vogensen SB, Brewster ME, Konraosdottir F 2007. Effects of cyclodextrins on drug delivery through biological membranes. *J Pharm Sci* 96(10):2532-2546.
45. Brewster ME, Noppe M, Peeters J, Loftsson T 2007. Effect of the unstirred water layer on permeability enhancement by hydrophilic cyclodextrins. *Int J Pharm* 342(1-2):250-253.
46. Loftsson T, Duchene D 2007. Cyclodextrins and their pharmaceutical applications. *Int J Pharm* 329(1-2):1-11.
47. Arima H, Yunomae K, Morikawa T, Hirayama F, Uekama K 2004. Contribution of cholesterol and phospholipids to inhibitory effect of dimethyl- β -cyclodextrin on efflux function of P-glycoprotein and multidrug resistance-associated protein 2 in vinblastine-resistant Caco-2 cell monolayers. *Pharm Res* 21(4):625-634.
48. Arima H, Yunomae K, Hirayama F, Uekama K 2001. Contribution of P-glycoprotein to the enhancing effects of dimethyl- β -cyclodextrin on oral bioavailability of tacrolimus. *J Pharmacol Exp Ther* 297(2):547-555.
49. Matsubara K, Irie T, Uekama K 1997. Spectroscopic characterization of the inclusion complex of a luteinizing hormone-releasing hormone agonist, buserelin acetate, with dimethyl- β -cyclodextrin. *Chem Pharm Bull (Tokyo)* 45(2):378-383.
50. Nagase Y, Arima H, Wada K, Sugawara T, Satoh H, Hirayama F, Uekama K 2003. Inhibitory effect of sulfobutyl ether β -cyclodextrin on DY-9760e-induced cellular damage: In vitro and in vivo studies. *J Pharm Sci* 92(12):2466-2474.

51. Nagase Y, Hirata M, Wada K, Arima H, Hirayama F, Irie T, Kikuchi M, Uekama K 2001. Improvement of some pharmaceutical properties of DY-9760e by sulfobutyl ether beta-cyclodextrin. *Int J Pharm* 229(1-2):163-172.
52. Ono N, Arima H, Hirayama F, Uekama K 2001. A moderate interaction of maltosyl-alpha-cyclodextrin with Caco-2 cells in comparison with the parent cyclodextrin. *Biol Pharm Bull* 24(4):395-402.
53. Tokihiro K, Arima H, Tajiri S, Irie T, Hirayama F, Uekama K 2000. Improvement of subcutaneous bioavailability of insulin by sulphobutyl ether beta-cyclodextrin in rats. *J Pharm Pharmacol* 52(8):911-917.
54. Tokihiro K, Irie T, Uekama K 1997. Varying effects of cyclodextrin derivatives on aggregation and thermal behavior of insulin in aqueous solution. *Chem Pharm Bull (Tokyo)* 45(3):525-531.
55. Piel G, Piette M, Barillaro V, Castagne D, Evrard B, Delattre L 2007. Study of the relationship between lipid binding properties of cyclodextrins and their effect on the integrity of liposomes. *Int J Pharm* 338(1-2):35-42.
56. Irie T, Uekama K 1997. Pharmaceutical applications of cyclodextrins. III. Toxicological issues and safety evaluation. *J Pharm Sci* 86(2):147-162.
57. Irie T, Uekama K 1999. Cyclodextrins in peptide and protein delivery. *Adv Drug Deliv Rev* 36(1):101-123.
58. Brewster ME, Loftsson T 2007. Cyclodextrins as pharmaceutical solubilizers. *Adv Drug Deliv Rev* 59(7):645-666.
59. Loftsson T, Duchene D 2007. Cyclodextrins and their pharmaceutical applications. *Int J Pharm* 329(1-2):1-11.
60. Davis ME, Brewster ME 2004. Cyclodextrin-based pharmaceuticals: past, present and future. *Nat Rev Drug Discov* 3(12):1023-1035.
61. Aungst BJ 2000. Intestinal permeation enhancers. *J Pharm Sci* 89(4):429-442.
62. Aungst BJ 1993. Novel formulation strategies for improving oral bioavailability of drugs with poor membrane permeation or presystemic metabolism. *J Pharm Sci* 82(10):979-987.
63. Hellriegel ET, Bjornsson TD, Hauck WW 1996. Interpatient variability in bioavailability is related to the extent of absorption: implications for bioavailability and bioequivalence studies. *Clin Pharmacol Ther* 60(6):601-607.

64. Lee VHL, Yamamoto A 1990. Penetration and enzymatic barriers to peptide and protein absorption. *Adv Drug Del Rev* 4:171-207.
65. Muranishi S 1990. Absorption enhancers. *Crit Rev Ther Drug Carrier Syst* 7(1):1-33.
66. Swenson ES, Curatolo W 1992. Intestinal Permeability enhancement for proteins, peptides, and other polar drugs: mechanisms and potential toxicity. *Adv Drug Del Rev* 8:39-92.
67. van Hoogdalem EJ, de Boer AG, Breimer DD 1989. Intestinal drug absorption enhancement: an overview. *Pharmacol Ther* 44(3):407-443.
68. Drewe J, Fricker G, Vonderscher J, Beglinger C 1993. Enteral absorption of octreotide: absorption enhancement by polyoxyethylene-24-cholesterol ether. *Br J Pharmacol* 108(2):298-303.
69. Kreutler CJ, Davis WW 1971. Normal and promoted GI absorption of water-soluble substances. 3. Absorption of antibiotics from stomach and intestine of the rat. *J Pharm Sci* 60(12):1835-1838.
70. Malik SN, Canaham DH, Gouda MW 1975. Effect of surfactants on absorption through membranes III: effects of dioctyl sodium sulfosuccinate and poloxalene on absorption of a poorly absorbable drug, phenolsulfonphthalein, in rats. *J Pharm Sci* 64(6):987-990.
71. Ichikawa K, Ohata I, Mitomi M, Kawamura S, Maeno H, Kawata H 1980. Rectal absorption of insulin suppositories in rabbits. *J Pharm Pharmacol* 32(5):314-318.
72. Walters KA, Dugard PH, Florence AT 1981. Non-ionic surfactants and gastric mucosal transport of paraquat. *J Pharm Pharmacol* 33(4):207-213.
73. Guarini S, Ferrari W 1984. Structural restriction in bile acids and non-ionic detergents for promotion of heparin absorption from rat gastro-intestinal tract. *Arch Int Pharmacodyn Ther* 271(1):4-10.
74. Feldman S, Gibaldi M 1969. Physiologic surface-active agents and drug absorption. I. Effect of sodium taurodeoxycholate on salicylate transfer across the everted rat intestine. *J Pharm Sci* 58(4):425-431.
75. Feldman S, Gibaldi M 1969. Physiologic surface-active agents and drug absorption II. Comparison of the effect of sodium taurodeoxycholate and ethylenediaminetetraacetic acid on salicylamide and salicylate transfer across the everted rat small intestine. *J Pharm Sci* 58(8):967-970.

76. Freel RW, Hatch M, Earnest DL, Goldner AM 1983. Dihydroxy bile salt-induced alterations in NaCl transport across the rabbit colon. *Am J Physiol* 245(6):G808-815.
77. Freel RW, Hatch M, Earnest DL, Goldner AM 1983. Role of tight-junctional pathways in bile salt-induced increases in colonic permeability. *Am J Physiol* 245(6):G816-823.
78. Kakemi K, Sezaki H, Konishi R, Kimura T, Murakami M 1970. Effect of bile salts on the gastrointestinal absorption of drugs. I. *Chem Pharm Bull (Tokyo)* 18(2):275-280.
79. Kakemi K, Sezaki H, Konishi R, Kimura T, Okita A 1970. Effect of bile salts on the gastrointestinal absorption of drugs. II. Mechanism of the enhancement of the intestinal absorption of sulfaguanidine by bile salts. *Chem Pharm Bull (Tokyo)* 18(5):1034-1039.
80. Kidron M, Bar-On H, Berry EM, Ziv E 1982. The absorption of insulin from various regions of the rat intestine. *Life Sci* 31(25):2837-2841.
81. Rafter JJ, Eng VW, Furrer R, Medline A, Bruce WR 1986. Effects of calcium and pH on the mucosal damage produced by deoxycholic acid in the rat colon. *Gut* 27(11):1320-1329.
82. Teichberg S, McGarvey E, Bayne MA, Lifshitz F 1983. Altered jejunal macromolecular barrier induced by alpha-dihydroxy deconjugated bile salts. *Am J Physiol* 245(1):G122-132.
83. Ziv E, Eldor A, Kleinman Y, Bar-On H, Kidron M 1983. Bile salts facilitate the absorption of heparin from the intestine. *Biochem Pharmacol* 32(5):773-776.
84. Tsutsumi K, Li SK, Hymas RV, Teng CL, Tillman LG, Hardee GE, Higuchi WI, Ho NF 2008. Systematic studies on the paracellular permeation of model permeants and oligonucleotides in the rat small intestine with chenodeoxycholate as enhancer. *J Pharm Sci* 97(1):350-367.
85. Anderberg EK, Lindmark T, Artursson P 1993. Sodium caprate elicits dilatations in human intestinal tight junctions and enhances drug absorption by the paracellular route. *Pharm Res* 10(6):857-864.
86. Ramakrishna BS, Mathan M, Mathan VI 1994. Alteration of colonic absorption by long-chain unsaturated fatty acids. Influence of hydroxylation and degree of unsaturation. *Scand J Gastroenterol* 29(1):54-58.

87. Sawada T, Ogawa T, Tomita M, Hayashi M, Awazu S 1991. Role of paracellular pathway in nonelectrolyte permeation across rat colon epithelium enhanced by sodium caprate and sodium caprylate. *Pharm Res* 8(11):1365-1371.
88. Tomita M, Hayashi M, Awazu S 1995. Absorption-enhancing mechanism of sodium caprate and decanoylcarnitine in Caco-2 cells. *J Pharmacol Exp Ther* 272(2):739-743.
89. Tomita M, Hayashi M, Horie T, Ishizawa T, Awazu S 1988. Enhancement of colonic drug absorption by the transcellular permeation route. *Pharm Res* 5(12):786-789.
90. Tomita M, Sawada T, Ogawa T, Ouchi H, Hayashi M, Awazu S 1992. Differences in the enhancing effects of sodium caprate on colonic and jejunal drug absorption. *Pharm Res* 9(5):648-653.
91. Tomita M, Shiga M, Hayashi M, Awazu S 1988. Enhancement of colonic drug absorption by the paracellular permeation route. *Pharm Res* 5(6):341-346.
92. Raoof AA, Chiu P, Ramtoola Z, Cumming IK, Teng C, Weinbach SP, Hardee GE, Levin AA, Geary RS 2004. Oral bioavailability and multiple dose tolerability of an antisense oligonucleotide tablet formulated with sodium caprate. *J Pharm Sci* 93(6):1431-1439.
93. Raoof AA, Ramtoola Z, McKenna B, Yu RZ, Hardee G, Geary RS 2002. Effect of sodium caprate on the intestinal absorption of two modified antisense oligonucleotides in pigs. *Eur J Pharm Sci* 17(3):131-138.
94. Beskid G, Unowsky J, Behl CR, Siebelist J, Tossounian JL, McGarry CM, Shah NH, Cleeland R 1988. Enteral, oral, and rectal absorption of ceftriaxone using glyceride enhancers. *Chemotherapy* 34(2):77-84.
95. Sekine M, Maeda E, Sasahara K, Okada R, Kimura K, Fukami M, Awazu S 1985. Improvement of bioavailability of poorly absorbed drugs. III. Oral acute toxicity and local irritation of medium chain glyceride. *J Pharmacobiodyn* 8(8):633-644.
96. Sekine M, Sasahara K, Hasegawa K, Okada R, Awazu S 1985. Improvement of bioavailability of poorly absorbed drugs. V. Effect of surfactants on the promoting effect of medium chain glyceride for the rectal absorption of beta-lactam antibiotics in rats and dogs. *J Pharmacobiodyn* 8(8):653-660.
97. Sekine M, Sasahara K, Okada R, Awazu S 1985. Improvement of bioavailability of poorly absorbed drugs. IV. Mechanism of the promoting effect of medium chain glyceride on the rectal absorption of water soluble drugs. *J Pharmacobiodyn* 8(8):645-652.

98. Sekine M, Terashima H, Sasahara K, Nishimura K, Okada R, Awazu S 1985. Improvement of bioavailability of poorly absorbed drugs. II. Effect of medium chain glyceride base on the intestinal absorption of cefmetazole sodium in rats and dogs. *J Pharmacobiodyn* 8(4):286-295.
99. Ueda I, Shimojo F, Kozatani J 1983. Effect of ethyl cellulose in a medium-chain triglyceride on the bioavailability of ceftizoxime. *J Pharm Sci* 72(4):454-458.
100. Unowsky J, Behl CR, Beskid G, Sattler J, Halpern J, Cleeland R 1988. Effect of medium chain glycerides on enteral and rectal absorption of beta-lactam and aminoglycoside antibiotics. *Chemotherapy* 34(4):272-276.
101. Aungst BJ, Saitoh H 1996. Intestinal absorption barriers and transport mechanisms, including secretory transport, for a cyclic peptide, fibrinogen antagonist. *Pharm Res* 13(1):114-119.
102. Takeichi Y, Baba K, Kinouchi Y, Iida Y, Umeno Y, Muranishi S, Nakai Y 1990. Combinative improving effect of increased solubility and the use of absorption enhancers on the rectal absorption of uracil in beagle dogs. *Chem Pharm Bull (Tokyo)* 38(9):2547-2551.
103. Swenson ES, Milisen WB, Curatolo W 1994. Intestinal permeability enhancement: efficacy, acute local toxicity, and reversibility. *Pharm Res* 11(8):1132-1142.
104. Aungst BJ, Saitoh H, Burcham DL, Huang S-M, Mousa SA, Hussain MA 1996. Enhancement of the intestinal absorption of peptides and non-peptides. *J Controlled Release* 41(1,2, Fifth International Symposium on Delivery and Targeting of Pesticides, Proteins and Genes, 1995):19-31.
105. Curatolo W, Ochoa R. 1994. Safety assessment of intestinal permeability enhancers. In deBoer AG, editor *Drug Delivery*: Harwood Publishers. p 367-389.
106. Swenson ES, Milisen WB, Curatolo W 1994. Intestinal permeability enhancement: structure-activity and structure-toxicity relationships for nonylphenoxypolyoxyethylene surfactant permeability enhancers. *Pharm Res* 11(10):1501-1504.

CHAPTER 2

STATEMENT OF THE PROBLEM

Efforts to improve gastrointestinal drug delivery have been on going for many years and the use of carrier molecules to improve solubility and transport of lipophilic drugs has become increasingly popular in recent decades. Although there is qualitative understanding of how cyclodextrin carriers improve drug transport, the complex interplay of the parameters involved is not well understood. The purpose of the present research project has been to quantify the effects of cyclodextrin carriers on the intestinal absorption of highly lipophilic (BCS class II) compounds and to examine the use of cyclodextrin carriers for more effectively presenting permeation enhancers to the surface of the ileum for the intestinal absorption enhancement of polar (i.e., BCS Class III) compounds. This will be accomplished through the following specific aims.

1. Develop a physical model that predicts the transport of a highly lipophilic weak acid molecule (the permeant) across a lipophilic membrane from aqueous buffered solutions in the presence of a cyclodextrin carrier. This model will account for the permeant and carrier concentrations and the following parameters: solution pH, permeant pKa, aqueous boundary layer (ABL) thickness, permeant-carrier binding constant(s), intrinsic membrane permeability coefficient, and diffusion coefficient(s). These parameters will be quantified using independent methods where feasible.

2. Experimentally determine the transport rate of a highly lipophilic weak acid molecule (capric acid) across a silicone polymer membrane in the presence of a hydroxypropyl- β -cyclodextrin (HPB) carrier, choosing experimental conditions that cover the range from ABL-controlled to membrane-controlled transport. The experimental results will be compared to those predicted from the model.
3. Experimentally determine the transport rate of a highly lipophilic weak acid molecule (capric acid) across the rat ileal membrane in the presence of a cyclodextrin carrier using the in situ single pass perfusion technique. The experimental results will be compared to those predicted from the model developed in vitro with the silicone polymer membrane. The model will then be modified to account for the villus structure of the rat ileum, and the experimental results will be analyzed using the villus model (VM).
4. Demonstrate the permeability enhancement in the rat ileum using solutions containing an intestinal membrane permeation enhancer (capric acid or chenodeoxycholic acid) in the presence and absence of a cyclodextrin carrier. The effect of the cyclodextrin carrier on the presentation of the permeation enhancer to the surface and its accompanying membrane enhancement will be experimentally determined and interpreted using the physical model predictions.

CHAPTER 3

TRANSPORT OF A LIPOPHILIC IONIZABLE PERMEANT (CAPRIC ACID) ACROSS A LIPOPHILIC MEMBRANE (SILICONE POLYMER MEMBRANE) FROM AQUEOUS BUFFERED SOLUTIONS IN THE PRESENCE OF HYDROXYPROPYL- β - CYCLODEXTRIN

3.1 Introduction

Many biologically active compounds have inadequate bioavailability for successful oral dosing because of poor biological membrane permeability, water solubility, and/or stability characteristics. One category of drug molecules that has been receiving much attention recently is that class of compounds which are both highly lipophilic and poorly water soluble (BCS classification class II).¹ For drug molecules in this category, an approach often taken to improve bioavailability is the inclusion of a solubilizing agent in the formulation to increase the drug solubility and to effect a greater maximum flux of drug into the blood stream.²⁻⁷

In recent years, cyclodextrins have received extensive attention as solubilizing agents in aqueous media because of their ability to form inclusion complexes with lipophilic drug molecules. Of particular interest, 2-hydroxypropyl- β -cyclodextrin (HPB) has been studied as a potential excipient in drug formulations because of its ability to

improve the drug delivery characteristics for a large number of molecules.⁸⁻¹⁶ HPB is highly water soluble, well tolerated at moderate doses, is not significantly absorbed in the gastrointestinal tract, and is cited in the FDA's list of Inactive Pharmaceutical Ingredients,⁸ making it a good example of an excipient for oral drug delivery formulations of poor solubility, high permeability drugs.

While there has been much progress from the standpoint of practical formulation development involving inclusion complexes, there has been relatively little progress from the standpoint of the quantitative mechanistic understanding of the interplay of certain key variables, and therefore it should be desirable to examine appropriate models both theoretically and experimentally that may advance the cause of more rational approaches in the area of formulation development of orally delivered, high lipophilicity/low solubility drug molecules. The present study builds upon earlier model studies done by Amidon et al.² who examined transport of progesterone across a silicone polymer membrane and the transport-enhancing effects of polysorbate-80 micelles in the aqueous medium. In the current study, a physical model approach is presented for the transport of a lipophilic weak acid molecule across a lipophilic biological membrane in the presence of a carrier in the aqueous phase with the particular purpose of obtaining a better understanding of the interplay of key variables involved. In the present case, the model situation is that where capric acid (HA) is the high lipophilicity weak acid molecule (playing the role of surrogate for a drug molecule), and its transport across a silicone polymer membrane (the surrogate for a lipophilic biological membrane) positioned between two aqueous compartments in the presence of the carrier HPB in the aqueous phase. The expected high silicone polymer membrane/water partition

coefficient and the expected high diffusivity of the capric acid molecule in the silicone polymer membrane¹⁷ is expected to allow for a significant influence of the aqueous boundary layer (ABL) on the overall capric acid transport rate. The model takes into account the capric acid and HPB concentrations, solution pH, aqueous boundary layer thickness, the capric acid dissociation constant, the capric acid/silicone membrane intrinsic permeability coefficient, the capric acid/HPB and the caprate ion/HPB binding constants, and the diffusion coefficients of all four species.

3.2 The Model and Equations Used in the Analysis of Experimental Data

Here we describe the general model with a principal aim of obtaining from it the equations for the interpretation of the experiments conducted in the present study. The model also serves as the template for the design of experimental strategies aimed at the quantitation or the confirmation thereof of species-specific diffusion coefficients, the capric acid dissociation constant, the binding constants for the two complexes, and the capric acid permeability coefficient of the ABL and that of the silicone membrane.

In an aqueous solution containing capric acid and HPB in equilibrium, the total caprate concentration (C_T) in the bulk donor solution, in the ABL, or in the solution at the membrane-solution interface, as the case may be, is

$$C_T = C^u + C^- + C^{*u} + C^{*-} \quad (3.1)$$

where C denotes concentration and the superscripts u , $-$, $*u$, and $*-$ represent the capric acid molecule (HA), caprate ion (A^-), capric acid-HPB complex (HA•HPB) and caprate

ion-HPB complex ($A^- \bullet \text{HPB}$) species, respectively. Since the concentration of each species is equal to the product of the molar fraction (F) of each species and C_T ,

$$C_T = (F^u + F^- + F^{*u} + F^{*-})C_T \quad (3.2)$$

where these fractions are related to the HPB concentration, pH, C_T , the acid dissociation constant (K_a) of capric acid, and the two binding constants, K^u (for $\text{HA} \bullet \text{HPB}$) and K^- (for $A^- \bullet \text{HPB}$). The steady-state flux across the ABL (J_{ABL}) from the stirred bulk donor solution to the membrane surface is the sum of the fluxes of all the caprate species across the ABL:

$$J_{\text{ABL}} = \left(\frac{(D^u F^u + D^- F^- + D^{*u} F^{*u} + D^{*-} F^{*-})}{h_{\text{ABL}}} \right) (C_{T,D} - C_{T,S}) \quad (3.3)$$

where the D 's are the diffusion coefficients, h_{ABL} is the ABL thickness, and $C_{T,D}$ and $C_{T,S}$ represent the total caprate concentration in the donor bulk solution and at the solution-membrane interface, respectively. The effective total caprate diffusion coefficient in the aqueous phase (D^{eff}) is:

$$D^{\text{eff}} = D^u F^u + D^- F^- + D^{*u} F^{*u} + D^{*-} F^{*-} \quad (3.4)$$

The effective total caprate permeability coefficient for the ABL ($P_{\text{ABL}}^{\text{eff}}$) is then:

$$P_{\text{ABL}}^{\text{eff}} = \frac{D^{\text{eff}}}{h_{\text{ABL}}} \quad (3.5)$$

It follows then that,

$$J_{ABL} = P_{ABL}^{eff} (C_{T,D} - C_{T,S}) \quad (3.6)$$

Taken together, Eqs 3.4 and 3.5 tacitly assume that there exists rapid chemical equilibria everywhere in the ABL and that there is no significant convective contribution to caprate transport in the ABL. When only capric acid molecules are able to partition at the solution/membrane interface and diffuse across the membrane into the receiver sink, the capric acid membrane flux (J_m)

$$J_m = P_m C_{T,S} \quad (3.7)$$

where the effective capric acid membrane permeability coefficient (P_m) is the product of the intrinsic membrane permeability coefficient (P_i) and the fraction of the free capric acid species (F^u):

$$P_m = P_i F^u \quad (3.8)$$

The intrinsic permeability coefficient is given by

$$P_i = \frac{k_{p,i} D_m}{h_m} \quad (3.9)$$

where $k_{p,i}$ is the intrinsic capric acid/silicone polymer partition coefficient, D_m is the diffusion coefficient of capric acid molecule in the silicone polymer membrane, and h_m is the membrane thickness. The continuity of the flow of mass at steady-state is given by

$$J_{ABL} = J_m = J \quad (3.10)$$

where J is the overall flux across the system. With Eqs 3.10, 3.6 and 3.7, the membrane surface total caprate concentration ($C_{T,S}$) is related to the total donor concentration ($C_{T,D}$) by

$$C_{T,S} = \frac{P_{ABL}^{eff} C_{T,D}}{P_{ABL}^{eff} + P_i F^u} \quad (3.11)$$

With Eqs 3.6, 3.10, and 3.11, the overall flux from the donor to the receiver sink is

$$J = \left(\frac{1}{\frac{1}{P_{ABL}^{eff}} + \frac{1}{P_i F^u}} \right) C_{T,D} \quad (3.12)$$

from which it is apparent that the total permeability coefficient (P_T) encompassing both the ABL and the membrane transport barriers is:

$$P_T = \frac{1}{\frac{1}{P_{ABL}^{eff}} + \frac{1}{P_i F^u}} = \frac{P_{ABL}^{eff}}{1 + \frac{P_{ABL}^{eff}}{P_i F^u}} \quad (3.13)$$

The mathematical form of the right-most side of Eq 3.13 permits one to readily assess the extent to which the overall transport is ABL-controlled and membrane-controlled. The permeability coefficient (P_T) in Eq 3.13 is predictable when the HPB concentration, pH, $C_{T,D}$, capric acid K_a , K^- , K^u , D^{eff} , h_{ABL} , and P_i are known. It is understood that the present physical model does not consider pH gradients within the ABL. Consequently, sufficiently high buffer capacity to maintain a constant pH everywhere is presumed.

Additionally, D^{eff} (see Eqs. 3.3 and 3.4) would be constant across the entire ABL for a given set of experimental conditions strictly only when the uncomplexed HPB, i.e., the free HPB (HPB_f) concentration is much greater than the concentrations of the complexes. This condition is met for all experiments in the present study. For the general case in which the HPB concentration may not be always much greater than the concentrations of the complexes, the finite element numerical method discussed in Chapter 4 may be employed to calculate the ABL-location dependent D^{eff} values for each experimental situation.

3.3 Strategy

The present work was expected to be particularly helpful in interpreting the results of the capric acid rat intestinal absorption experiments which have been concurrently conducted in our laboratory and the results for which are presented in Chapter 4. In the present study, the physical model is developed and tested with a silicone polymer membrane mounted between two aqueous phases in a side-by-side diffusion cell system. Silicone membranes have been commonly used as in vitro surrogates in the attempt to mimic characteristics of biological membranes.^{18,19} Key parameters entering into the equations for the physical model are to be determined experimentally by independent (or essentially independent) methods. The capric acid K_a and the capric acid/HPB binding constants (K^u and K^-) are determined by equilibrium silicone polymer membrane partitioning experiments and/or by selected silicone membrane capric acid transport studies; the free and the complexed caprate species diffusion coefficients are determined from fritted glass disk diffusion experiments; the

intrinsic silicone membrane capric acid permeability coefficient and the effective ABL thicknesses are determined from best-fit analyses of selected data from silicone membrane/capric acid transport experiments over a range of conditions particularly sensitive to these parameters.

The buffers used in the present study are all at an ionic strength of 0.37 M as this is the ionic strength of the media employed in the rat intestinal perfusion experiments.^{20,21} For the same reason, all experiments involved in the determination of the model parameters as well as all of the main transport experiments were conducted in appropriate media at the ionic strength of 0.37 M. The buffer capacities, ranging from 9.5×10^{-3} to 6×10^{-3} M for 0.01 M citrate buffers, pH 3.0 to 6.0, and 3.1×10^{-2} M for 0.057 M phosphate buffers, pH 7.0 and 7.4, were all sufficiently large so that the additions of 5×10^{-5} M cold capric acid would have had inconsequential effects ($\Delta\text{pH} \leq 0.005$) on the buffer pH. Therefore, no significant pH gradients across the ABL were anticipated.

The main capric acid transport experiments of this study are conducted with a) the silicone membrane alone (SM) in the diffusion chamber or b) the silicone membrane plus six Millipore membranes assembled together and held closely against the silicone membrane on the donor compartment side (SM-MM). The latter is essentially a composite membrane possessing a significantly greater effective ABL thickness than in the SM case, this to more closely approximate the magnitude of the effective ABL thickness of the rat intestinal tract. Although the capric acid-to-HPB concentration ratios in the present experiments were always very much less than unity (i.e., HPB concentration $\gg C_T$), the ratios were varied in conjunction with pH to provide a wide

range of conditions that not only enabled the validation/quantitation of species-dependent physicochemical parameters, but also more effectively demonstrated the quantitative interplay of multiple factors. The receiver compartment is always maintained at pH 9.5 with adequate buffer capacity for the purpose of efficient extraction of capric acid from the membrane and the elimination of any significant ABL resistance in the receiver chamber. All experiments are performed at 30°C as this has been the mean temperature of the perfusate in the in situ rat intestinal perfusion experiments.

While being a surrogate for the weak acid lipophilic drug molecule in the present study, capric acid has been commonly investigated as a possible intestinal drug absorption enhancer for low permeability, highly polar drug molecules.²²⁻²⁴ Therefore, a major independent reason for using capric acid and HPB in the present study is that we have been investigating this combination in exploratory in situ studies to determine the modulating influence of HPB on the biomembrane transport enhancement of highly polar compounds in the rat ileum by capric acid. The results of this exploratory investigation are discussed in Chapter 5.

3.4 Experimental

3.4.1 Chemicals and reagents

Capric acid and caprylic acid were purchased from Sigma-Aldrich Company (St. Louis, MO). [¹⁴C]Urea, [¹⁴C]mannitol, [¹⁴C]sucrose, [¹⁴C]capric acid, and [¹⁴C]caprylic acid of radiochemical purity ≥97% were obtained from Moravek Biopharmaceuticals (Brea, CA). Hydroxypropyl-β-cyclodextrin (HPB) was a generous gift from Roquette America (Keokuk, IA). Trifluoroacetic acid was obtained from Acros (New Jersey,

USA). Dimethyl silicone polymer membranes (100 μm thick, SSP-M823) obtained from Specialty Silicone Products (Ballston Spa, NY) were cut into 20 mm diameter disks. Millipore filter membranes (0.22 μm) were obtained from Millipore Corp. (Bedford, MA). Borate buffer pH 9.5 (Item No. 2307) was obtained from GFS Chemicals (Columbus, OH). All other chemicals and reagents were obtained from Sigma-Aldrich Company (St. Louis, MO).

3.4.2 Methods

3.4.2.1 Determination of the capric acid pK_a (at ionic strength=0.37)

and the intrinsic capric acid aqueous-silicone polymer partition

coefficient, $k_{p,i}$, by the silicone membrane partitioning method

Citrate buffers (10 mM) at pH 3.0, 3.5, 4.0, 4.5, 4.7, 5.0, and 5.5, and phosphate buffers (57 mM) at pH 6.0 and 6.5, all with 0.05 mM cold sodium caprate and 0.02% sodium azide, were adjusted to 0.37 ionic strength using sodium chloride. All pH measurements were conducted with an Orion 320 pH meter manufactured by Thermo Electron Corporation calibrated with pH 4.0, 7.0, and/or 10.0 Fisher Scientific standard pH buffers. A trace amount of $[\text{C}^{14}]$ capric acid (0.01-0.1 $\mu\text{Ci/ml}$) was added to each buffer solution. A 5 ml aliquot of each solution was added to a 20 ml scintillation vial containing a preweighted silicone polymer membrane disk and equilibrated at 30 $^{\circ}\text{C}$ in a shaking water bath for 48, 72, or 96 hours. After equilibration, a 1ml sample of the equilibrated solution was pipetted into 10 ml of scintillation cocktail in a scintillation vial; the silicone disk was then removed and rinsed for 10 seconds in distilled water adjusted to pH 3.0 using 1 molar hydrochloric acid. The silicone disk was then dried

with a paper towel and transferred into a 20 ml scintillation vial. Then 200 μl of 100% trifluoroacetic acid was added into the vial and the disk was allowed to completely dissolve (10 min); then 10 ml of scintillation cocktail was added to this solution. Both the equilibrated aqueous solution sample and the dissolved silicone disk sample were assayed using the Packard TriCarb 1900TR liquid scintillation counter. The apparent partition coefficient, $k_{p,\text{app}}$, was calculated by

$$k_{p,\text{app}} = \frac{C_{s,p}}{C_{\text{aq}}} \quad (3.14)$$

where $C_{s,p}$ and C_{aq} are the capric acid concentration (mole/cc) in the silicone polymer and total caprate concentration in the aqueous phase (mole/cc), respectively. The intrinsic partition coefficient ($k_{p,i}$) and $\text{p}K_a$ were then simultaneously determined by best-fitting the data to Eq 3.15. A good fit of all the data to Eq 3.15 with the two best-fit parameters ($k_{p,i}$ and $\text{p}K_a$) would also directly suggest that only the unionized capric acid molecule may partition into the silicone membrane polymer.

$$k_{p,\text{app}} = \frac{k_{p,i}}{1 + 10^{(\text{pH} - \text{p}K_a)}} \quad (3.15)$$

Experiments were performed in triplicate for each pH condition. This procedure was repeated using caprylic acid at an ionic strength of 0.1 to validate the method by comparing experimentally determined caprylic acid K_a values to literature values.

3.4.2.2 HA•HPB and A⁻•HPB binding constants, K^u and K⁻

The model assumes that HPB forms only 1:1 complexes with both the neutral and the anionic capric acid species; this assumption is consistent with the diffusion coefficient data (to be discussed later) and with results of transport experiments with 500 molecular weight cut-off membranes at various concentrations of HPB and total caprate (data not shown). The model also assumes that uncomplexed HPB (i.e., HPB_f in Eq 3.16), exists only as monomers. This is considered to be a reasonable assumption by noting, for example, that the water solubility of corticosterone (a steroid for which its interaction with HPB in aqueous solutions is best explained by the formation of a one-to-one complex) increases linearly with increasing free HPB concentration over the HPB concentration range of the present study.¹⁴

The following equation was used to determine K^u

$$K^u = \frac{C^{*u}}{C^u[\text{HPB}_f]} \quad (3.16)$$

where [HPB_f] denotes the free HPB concentration. C^u and C^{*u} were determined from

$$F^u = C^u / C_T \quad (3.17)$$

$$F^{*u} = C^{*u} / C_T \quad (3.18)$$

Because, as will be seen, the partitioning of the caprate ion into the silicone polymer membrane is negligible compared to the unionized capric acid molecule, F^u can be determined from

$$F^u = \frac{k_{p,app}}{k_{p,i}} \quad (3.19)$$

$k_{p,app}$ was experimentally determined using the same method as in Section 3.4.2.1 at pH 3.0 (essentially 100% unionized capric acid), ionic strength = 0.37, and 30°C in the presence of 0, 0.33, 1, and 3 mM HPB. How $k_{p,i}$ for capric acid was determined independently has already been discussed Section 3.4.2.1. At low pH, F^{*u} could be determined from F^u because $F^u + F^{*u} \approx 1$ (At pH 3.0, the uncertainty in F^{*u} because of this approximation will be seen to be less than 3% over the HPB concentration range of the present study).

In the case of K^- , where

$$K^- = \frac{C^{*-}}{C^- [HPB_f]} \quad (3.20)$$

the apparent partition coefficient ($k_{p,app}$) of capric acid for silicone membrane at high pH in the presence of HPB was too low to permit an accurate determination of K^- . Therefore, K^- was determined from a least squares best-fit of select data at pH 7.4 and pH 7.0 on capric acid transport across one silicone membrane in the presence of varying concentrations of HPB in the donor chamber at 30°C.

3.4.2.3 Determination of aqueous diffusion coefficients

Diffusion cell transport experiments were designed for determining the diffusion coefficients of the four species– the capric acid molecule (HA), the caprate ion (A^-), $HA \bullet HPB$, and $A^- \bullet HPB$. The experiments were conducted at 30°C with various HPB

concentrations in a pH 7.4 buffer and in a pH 3.0 buffer. The dominant species were expected to be the caprate ion and $A^- \bullet HPB$ at pH 7.4 and the capric acid species and $HA \bullet HPB$ at pH 3.0. The pH 7.4 buffer was comprised of 57 mM $NaH_2PO_4 \cdot H_2O$ and 79 mM Na_2SO_4 . The low pH buffer was 10 mM citric acid adjusted to pH 3.0 with 10 M NaOH. For both buffers, the ionic strength was adjusted to 0.37 with reagent grade sodium chloride. The pH 7.4 buffer was also used in the single pass rat ileum perfusion studies (Chapter 4). The diffusion cell experiments employed a method described by Peck et al.²⁵ Briefly, a glass tube containing an embedded, medium fritted glass disk (LG-7160-140) (thickness of 2.5 mm, nominal pore size of 10-15 μm and an inside diameter of 10 mm) was obtained from Wilmad-Labglass (Buena, NJ) and permanently fused into a side-by-side diffusion cell system at the University of Utah glass shop. These cells were constructed to have ~3 ml donor and receiver chambers and a diffusional area (A) of 0.78 cm^2 . Teflon-coated magnetic stir bars (2mm \times 6mm) provided continuous stirring in the donor and receiver chambers during a transport experiment, and the temperature was maintained at 30°C by a circulating water bath. Removable stopcocks were used to prevent convective flow between the two chambers at the start of and during the transport experiment.

The experiment was initiated by filling the donor compartment with the donor solution of a solute of interest and then sealing it off using a stopcock. The receiver compartment was filled with 2.5 ml of the receiver solution and left open for sampling. In the capric acid diffusion cell experiments, the composition of the donor and receiver was always the same except for trace levels of [^{14}C]capric acid in the donor solution. A

1ml sample of the receiver solution was taken with replacement of fresh receiver solution at predetermined time points. Two 20 μ l donor solution samples were taken at the beginning and the end of the experiment to determine initial and final donor solute concentration. Samples were mixed with 10 ml Ultima Gold scintillation cocktail, assayed by scintillation counting, and the fritted disk permeability coefficient was calculated from

$$P_T = \frac{1}{AC_D} \frac{dQ}{dt} \quad (3.21)$$

where C_D is the solute concentration in the donor compartment and $\frac{dQ}{dt}$ is the steady-state slope of the cumulative amount of solute transported vs. time plot. C_D was determined from the average of the 20 μ l donor samples (C_D changed less than 5% over the course of a typical experiment). The aqueous diffusion coefficient is then calculated by

$$D_X = \frac{P_{T,X}}{P_{T,R}} D_R \quad (3.22)$$

where the subscripts X and R denote the solute of interest and the reference solute, respectively. [14 C]Sucrose was used as the reference solute. The experimental diffusion coefficients for the caprate ion and the capric acid species were determined at pH 7.4 and pH 3.0, respectively, using the buffers and range of conditions described above. The experimental diffusion coefficients for the complexes, $A^- \bullet \text{HPB}$ and $\text{HA} \bullet \text{HPB}$, were

determined over a range of HPB concentrations in the pH 7.4 phosphate buffer and at 30 mM HPB in the pH 3.0 citrate buffer, respectively. The diffusion coefficients for [^{14}C]urea and [^{14}C]mannitol were also determined at pH 3.0 and/or 7.4 (ionic strength = 0.37) for comparisons with temperature- and ionic strength-corrected literature values.

3.4.2.4 Viscosity measurements

A size 25 kinematic viscometer (Technical Glass Products Inc., Dover, NJ) was used to obtain kinematic viscosity values for the various solutions described in Section 3.4.2.3. All measurements were done in triplicate.

3.4.2.5 Capric acid transport experiments: silicone membrane alone (SM)

or silicone membrane plus six millipore membranes (SM-MM)

A 20 mm diameter, 100 μm thick silicone membrane alone or together with six Millipore membranes was mounted in a side-by-side diffusion cell having a surface area (A) of 0.78 cm^2 . The donor and receiver solution volumes were 2 ml each. The donor and receiver solutions were stirred at approximately 450 rpm using a magnetic stir bar (2mm \times 6mm), and the experiment was maintained at 30°C by a circulating water bath. The buffers for the donor solutions were citrate (for pH 3.0-5.5) or phosphate (for pH 6.0-7.4) described in Section 3.4.2.3, with the pH adjusted using 10 M NaOH. The receiver solution buffer was always the pH 9.5 borate buffer, this effectively eliminating any aqueous boundary layer resistance for capric acid transport in the receiver chamber side of the silicone membrane. The capric acid transport experiments were conducted with a trace concentration (0.04-0.2 $\mu\text{Ci/ml}$) of [^{14}C]capric acid present in the donor chamber

and with the HPB concentration (0-30 mM) and 0.05 mM cold capric acid and 0.02% sodium azide in both the donor and receiver chambers.

The transport experiment was initiated by loading the donor and receiver chambers with 2ml of donor and receiver solution, respectively. One-half (i.e., 1ml) of the donor solution and all of the receiver solution were replaced at predetermined time points to allow [^{14}C]capric acid transport to reach steady state. After steady-state was attained, 1ml receiver samples were taken with replacement and 20 μl donor samples were taken at predetermined time points. The sampling time points were chosen such that the receiver chamber had gained sufficient concentration in 1ml buffer for assay, and the donor capric acid concentration remained within 5% of the initial concentration over the duration of the experiment. After taking a set of samples, 1ml of the donor solution was replaced with fresh donor solution, the receiver chamber solution was removed as completely as possible by pipette and then rinsed and replenished with 2ml of fresh receiver solution, and another transport run was conducted. This process was repeated until four sets of samples were taken for a given condition. The samples were mixed with 10 ml scintillation cocktail and analyzed by scintillation counting. The experimental total permeability coefficient (P_T) was calculated using the same Eq 3.21 used in the diffusion coefficient determination.

3.4.2.6 Six millipore membranes (MM) only transport experiments

Six Millipore membranes were wetted with buffer solution under vacuum to remove any air bubbles, assembled and mounted as a composite membrane in the same side-by-side diffusion cell used for silicone transport studies. The donor and receiver

solutions consisted of either pH 3.0 citrate buffer or pH 7.4 phosphate buffer and either 0 or 30 mM HPB. These buffer solutions were prepared in the same manner as described in Section 3.4.2.3. The donor solution also included trace (0.01-0.1 $\mu\text{Ci/ml}$) $[\text{C}^{14}]$ capric acid or $[\text{C}^{14}]$ mannitol. The experiments were performed in a manner similar to that described in Section 3.4.2.4 and the P_T values calculated.

3.5 Results

3.5.1 Key parameters associated with the capric acid transport across the silicone membrane

The independently determined parameters that are involved in the physical model calculations of the transport of capric acid across silicone membrane in the presence of HPB are summarized in Table 3.1. The details are discussed in the following sections.

3.5.1.1 Capric acid pK_a and the intrinsic capric acid aqueous-silicone polymer partition coefficient, $k_{p,i}$

The capric acid apparent partition coefficients ($k_{p,app}$) calculated from the experimental data using Eq 3.14 were found to be independent of time from 48-96 hours, verifying that capric acid was in equilibrium with the silicone membrane within 48 hours. Fig 3.1 shows the experimentally determined $k_{p,app}$. The solid line represents the least-squares best-fit of the experimental $k_{p,app}$ to Eq 3.15. Briefly, the experimental $k_{p,app}$ at pH 3.0 was used as the initial guess for $k_{p,i}$, and the least-squares best-fit pK_a was determined using the pH 3.5-5.5 experimental data according to Eq 3.15. This pK_a was then used in Eq 3.15 to find the least-squares best-fit of $k_{p,i}$ to the pH 3.5-5.5 data. This

Table 3.1 Key parameters associated with the transport of capric acid across the silicone polymer membrane in the presence of hydroxypropyl- β -cyclodextrin (HPB).

| Parameter | Symbol | Value |
|--|-----------------|----------------------------------|
| Aqueous boundary layer thickness for SM (cm) | $h_{ABL,SM}$ | 0.012(\pm 0.002) |
| Effective aqueous boundary layer thickness for SM-MM (cm) | $h_{ABL,SM-MM}$ | 0.23(\pm 0.03) |
| Intrinsic permeability coefficient of capric acid (cm/s) | P_i | 0.018(\pm 0.001) |
| Diffusion coefficient of capric acid or the caprate ion (cm ² /s) | D^f | 6.9(\pm 0.5) $\times 10^{-6}$ |
| Diffusion coefficient of HA \bullet HPB or A ⁻ \bullet HPB (cm ² /s) | D^* | 2.9(\pm 0.2) $\times 10^{-6}$ |
| HA \bullet HPB binding constant mM ⁻¹ | K^u | 7.5(\pm 0.3) |
| A ⁻ \bullet HPB binding constant mM ⁻¹ | K^- | 2.5(\pm 0.2) |
| Capric acid pK _a at ionic strength = 0.37 | pK _a | 4.53(\pm 0.03) |

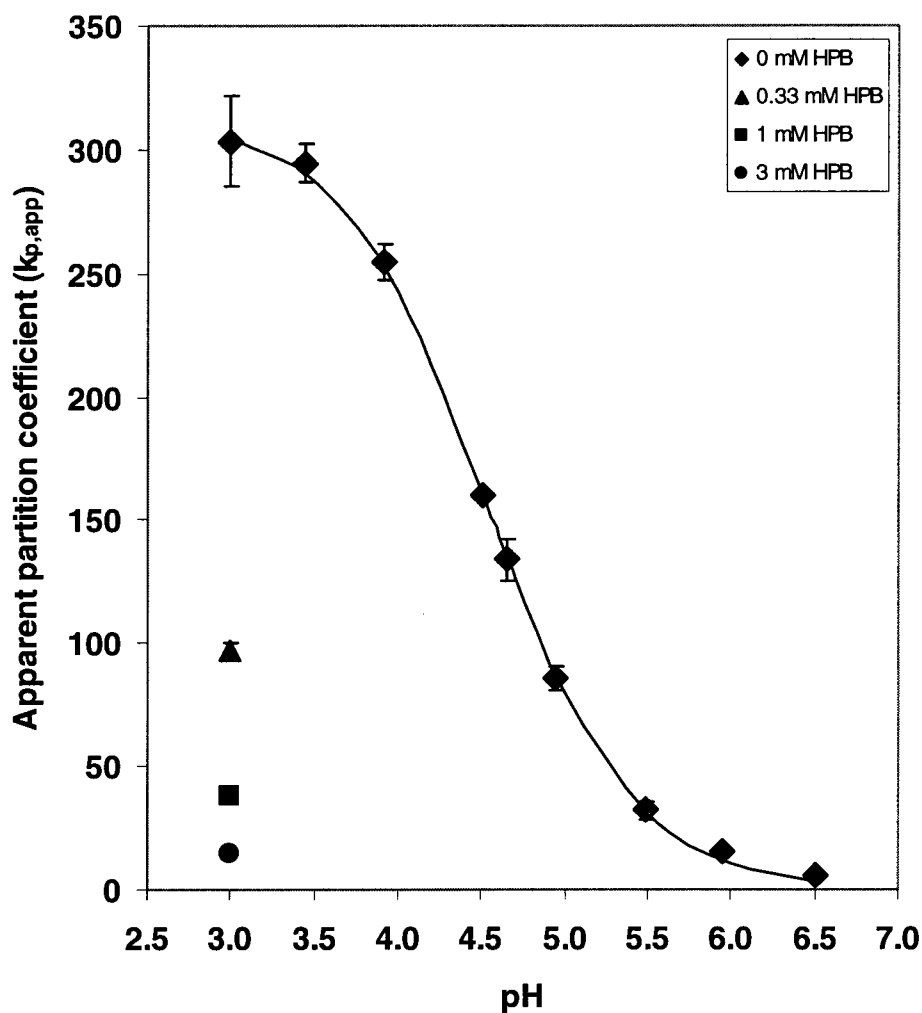


Fig 3.1 The apparent partition coefficient ($k_{p,app}$) for capric acid partitioning into silicone polymer membrane in 10 mM citrate buffers and 57 mM phosphate buffers ranging from pH 3.0 to pH 6.5 (ionic strength = 0.37). The curve represents best-fitting Eq 3.15 to the experimental $k_{p,app}$ data and the best-fit values of pK_a and $k_{p,i}$ were 4.53 (± 0.03) and 315 (± 14), respectively. The apparent partition coefficients for capric acid at pH 3.0 in the presence of 0.33, 1, and 3 mM hydroxypropyl- β -cyclodextrin (HPB) are also shown.

new $k_{p,i}$ was then, in turn, used in Eq 3.15 to find the least-squares best-fit pK_a to the pH 3.5-5.5 data. This process was repeated until successive iterations resulted in no further changes in the $k_{p,i}$ or the pK_a .

The results of the best-fitting procedure yielded a $k_{p,i}$ value of 315 (± 14) and a pK_a value of 4.53 (± 0.03). Fig 3.1 demonstrates the good fit of the data to Eq 3.15 over the entire range of the $k_{p,app}$ values. In order to increase the level of confidence in the pK_a determination method (silicone partitioning), the pK_a of caprylic acid was also determined at 25°C and 0.1 ionic strength. This experimentally determined pK_a value of caprylic acid was then compared to literature values²⁶ that were corrected for ionic strength using the extended Debye-Huckel equation and Kielland's ion size parameter of 6 for the caprylic acid ion.^{27,28} The experimental pK_a of caprylic acid at 0.1 ionic strength was determined to be 4.69 (± 0.03) with a $k_{p,i}$ of 14.2 (± 0.7). The literature value of the caprylic acid pK_a after correction for ionic strength was 4.71. The experimental pK_a values and the corrected literature pK_a values for caprylic acid were the same within experimental error, validating the silicone polymer membrane partition method for the determination of the capric acid pK_a at 30°C and 0.37 ionic strength.

3.5.1.2 HA• HPB and A⁻• HPB binding constants, K^u and K^-

K^u was determined from the results of the silicone polymer membrane partitioning experiments in the presence of 0.3, 1.0, and 3.0 mM HPB at pH 3.0 as described in Section 3.4.2.2. The apparent partition coefficients ($k_{p,app}$) for capric acid partitioning into silicone polymer membrane at varying concentrations of HPB are shown in Fig 3,1, and the F^u and K^u for each condition are presented in Table 3.2. K^- was

Table 3.2 The capric acid/HPB binding constant (K^u) as determined from silicone polymer membrane partitioning coefficients at pH 3.0 in the presence of varying concentrations of HPB.

| HPB | $k_{p,app}$ | F^u | K^u |
|----------------------|-------------|-------|-------------------|
| 0 | – | 0.97 | – |
| 0.33 | 97 | 0.31 | 7.7 |
| 1 | 38 | 0.12 | 7.6 |
| 3 | 14 | 0.045 | 7.1 |
| Average (SD) $K^u =$ | | | 7.5 (± 0.3) |

determined as a best-fit K^- value with silicone polymer membrane alone capric acid transport data at pH 7.0 and 7.4 obtained in the presence of varying concentrations of HPB. The effect of the negative charge on the HPB binding constants have been reported by others for various ionizable lipophilic compounds.^{13,29} Finding K^u to be approximately three times larger than K^- is considered to be quite reasonable.

3.5.1.3 Aqueous diffusion coefficients

Sucrose has a well defined diffusion coefficient³⁰ and has been frequently used as a standard,^{25,31} therefore, sucrose was used as the fritted glass disk cell reference solute for determining the aqueous diffusion coefficients using Eq 3.22. The aqueous diffusion coefficient of sucrose at 30°C taken from Ribeiro et al.³² was found to be 5.8×10^{-6} cm²/s after correction for viscosity using:

$$D_E = \frac{\eta_L T_E}{\eta_E T_L} D_L \quad (3.23)$$

where η is the viscosity, T is the absolute temperature, and D is the diffusion coefficient for the experimental and literature values (subscripts E and L, respectively).

Table 3.3 presents the experimentally determined diffusion coefficients or effective diffusion coefficients and Table 3.4 presents the diffusion coefficients for the caprate•HPB complexes. The experimentally determined diffusion coefficients of urea and mannitol were found to be in good agreement with literature values^{25,31-33} after correction for temperature and viscosity. D^{*-} , the diffusion coefficient of the A^- •HPB complex, was found by best-fitting all of the A^- •HPB in Table 3.3 to Eq 3.4. D^{*u} , the diffusion coefficient of the HA•HPB complex, was then calculated from the pH 3.0, 30

Table 3.3 Diffusion coefficients or effective diffusion coefficients (all at 30°C) for capric acid (HA), caprate ion (A⁻), mannitol, sucrose, and urea as a function of the hydroxypropyl-β-cyclodextrin (HPB) concentration (n≥3).

| System | pH | HPB conc. (mM) | Diffusion coefficient or effective diffusion coefficient (cm ² /s) |
|---------------------|-----|-------------------|--|
| Sucrose | 7.4 | 0 | 5.8(± 0.4)×10 ^{-6a,b} |
| Urea | 7.4 | 0 | 1.4(± 0.1)×10 ^{-5b} |
| Mannitol | 7.4 | 0 | 7.0(± 0.5)×10 ^{-6b} |
| Mannitol | 7.4 | 30 | 6.3(± 0.2)×10 ^{-6b} |
| Caprate ion | 7.4 | 0 | 6.7(± 0.5) ×10 ^{-6b} |
| Capric acid | 3.0 | 0 | 7.1(± 0.2) ×10 ^{-6b} |
| A ⁻ /HPB | 7.4 | 0.12 | 5.8(± 0.2) ×10 ^{-6c} |
| A ⁻ /HPB | 7.4 | 0.33 | 4.9(± 0.4)×10 ^{-6c} |
| A ⁻ /HPB | 7.4 | 1 | 3.6(± 0.4)×10 ^{-6c} |
| A ⁻ /HPB | 7.4 | 3 | 3.4(± 0.4)×10 ^{-6c} |
| A ⁻ /HPB | 7.4 | 10 | 3.3(± 0.4)×10 ^{-6c} |
| A ⁻ /HPB | 7.4 | 15 | 3.2(± 0.2)×10 ^{-6c} |
| A ⁻ /HPB | 7.4 | 30 | 3.0(± 0.2)×10 ^{-6c} |
| HA/HPB | 3.0 | 30 | 2.8(± 0.1)×10 ^{-6c} |

^a Taken from reference³² and corrected for viscosity.

^b Diffusion coefficient

^c Effective diffusion coefficient

Table 3.4 Diffusion coefficients of the complexes calculated from the effective coefficients.

| Species | pH | HPB conc. (mM) | Diffusion coefficient of the complex (cm^2/s) |
|---------------------------------|-----|----------------|---|
| $\text{A}^- \bullet \text{HPB}$ | 7.4 | 1 | $2.9(\pm 0.5) \times 10^{-6}$ |
| $\text{A}^- \bullet \text{HPB}$ | 7.4 | 3 | $3.0(\pm 0.6) \times 10^{-6}$ |
| $\text{A}^- \bullet \text{HPB}$ | 7.4 | 10 | $3.1(\pm 0.5) \times 10^{-6}$ |
| $\text{A}^- \bullet \text{HPB}$ | 7.4 | 15 | $3.1(\pm 0.3) \times 10^{-6}$ |
| $\text{A}^- \bullet \text{HPB}$ | 7.4 | 30 | $2.9(\pm 0.2) \times 10^{-6}$ |
| $\text{HA} \bullet \text{HPB}$ | 3.0 | 30 | $2.7(\pm 0.1) \times 10^{-6}$ |

mM HPB data (Table 3.3) and Eq 3.4. D^- and D^u differed by only a few percent. Likewise, D^{*-} and D^{*u} also differed by only a few percent. Therefore, in order to simplify the calculations involved in the theoretical analysis of the experimental capric acid transport data, a single diffusion coefficient was selected for each pair by averaging the two values such that $D^- \cong D^u = D^f$ and $D^{*-} \cong D^{*u} = D^*$ where D^f is the diffusion coefficient for both the free capric acid species and the caprate ion species, and D^* is the diffusion coefficient for both of the complex species. Hence only D^f and D^* are given in Table 3.1. Therefore, for the present system Eq 3.4 reduces to

$$D^{\text{eff}} = D^f F^f + D^* F^* \quad (3.24)$$

where F^f and F^* are the sum of the fractions of the two free caprate species and that of the two complexes, respectively.

Because the viscosity of the buffer solution increased with increasing HPB concentration (up to ~15% at 30 mM HPB, see Fig 3.2), the dependency of the individual diffusion coefficients upon the HPB concentration was considered. D for mannitol decreased by around 10% in the presence of 30 mM HPB, which is consistent with the viscosity increase at 30 mM but which is also within the data scatter. Within the data scatter (mostly 5 to 15%), the diffusivity of $A^- \bullet \text{HPB}$, was found to be relatively constant with respect to the HPB concentration (Table 3.4) and the diffusivity of $\text{HA} \bullet \text{HPB}$, at 30 mM was essentially the same as that of $A^- \bullet \text{HPB}$. The constancy of the diffusivity of the $A^- \bullet \text{HPB}$ complex over the HPB concentration range supports the one-to-one assumption

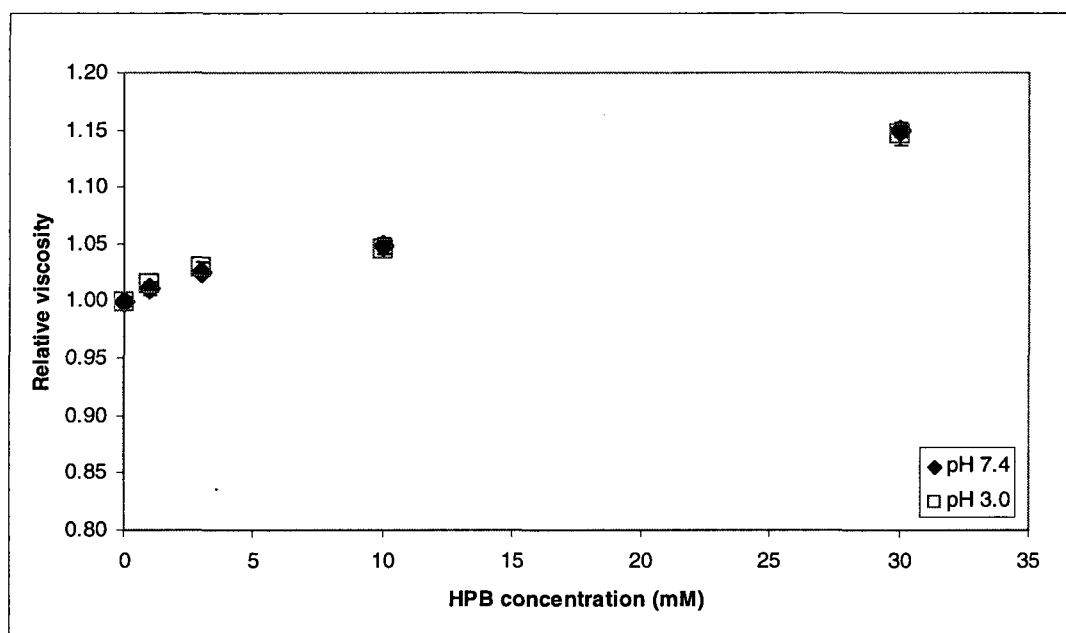


Fig 3.2 Relative buffer viscosity as a function of the hydroxypropyl- β -cyclodextrin (HPB) concentration of pH 3.0 and 7.4 buffer solutions.

for the stoichiometry of the complex. In any case, we are able to consider D^* to be independent of HPB concentration in the model calculations.

3.5.1.4 The determination of P_i and $h_{ABL,SM}$ from experiments

with the silicone polymer membrane alone (SM) case

P_i and $h_{ABL,SM}$ were determined simultaneously from a procedure involving best-fitting Eq 3.25 to a set of selected capric acid transport data (i.e., the P_T values) obtained with the silicone polymer membrane alone (SM) case over a range of pH and in the absence of HPB (see Fig 3.3).

$$P_T = \frac{P_{ABL,SM}}{1 + \frac{P_{ABL,SM}}{P_i F^u}} = \frac{D^f}{h_{ABL,SM} + \frac{D^f}{P_i F^u}} \quad (3.25)$$

where $P_{ABL,SM}$ is the aqueous boundary layer permeability coefficient for the capric acid molecule or that for the free caprate ion. Eq 3.25 comes from Eq 3.13: it follows from Eqs 3.4 and 3.5, when HPB is absent in the system, $P_{ABL}^{eff} = P_{ABL,SM}$ and

$P_{ABL,SM} = \frac{D^f}{h_{ABL,SM}}$, where $D^f = 6.9 \times 10^{-6} \text{ cm}^2/\text{s}$ (see Table 3.1), and F^u is only a function of

the pK_a (4.53) and pH (see Section 3.8, Appendix B). The best-fit curve is in good agreement with the experimental results over the entire pH range with less than 5% deviation and yielded a $h_{ABL,SM}$ value of 0.012 cm and a P_i value of 0.018 cm/s . Experimental variability was greatest in the low pH region ($pH > pK_a$) where transport of the lipophilic capric acid was expected to be most sensitive to variations in the hydrodynamics of the diffusion cell system. The capric acid transport kinetics was 95-

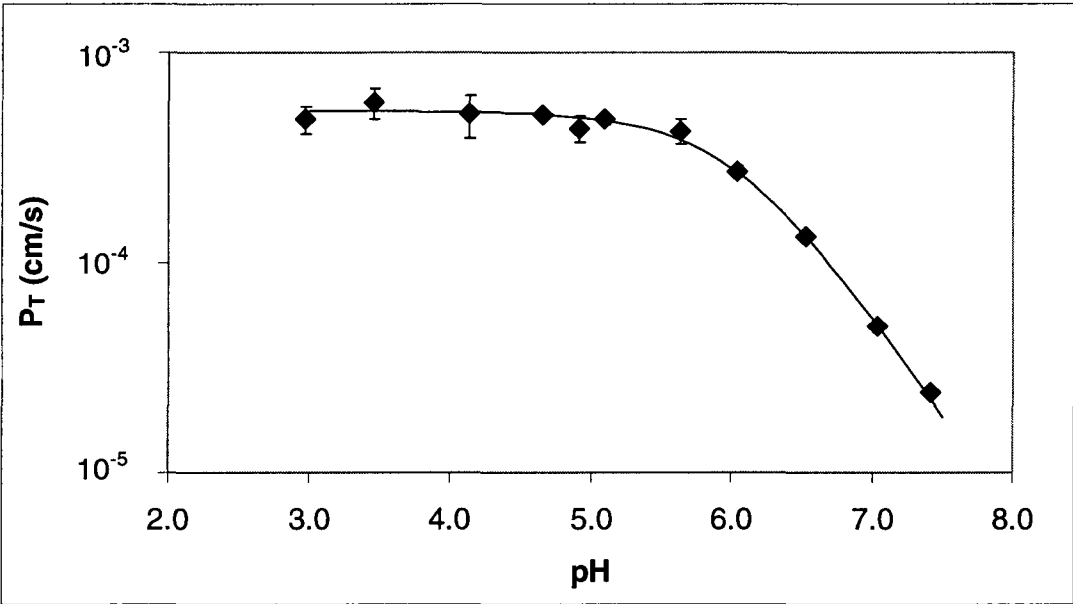


Fig 3.3 Total permeability coefficient (P_T) for capric acid transport across the silicone polymer membrane as a function of pH. Eq 3.25 with an input pK_a value of 4.53 and a D^f value of $6.9 \times 10^{-6} \text{ cm}^2/\text{s}$ was best-fitted to the experimental data (\blacklozenge). The best-fit procedure simultaneously yielded a best $h_{ABL,SM}$ value of 0.012 cm and a best P_i value of 0.018 cm/s).

97% ABL-controlled over the pH range of 3.0 to 5.5 and then markedly became increasingly membrane controlled with increasing pH. At pH 7.5, it was 97% membrane-controlled. The good fit of the data, particularly in the high pH region, is also direct evidence that caprate ion transport across the silicone polymer membrane was negligible, and that therefore P_i accurately represented the transport of the neutral capric acid molecule across the silicone polymer membrane in the present system.

3.5.1.5 Six Millipore membrane (MM) transport

Table 3.5 shows P_T values for the transport of capric acid and mannitol across an assembly of six Millipore membranes in the presence and absence of 30 mM HPB at pH 3.0 and 7.4. These transport experiments were performed to provide an independent estimate of the effective ABL thickness that the six Millipore membranes would provide as a surrogate ABL in the SM-MM experiments. The P_T ratio for free capric acid to the HA•HPB complex was determined at pH 3.0 and 7.4 and compared to the same ratio as determined in the fritted disk diffusion coefficient studies. These ratios were consistent, which confirmed the absence of any significant diffusional pore hindrances (i.e., a hindrance factor of unity) for the transport of capric acid or the complex across the Millipore filters. Transport for all molecules was independent of pH within the scatter of the data which ruled out any pH specific effects. Because mannitol and capric acid had a similar molecular weight (180 and 172 Da, respectively), the total permeability coefficients (P_T) for these molecules were compared at high and low pH. The similarity of the P_T values of the two molecules ruled out lipophilicity dependent anomalies. The transport of mannitol in the presence and absence of 30 mM HPB was compared to rule

Table 3.5 Total permeability coefficient (P_T) for transport of mannitol and of caprate species across six Millipore membranes in the presence and absence of 30 mM hydroxypropyl- β -cyclodextrin (HPB) at pH 3.0 and 7.4. ($n \geq 3$)

| Species | pH | HPB concentration (mM) | P_T (cm/s) |
|----------|-----|------------------------|--------------------------------|
| Mannitol | 7.4 | 0 | $2.5(\pm 0.36) \times 10^{-5}$ |
| Mannitol | 7.4 | 30 | $2.3(\pm 0.27) \times 10^{-5}$ |
| Mannitol | 3.0 | 0 | $2.5(\pm 0.22) \times 10^{-5}$ |
| Mannitol | 3.0 | 30 | $2.6(\pm 0.15) \times 10^{-5}$ |
| Caprate | 7.4 | 0 | $2.0(\pm 0.21) \times 10^{-5}$ |
| Caprate | 7.4 | 30 | $8.5(\pm 0.94) \times 10^{-6}$ |
| Caprate | 3.0 | 0 | $2.3(\pm 0.51) \times 10^{-5}$ |
| Caprate | 3.0 | 30 | $1.0(\pm 0.07) \times 10^{-5}$ |

out any viscosity or HPB concentration-dependent anomalies, and the results were found to be consistent with the results of the fritted disk diffusivity experiments. Therefore, the six Millipore system was determined to be an acceptable surrogate ABL for the study of capric acid transport across the silicone polymer membrane in the presence of HPB.

As an aside, a theoretical, surrogate ABL thickness of a six Millipore membrane assembly ($h_{MM,theo}$) was calculated from

$$h_{MM,theo} = \frac{h}{\epsilon} \quad (3.26)$$

where the actual thickness of six Millipore membranes (h) of 0.075 cm was determined using a micrometer and a porosity (ϵ) of 0.7 and a pore diameter of 0.22 μm were obtained from the manufacturer. Based on Eq 3.26 the $h_{MM,theo}$ was found to be 0.11 cm. The experimentally determined surrogate ABL thickness for the six Millipore membrane assembly, h_{MM} , was obtained from the results of the mannitol transport experiments (Table 3.5) using

$$h_{MM} = D_{\text{Mannitol}} \left(\frac{1}{P_{T,MM}} - \frac{1}{2P_{ABL,SM}} \right) \quad (3.27)$$

Here $P_{T,MM}$ is the experimentally determined mannitol permeability coefficient for

the six Millipore membrane assembly (Table 3.5) and $P_{ABL,SM} = \frac{D_{\text{mannitol}}}{h_{ABL,SM}}$ where D_{mannitol}

is the mannitol aqueous diffusion coefficient (Table 3.3) and $h_{ABL,SM} = 0.012$ cm is the ABL thickness for the system, previously defined (Table 3.1). The calculation with Eq

3.27 gives $h_{MM}=0.27 (\pm 0.04)$ cm. Independent of the calculation based on Eq 3.27, a value for $h_{MM}=$ of $0.23 (\pm 0.03)$ cm was obtained from the model best-fitting of capric acid transport data obtained in the silicone membrane plus six Millipore membrane (SM-MM) system discussed in Section 3.5.2. Differences between the theoretical, surrogate ABL thickness of $h_{MM,theo} = 0.11$ cm based on Eq 3.26 and the experimentally deduced h_{MM} values are likely caused by several factors including Millipore membrane effective tortuosity values greater than unity and/or effective porosity values less than 0.7. The relatively small difference between the h_{MM} values determined by the six Millipore alone experiments and Eq 3.27 and those based on the best-fit values to the silicone plus six Millipore membrane transport of the SM-MM experiments are within experimental error. In the model calculations, the value of $h_{MM}=0.23$ cm has been employed.

3.5.2 Capric acid transport experiments with the silicone membrane plus six Millipore membranes (SM-MM) system

Fig 3.4 shows a family of log-log plots of capric acid P_T versus HPB concentration ranging from 0-30 mM as a function of pH from 5.0-7.4 wherein the initial capric acid concentration, C_T , is comprised of 0.05 mM (cold) and 0.004 mM (radiolabeled). Generally, P_T decreases nonlinearly with increasing HPB concentration within each pH situation. It is observed that, using the parameter values in Table 3.1 and Eq 3.13, the model-predicted P_T values agree remarkably well with the experimental results over the entire range of the experimental conditions, as indicated by the solid curves. This underscores the validity of the physical model and the systematic approach to the conduct of independent studies to determine key transport and thermodynamic

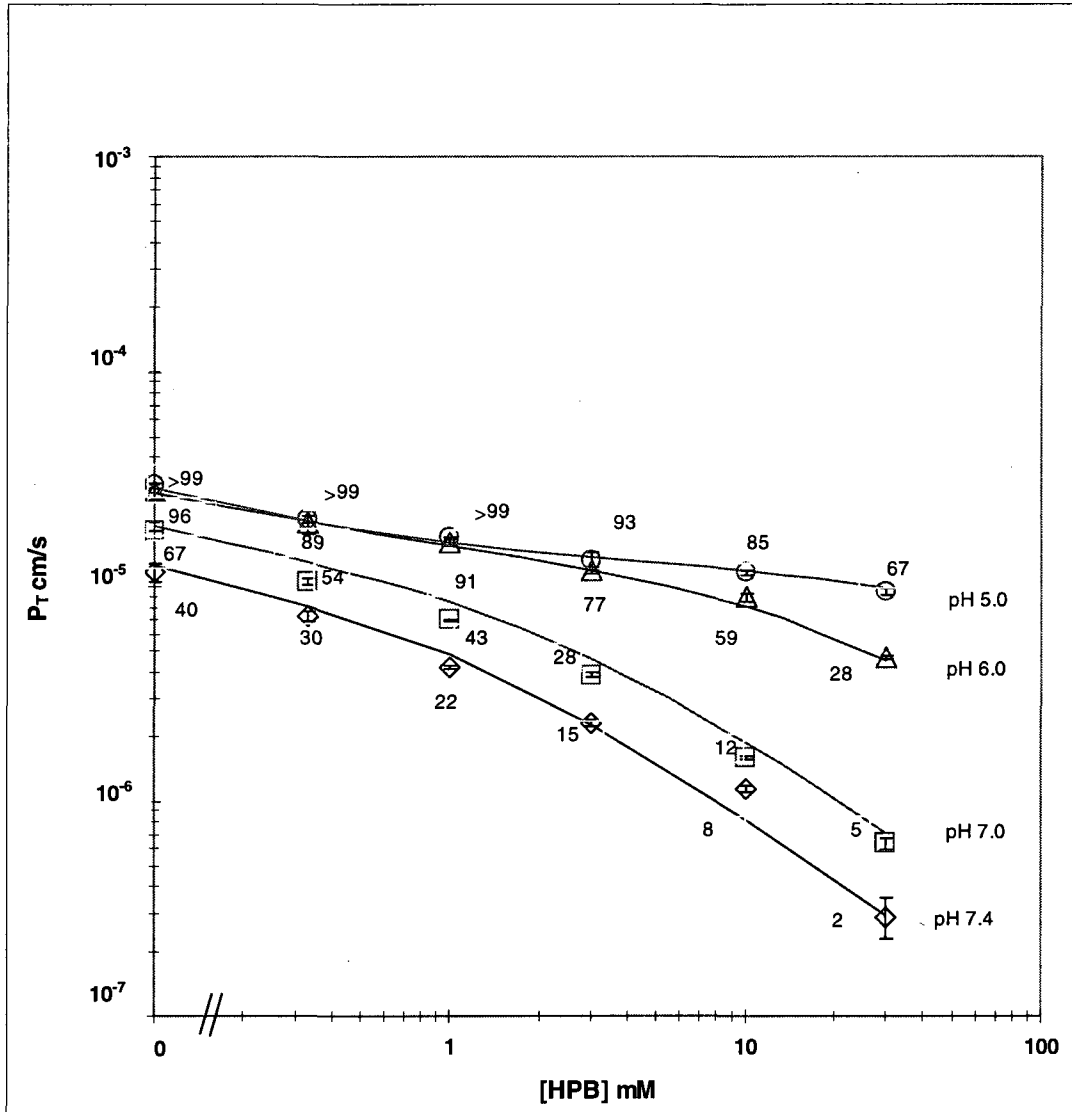


Fig 3.4 Total permeability coefficient (P_T) for capric acid transport across the silicone membrane plus six Millipore filter (SM-MM) situation as a function of pH and hydroxypropyl- β -cyclodextrin (HPB) concentration. The solid curves represent the model-predicted values. The numbers represent the percent aqueous boundary layer (ABL) controlled transport.

parameters. The transport behavior of capric acid is attributed the multivariable interrelationships of the transport parameters (i.e., diffusion coefficients, intrinsic membrane permeability coefficient, effective aqueous boundary layer thickness) and the thermodynamic parameters (i.e., pH, pK_a , partition coefficient, complexation equilibria, and species concentration) within the context of the transport barrier of the donor-side ABL and the silicone polymer membrane in series. Here, the governing diffusional resistance of the donor side effective ABL is due to the highly porous six Millipore membrane assembly for which the surrogate h_{ABL} is 0.23 cm. Any contribution to the donor side diffusional resistance from the stirring-dependent, actual ABL of ~ 0.012 cm is negligible. The receiver side ABL is effectively “short-circuited” by the pH 9.5 buffer condition.

Focusing first on the pH 5.0 results (Fig 3.4), P_T is 3.0×10^{-5} cm/s in the absence of HPB in which case the passage of capric acid across the composite membrane system is essentially 100% effective ABL-controlled, i.e., by the six Millipore membrane assembly portion of the composite membrane. In the presence of HPB at 0.33 mM and 1.0 mM, the P_T value has decreased to 2.1×10^{-5} cm/s and 1.7×10^{-5} cm/s, respectively. It can be noted, however, that in both instances the transport kinetics was still $\sim 100\%$ effective ABL controlled. When the HPB concentration was increased to 30 mM, P_T decreased further to 9.5×10^{-6} cm/s and now the transport kinetics was 67% ABL-controlled and 33% silicone membrane-controlled. This behavior is the result of the following interrelationships. From a thermodynamic point of view, as the $[HPB]/C_T$ ratio in the donor chamber increases, the free caprate fractions (capric acid molecule and the caprate

ion) decreases nonlinearly while the complementary fractions of caprate-HPB complexes increases nonlinearly. Since the effective aqueous diffusion coefficient is a sum of species-weighted diffusion coefficients (Eq 3.4), the permeability coefficient of the effective ABL ($P_{ABL}=P_{ABL,SM-MM}$) decreases nonlinearly with increasing HPB concentration, reaching a limiting value dictated by Eq 3.5 and the aqueous diffusivities of the HA•HPB complexes. At pH = 5.0, this limiting value for D^{eff} is essentially attained at [HPB] ~10 mM. In addition to this, since only the free, lipophilic unionized species (HA) may partition at the aqueous-silicone membrane interface, the effective silicone membrane permeability coefficient, P_m (see Eq 3.8), concomitantly also decreases nonlinearly with increasing (HPB) concentration. The consequence of both of these two factors is that the relative magnitudes of $P_{ABL,SM-MM}$ and P_m will determine the extent to which the overall passive permeation processes described in P_T is ABL- and/or silicone membrane-controlled (Eq 3.13).

In the case of pH 7.4 and comparing it to the pH 5.0 case, the displacement of P_T to smaller values at each HPB concentration is largely influenced by the interplay of pH/pK_a, the predominance of free caprate ion (A^-) and $A^-•HPB$ fractions, and the restriction that only free capric acid molecule (HA) may permeate the silicone membrane. Hence, it is observed that the overall transport kinetics is less ABL controlled in the absence of HPB and becomes more membrane-controlled with increasing HPB concentration.

3.5.3 Transport experiments with silicone membrane alone (SM)

The transport experiments of capric acid with SM in the presence of HPB was to show the effects of HPB on capric acid transport when the ABL is thin (0.012 cm) compared to the previously discussed (SM-MM) thick (0.23 cm) ABL case. This SM case may be regarded as typical of single silicone membrane transport situation with conventional hydrodynamic conditions (stirred aqueous compartments). The experiments were conducted under the same solution conditions as in the SM-MM case, and the results are presented in Fig 3.5. As with the SM-MM case, the model predicted P_T for capric acid transport across SM agree quite well over the entire ranges of pH and HPB concentrations and covers, for the most part, the 100 percent ABL-controlled to the 100 percent membrane-controlled range. The capric acid transport behavior in the SM case (Fig 3.5) is seen to differ from the SM-MM case (Fig 3.4) as follows. Because of the much thinner ABL (0.012 cm vs. 0.23 cm) in the case of SM, capric acid transport is more membrane-controlled (rather than ABL-controlled) over a wider range of conditions relative to the SM-MM case (Fig 3.4). Thus, convergence to ABL-controlled transport in the absence of HPB occurs at lower pH, i.e., around pH 4 to 5 in the SM case, instead of around pH of 6 to 7 as seen in the case of the SM-MM. For the same reason, the dependence of capric acid transport upon the HPB concentration at constant pH is steep over the entire HPB concentration range for the high pH situations (\sim pH 7.0) in Fig 3.5 (SM case) but not as much in Fig 3.4 (SM-MM case). This is because, in the latter case, the capric acid transport is already substantially ABL-controlled at zero or low HPB concentrations even at pH 7.0 and becomes predominantly membrane-controlled only at the high HPB concentrations. It should be noted that, in the comparison of the physical

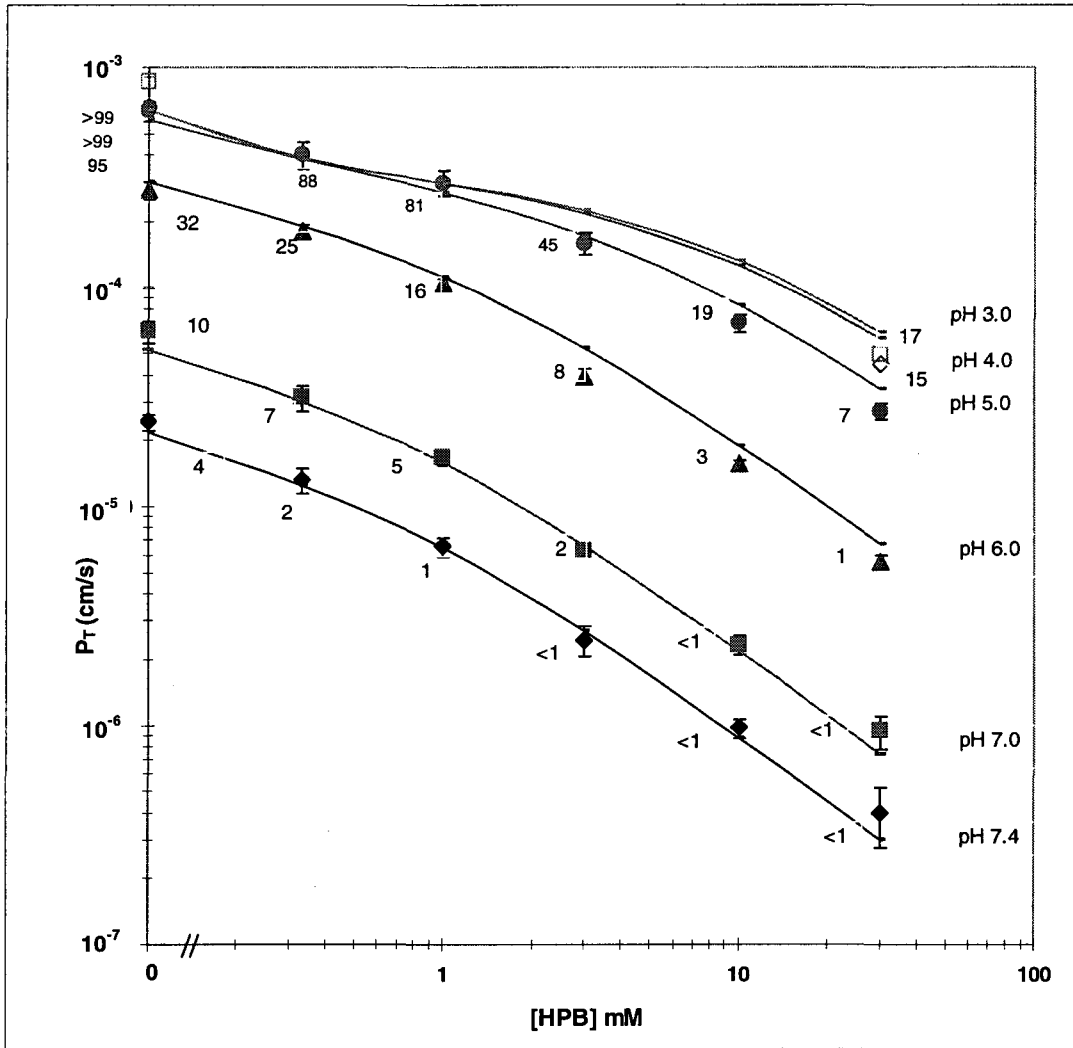


Fig 3.5 Total permeability coefficient (P_T) for capric acid transport across the silicone membrane alone (SM) as a function of pH and hydroxypropyl- β -cyclodextrin (HPB) concentration. The solid lines represent the model-predicted values. The numbers are the percent aqueous boundary layer (ABL) controlled.

model predictions with the experimental data, the SM case is more sensitive than the SM-MM case to more of the parameters in Table 3.1 over the range of conditions investigated. This is because of the greater influence of the ABL in the case of SM-MM. This does raise the question of how well the physical model would have been tested if we had experimental data only from the SM-MM case. The membrane-controlled conditions are particularly sensitive to the pK_a , P_i , and K^- , while the ABL-controlled conditions are primarily sensitive to the diffusion coefficients and both K^- and K^+ . The good agreement between physical model predictions and the experimental data employing both the SM and the SM-MM cases is therefore strong evidence for the validity of the physical model and that of the input parameters (Table 3.1) used in the calculations.

3.5.4 Radiochemical impurity corrections for capric acid transport and for the transport parameter values

At the beginning of the present research, the stock [^{14}C]capric acid was checked for radiochemical purity by HPLC fraction collection with 98-100% of the DPM recovered in the capric acid peak (retention time of 11 min). This was in agreement with manufacturer's claims ($\geq 97\%$). Initial silicone membrane alone (SM) [^{14}C]capric acid transport experiments however suggested, in some cases, a higher percentage of radiochemical impurity(ies) in the receiver chamber than expected, especially at high pH and high HPB concentration. Therefore a special set of high concentration (14 $\mu\text{Ci/ml}$) [^{14}C]capric acid transport experiments were conducted with the aim to more quantitatively assess the impurity problem. The results of these experiments allowed for the determination of the initial concentration of the impurity and the impurity

permeability coefficient. This information allowed us to make corrections for the effect of the impurity upon the capric acid fluxes, and these corrections have been incorporated in the results presented in Figs 3.3, 3.4, and 3.5. Corrections were also estimated for those transport parameters affected by the impurity and in all cases these were within experimental error. The details of the impurity study are presented in Appendix A.

3.6 Discussion

In light of the results demonstrated by Fig 3.4 and Fig 3.5, we may now discuss a scenario of how the presence of a cyclodextrin such as HPB in a formulation may improve the bioavailability of a drug.

3.6.1 Flux of drug X across SM-MM at unit thermodynamic activity (saturated solutions)

Let us discuss the potential implications of the results of the SM-MM studies of capric acid transport as it may apply to a typical aqueous-based drug formulation problem involving a hypothetical weak acid drug, X, having the same parameter values as those of the capric acid-silicone polymer membrane system (Table 3.1). The saturated solution of crystals of X in any formulation will possess a thermodynamic activity, $a=1$. Therefore, excluding supersaturated solutions from consideration, any pharmaceutical solution formulation of drug X at $a=1.0$ would be that possessing the potential for providing the maximum flux, J_{\max} , across the membrane system. We may now define $R_{J,\max}$ as the ratio of J_{\max} ($=J_{\max,f}$) of a test HPB formulation of drug X to J_{\max} ($=J_{\max,o}$) of the saturated solution of X in essentially pure water at low pH (i.e., $\text{pH} \ll 4.53$). $R_{J,\max}$ should then be a measure of the transport flux enhancement for any HPB formulation of drug X at

saturation relative to the saturated solution of X in water at low pH where only the unionized species of X is present in solution. From Eqs 3.1, 3.4, 3.5, and 3.12 and using the same terminology and symbols for the drug X/HPB system as for the capric acid/HPB system, we may write

$$J_{\max,o} = C_{\text{sat so ln}}^u \left(\frac{1}{\frac{h_{\text{ABL}}}{D^u} + \frac{1}{P_i}} \right) \quad (3.28)$$

And

$$J_{\max,f} = C_{\text{sat so ln}}^u \left(\frac{1}{F^u} \right) \left(\frac{1}{\frac{h_{\text{ABL}}}{D^{\text{eff}}} + \frac{1}{P_i F^u}} \right) \quad (3.29)$$

Therefore,

$$R_{J,\max} = \frac{J_{\max,f}}{J_{\max,o}} = \frac{\left(\frac{h_{\text{ABL}}}{D^u} + \frac{1}{P_i} \right)}{\frac{h_{\text{ABL}}}{D^{\text{eff}}} + \frac{1}{P_i F^u}} \quad (3.30)$$

Here $C_{\text{sat so ln}}^u$ is the concentration of the saturated solution of X in pure water at low pH ($\text{pH} \ll \text{pK}_a$), $h_{\text{ABL}} = h_{\text{ABL,SM-MM}}$ (Table 3.1), and all other terms have been previously defined.

Fig 3.6 presents plots of $R_{J,\max}$ versus HPB concentration at different pH of the hypothetical formulations. Several outcomes of interest relative to formulation performance now become clear that were not easily discernable from Fig 3.4, and the interplay of pH, HPB concentration, h_{ABL} , and P_i becomes more apparent. With respect to the addition of HPB, it can be seen in Fig 3.6 that the greatest influence of HPB upon the X flux enhancement takes place at the lowest pH (i.e., $\text{pH} \ll 4.53$) with the 30 mM case increasing the flux by around 30-fold over the formulation of X alone. The least increased X flux enhancement from the addition of HPB occurs with the pH 7.4 case, with the 30 mM case increasing the X flux by less than 2-fold over the X alone formulation at pH 7.4. It can also be seen from Fig 3.6 that, at $a=1$, the X flux increases with increasing pH for a given HPB concentration. This demonstrates that the X anion may have an effect similar to that of the $\text{X}\cdot\text{HPB}$ and the $\text{X}^-\cdot\text{HPB}$ complexes, i.e., to act as a carrier for X across the ABL (but it must be remembered that the formulation is assumed to possess high buffer capacity in the present calculations). From the mechanistic standpoint, in the steady-state transport of the unionized and the ionized X species across the ABL with adequate buffer capacity in the aqueous phase to preclude any significant pH gradients in the ABL, the ratio of the ionized to unionized drug species increases with increasing pH and therefore the ratio of the fluxes of the two species increases; and, because at $a=1$ the unionized concentration of X is constant in the donor chamber solution, the total flux of X may also increase as long as the overall transport of X is sufficiently ABL controlled. It is interesting to note that, while in going from 0 HPB to 30 mM HPB, the percent increase in $R_{J,\max}$ is greatest for the lowest pH and the least for the highest pH, the $R_{J,\max}$ value at 30 mM HPB at the highest pH is still

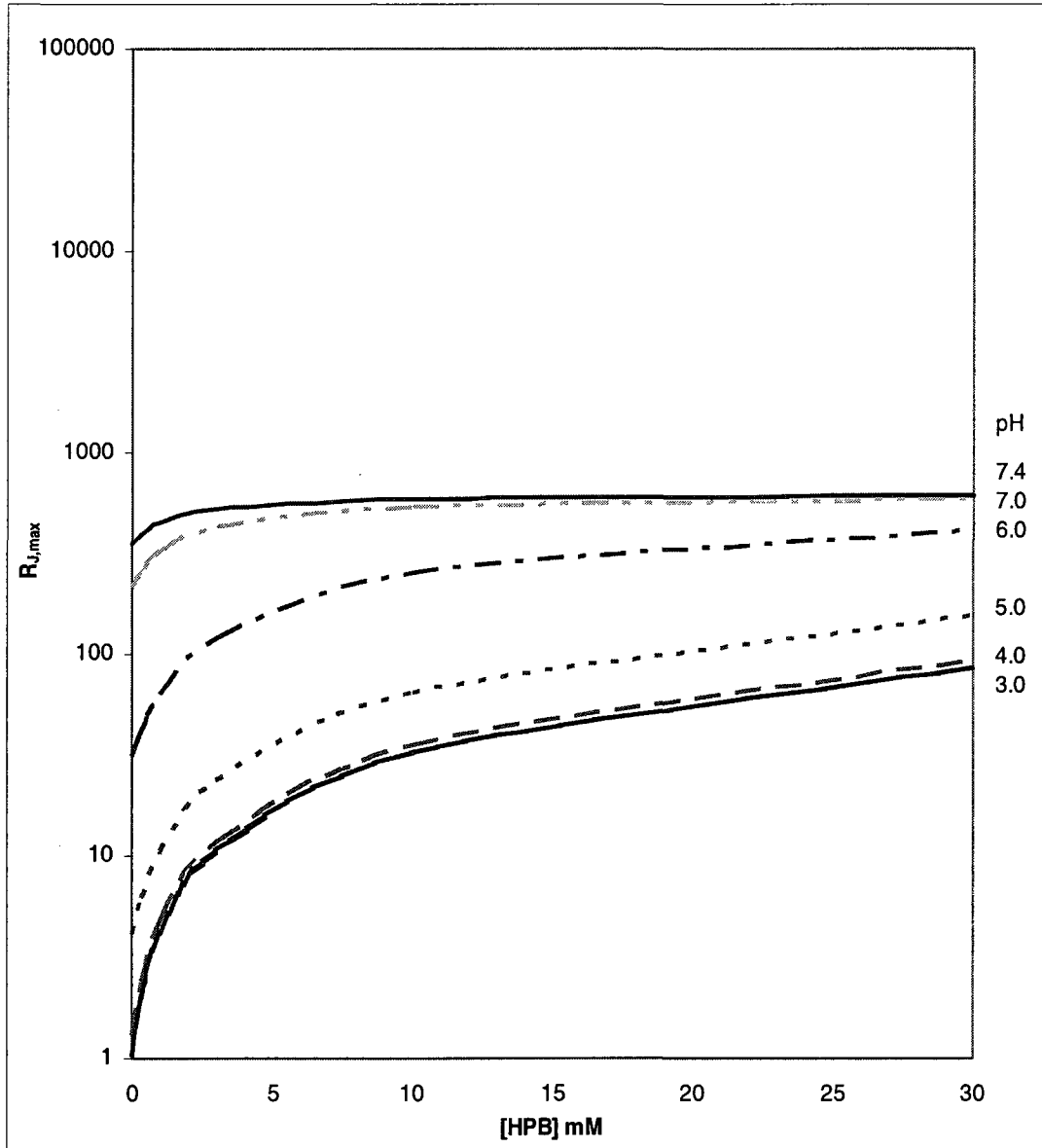


Fig 3.6 The influences of the HPB concentration and pH upon the flux enhancement factor, $R_{J,max}$, for saturated solutions of drug X across the silicone membrane plus six Millipore membrane filters (SM-MM).

considerably greater than for 30 mM HPB at the lowest pH. This points out that pH can be more important than the HPB concentration in enhancing the flux for the drug X system with the Table 3.1 parameters.

Even though only the free, unionized X molecule can traverse the silicone membrane, all four of the X species can traverse the ABL. Therefore, the complexes and the X anion species can help increase the X flux across the system, but only to the extent that it can effectively reduce the transport resistance of the ABL. There would be no further benefit of increasing the carrier concentration when X transport becomes essentially membrane-controlled. This can be seen by the plateau in Fig 3.6 at the two highest pHs. A carrier cannot increase the X flux beyond this point because this value represents membrane-controlled transport limit.

3.6.2 Flux of drug X across the rat ileum

at unit thermodynamic activity

It should now be instructive to apply the above results in examining flux enhancement of drug X in the scenario of in situ drug absorption studies of the rat ileum. For the physical model calculations of drug X transport in the rat ileum, all of the parameters of Table 3.1 would apply except for the intrinsic permeability coefficient (P_i) and the aqueous boundary layer thickness (h_{ABL}). For the rat ileum calculations, we may employ $P_i = 3.5$ cm/s and $h_{ABL} = h_{ABL,ileum} = 0.117$ cm; both of these parameter values are taken from the results of a study of the influence of HPB on capric acid absorption in the rat ileum (Table 4.6 in Chapter 4).

Fig 3.7 presents plots of $R_{J,max}$ vs. HPB concentration at various pH conditions for the rat ileum case. In comparing Fig 3.7 to Fig 3.6, we note a number of points of interest. At low pH ($pH \ll 4.53$) at which only the free unionized drug X and the X•HPB complex species should exist, the plots in the two figures converge to a common limiting curve. This is because transport across the silicone membrane and the rat ileum is essentially 100% ABL-controlled throughout the HPB concentration range and consequently, the ABL thickness in each case cancels out in the calculation of $R_{J,max}$. At high pH, there are significant differences between the Fig 3.7 and Fig 3.6. In Fig 3.6, as noted already, the curves at high pH exhibit little dependence upon HPB concentration and essentially converge to a constant plateau as a function of pH at around pH 7.4. In contrast to this behavior, the curves at pH 7.4 in Fig 3.7 continue an upward displacement with increasing pH and continue to exhibit a moderate-to-strong HPB concentration dependence everywhere. On the latter point, at pH 7.4 in going from zero HPB to 30 mM HPB, the $R_{J,max}$ value increases by a factor of around 30 in the case of the rat ileum while, as noted earlier in the case of SM-MM, this increase was less than a factor of two. These differences between Fig 3.6 and Fig 3.7 are largely the result of the much larger P_i for the rat ileum (i.e., 3.5 cm/s for the rat ileum vs. 0.018 cm/s for the silicone polymer membrane) and of the quantitative interplay between the respective effective permeability coefficient, P_{ABL}^{eff} , and F^u . The above comparison between the SM-MM results (Fig 3.6) and the rat ileum results (Fig 3.7) points to the potential value of the physical model approach in formulation development of highly lipophilic, low solubility drug molecules in oral delivery. To have had only the experimental silicone membrane transport data for drug X and some intuitive judgment to assess the potential of HPB as a drug carrier could

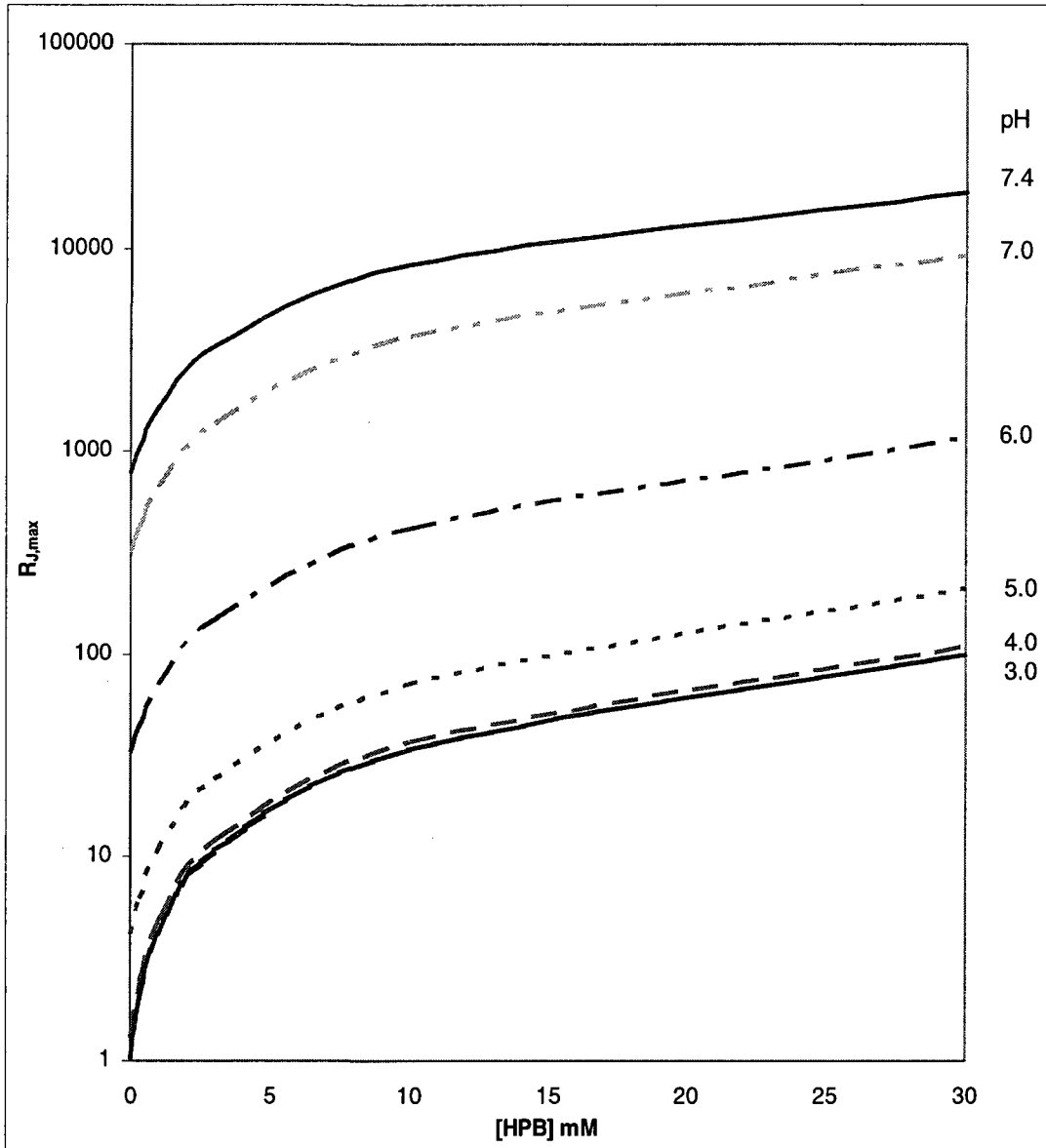


Fig 3.7 The influences of the HPB concentration and pH upon the flux enhancement factor, $R_{J,max}$, for saturated solutions of drug X transport across the rat ileum.

have led to the erroneous conclusion that there would be little or no favorable effect of HPB, in vivo, to enhance absorption of drug X. The physical model approach may thus provide the framework for the measurements of key parameters and their quantitative relationships which could then be applied judiciously to predicting in vivo situations.

3.7 Appendix A. Radiochemical Impurity Corrections **for Capric Acid Transport Parameter Values**

An initial set of transport experiments was carried out with a high concentration (14 $\mu\text{Ci/ml}$) of [^{14}C]capric acid in the donor chamber, and the amount of the impurity transported into the receiver chamber at 100 minutes determined. The conditions of the experiments otherwise were as described in Section 3.4.2.5. The results are presented in Fig 3.8. Importantly, the impurity fluxes (data not shown), when normalized for the total DPM in the donor chamber solution, were found to be essentially the same in all of the experiments. This immediately indicated that the thermodynamic activity of the transported impurity species in the donor chamber was independent of both the pH and the HPB concentration. Based upon this information, the following experiment was conducted.

A silicone membrane alone transport experiment with an initial donor solution of 14 $\mu\text{Ci/ml}$ [^{14}C]caprate plus 30 mM HPB at pH 7.4 was run for 1500 minutes with complete replacement of the receiver chamber solution at 100 minute intervals, and each of these receiver chamber solutions was analyzed for the total amount of the impurity. The initial impurity concentration (DPM/ml) in the donor chamber, $C_{\text{imp,init}}$, was calculated using the following mass balance equation:

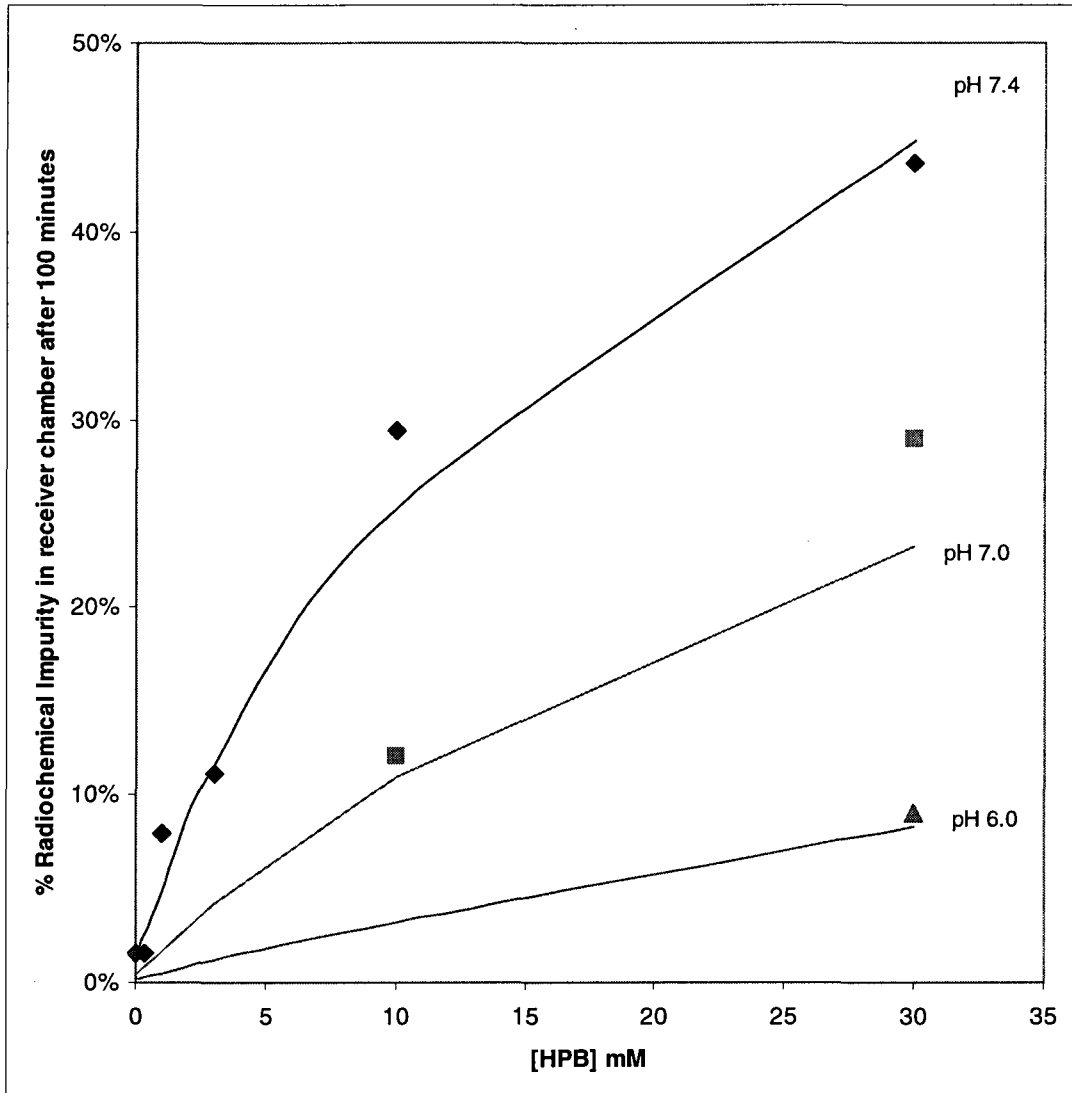


Fig 3.8 Experimental and predicted percent radiochemical impurity in the receiver chamber after 100 minutes. The percent radiochemical impurity in the receiver chamber at 100 minutes during [^{14}C]capric acid transport across the silicone membrane alone under various pH and HPB concentration conditions (symbols). The curves are the predicted values based upon a model analysis of the impurity issue.

$$C_{\text{imp,init}} = \frac{1}{V_D} \left(\frac{\sum A_{\text{imp,tot}}}{1 - \frac{A_{\text{imp,1500}}}{A_{\text{imp,100}}}} \right) \quad (3.31)$$

Here $\sum A_{\text{imp,tot}}$ is the total cumulative amount of the impurity transported into the receiver chamber over the 1500 minute run; $A_{\text{imp,100}}$ is the amount of impurity (DPM) found in the 0-100 minute receiver solution; $A_{\text{imp,1500}}$ is the amount of impurity (DPM) found in the 1400-1500 minute receiver solution; $V_D = 2.0$ ml is the volume of the donor solution. Then, the percent radiochemical impurity in the stock [^{14}C]capric acid solution may be calculated from

$$\% \text{ impurity} = \frac{C_{\text{imp,init}}}{C_{\text{DPM,tot}}} \quad (3.32)$$

where $C_{\text{DPM, tot}}$ is the total initial radioactivity concentration (DPM/ml) in the donor chamber. Eq 3.31 has assumed that the impurity transport is a first order process. Using Eqs 3.31 and 3.32, the stock [^{14}C]capric acid solution was determined to have a 0.64% impurity which was in agreement with the manufacturer's claims. However, when the fraction of the free capric acid species available for transport is very small (i.e., $F^U \ll 1$), this small amount of impurity in the stock [^{14}C]capric acid solution is responsible for a significantly high percentage of the radiochemical flux. Fig 3.8 shows the experimental and predicted percent impurity in the receiver chamber after 100 minutes for several capric acid transport conditions. The predicted values were based on the experimental permeability coefficient of the radiochemical impurity, P_{imp} ,

$$P_{\text{imp}} = \frac{J_{\text{imp}}}{C_{\text{imp}}} \quad (3.33)$$

where J_{imp} is the experimental impurity flux and C_{imp} is the impurity concentration in the donor chamber. As noted earlier, $J_{\text{imp}}/C_{\text{imp}}$ was found to be constant in all experiments, corresponding to $P_{\text{imp}}=4.6 \times 10^{-5}$ cm/s. The constancy of the P_{imp} value importantly verified that the thermodynamic activity of the impurity was insensitive to pH and the HPB concentration over the range of conditions studied. This outcome allowed for the direct prediction of the theoretical values in Fig 3.7 using Eq 3.33. The P_{imp} value has also permitted impurity corrections to be applied to the experimental data presented in Figs 3.4 and 3.5. These figures can be compared with Figs. 3.9 and 3.10, in which the experimental data and the model-predicted curves are based on the uncorrected P_T data. The corrections were important only at high pH and high HPB concentrations. Where they were important, they generally improved the fit of the experimental data to the model predictions.

In addition to the impurity correction of P_T values for capric acid transport across the silicone polymer membrane, the impact of the impurity upon the determination of the capric acid pK_a and the caprate/HPB binding constants K^u and K^- was also assessed. The capric acid pK_a was experimentally determined from capric acid partitioning between the silicone polymer membrane and the aqueous phase. The maximum possible errors arising from the impurity(ies) in the partition coefficient experiments can be assessed by examining the two extreme cases: none or all of the impurity partitions into the silicone polymer. In the case where none of the impurity partitions into the silicone phase, the capric acid concentration in the silicone ($C_{s,p}$) will be correct and the aqueous

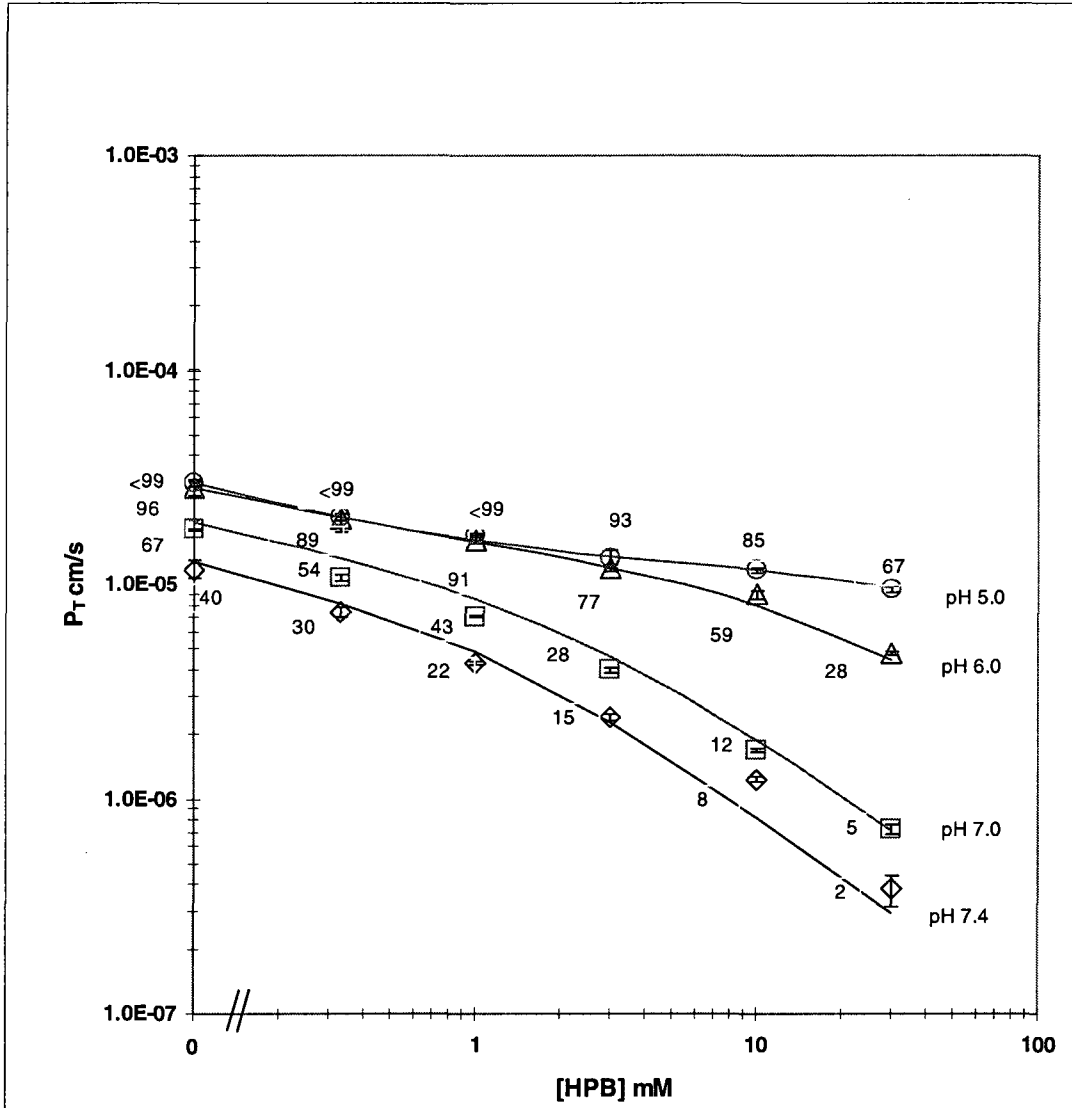


Fig 3.9 The results presented here (both the experimental and the model-predicted values) are the same as those of Fig 3.4 except the corrections for the impurity fluxes were not made.

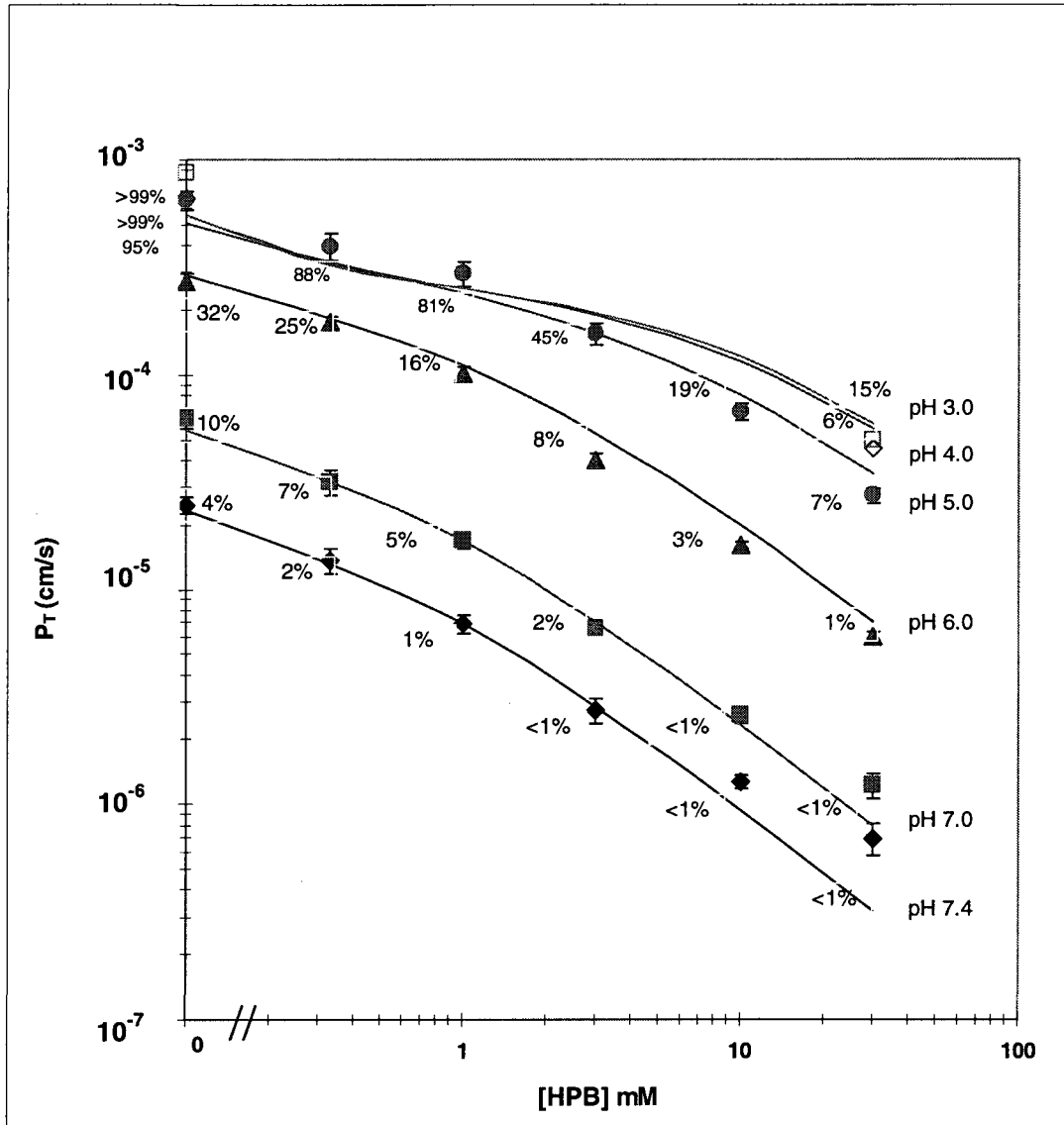


Fig 3.10 The results presented here (both the experimental and the model-predicted values) are the same as those of Fig 3.5 except the corrections for the impurity fluxes were not made.

concentration (C_{aq}) will have maximum error (see Eq 3.14). Recall that the initial concentration of impurity was 0.64%; however, as capric acid partitions into silicone, the impurity is left behind, and the fraction of the impurity in the aqueous phase is increased. This situation will be most extreme for the low pH case (i.e., pH 3.5) where the partitioning of capric acid into the silicone phase is greatest (i.e., the highest $k_{p,app}$, see Fig 3.1). For this case, the aqueous concentration of the total radioactivity (DPM/ml) at equilibrium would have been reduced to 57% of its initial concentration while the concentration of the impurity in the aqueous phase would have remained unchanged. This would have increased the radioactive impurity fraction from 0.64% to 1.12% of the total radiolabeled material in the aqueous phase, which would still be negligible. For the other extreme case where all of the impurity partitions into the silicone membrane, the capric acid concentration in the aqueous phase (C_{aq}) will remain as correct and the capric acid concentration in silicone ($C_{s,p}$; see Eq 3.14) would have maximum error. The maximum error would occur at the highest pH (i.e., pH 5.5 was the highest pH for which data were used in the best-fit procedure to determine the pK_a value of capric acid.) because it would correspond to having the smallest fraction of capric acid partitioning into silicone (i.e., it has the lowest $k_{p,app}$). In the pH 5.5 experiment, the total DPM in the system were 450,000 DPM, of which 35,000 were in the silicone membrane at equilibrium. The total amount of impurity in the system was 2,880 DPM ($450,000 \times 0.0064$). If all of the impurity DPM partitioned into the silicone membrane, the experimental C_{aq} at pH 5.5 would have had an 8.2% error, with the lower pH data exhibiting smaller errors. In order to assess the maximum possible effect the impurity could have on the pK_a determination, the pK_a was reevaluated after subtracting all the

assumed impurity DPM from the silicone phase. The result was a pK_a of $4.51(\pm 0.03)$ and a $k_{p,i}$ of $311(\pm 14)$, both which are within the experimental error of the original evaluation. Because the true partition coefficient of the impurity was not known and the maximum effect was negligible, the original pK_a and $k_{p,i}$ values were retained for use in all calculations.

The determination of K^u required silicone partitioning studies at pH 3.0 with 0, 0.33, 1, and 3 mM HPB, where the $k_{p,app}$ values were 303, 97, 38, and 14, respectively (see Fig 3.1). If we again assume that all the impurity partitions into the silicone phase, then as before the most extreme error due to impurity would occur when $k_{p,app}$ is lowest (i.e., the 3 mM HPB case). In this case there were 430,000 DPM in the system, of which 17,000 DPM would have been in the silicone at equilibrium. If all the impurity (2750 DPM) is assumed to have partitioned into the silicone phase, then the actual $k_{p,app}$ would have been 17% lower than the experimentally determined $k_{p,app}$, with the lower HPB conditions experiencing lower maximum errors. Reevaluating K^u under this extreme case where the impurity had an infinitely high silicone partition coefficient by subtracting all the impurity DPM from the silicone phase for all cases yielded a K^u value of $7.7 (\pm 0.3)$, which is within experimental error of the reported value ($7.5 (\pm 0.3)$, see Table 3.1). Therefore, no corrections were made to K^u . K^- needed no evaluation since it was determined by best-fitting to impurity-corrected silicone transport data. In conclusion, only the P_T values needed correcting for the small amount of impurity present in the stock [^{14}C]capric acid solution. Table 3.6 compares the uncorrected to the corrected for the worst cases for pK_a , $k_{p,i}$, and K^u .

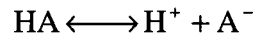
Table 3.6 A comparison of parameters and P_T results before and after correction for the worst case situation involving the radiolabeled impurity(ies).

| | No correction | Corrected |
|-----------|-----------------------|----------------------|
| pK_a | 4.53(\pm 0.03) | 4.51(\pm 0.03) |
| $k_{p,i}$ | 315(\pm 14) | 311(\pm 14) |
| K^u | 7.5(\pm 0.3) | 7.7(\pm 0.3) |
| P_T | See Figs 3.9 and 3.10 | See Figs 3.4 and 3.5 |

3.8 Appendix B. Equilibrium Reactions, Species

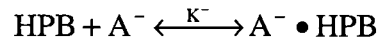
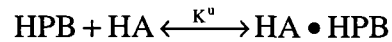
Concentrations and Fractions

The equilibrium reaction of capric acid (HA) and its acid dissociation constant K_a , are



$$K_a = \frac{[H^+][A^-]}{[HA]} \quad (3.34)$$

For the complexes of HPB with the caprate species, $HA \bullet HPB$ and $A^- \bullet HPB$, the equilibria are:



The binding constants K^u and K^- , are:

$$K^u = \frac{C^{*u}}{C^u [HPB_f]} \quad (3.35)$$

$$K^- = \frac{C^{*-}}{C^- [HPB_f]} \quad (3.36)$$

where C^{*u} , C^{*-} , and $[HPB_f]$ are the concentrations of the $HA \bullet HPB$, $A^- \bullet HPB$, and free HPB, respectively. The total caprate concentration, C_T , is

$$C_T = C^u + C^- + C^{*u} + C^{*-} \quad (3.37)$$

And, in terms of the fraction (F) of each species,

$$C_T = (F^u + F^- + F^{*u} + F^{*-})C_T \quad (3.38)$$

The total concentration of all HPB species, $[HPB_T]$, is

$$[HPB_T] = [HPB_f] + C^{*u} + C^{*-} \quad (3.39)$$

Solving for the concentration of each species in Eq 3.37 with the aid of Eqs 3.34, 3.35, 3.36, and 3.39, one obtains expressions which take into account the pH and pK_a , the binding constants K^u and K^- , and the $[HPB_T]$ and C_T .

Capric acid species

$$C^u = \frac{C_T}{\beta + \alpha[HPB_f]} \quad (3.40)$$

$$[HPB_f] = \frac{[HPB_T]}{1 + \alpha C^u} \quad (3.41)$$

$$\alpha\beta(C^u)^2 + [\beta + \alpha[HPB_T] - \alpha C_T] C^u - C_T = 0 \quad (3.42)$$

where

$$\alpha = K^u + K^- (10^{(pH-pK_a)}) \quad (3.43)$$

$$\beta = 1 + 10^{(pH-pK_a)} \quad (3.44)$$

Caprate ion species

$$C^- = \frac{C_T}{\beta' + \alpha' [HPB_f]} \quad (3.45)$$

$$[HPB_f] = \frac{[HPB_T]}{1 + \alpha' C^-} \quad (3.46)$$

$$\alpha' \beta' (C^-)^2 + [\beta' + \alpha' [HPB_T] - \alpha' C_T] C^- - C_T = 0 \quad (3.47)$$

$$\alpha' = K^- + K^u (10^{(pK_a - pH)}) \quad (3.48)$$

$$\beta' = 1 + 10^{(pK_a - pH)} \quad (3.49)$$

HPB • A⁻ Complex

$$C^{*-} = \frac{C_T}{1 + \frac{K^u (\beta' - 1)}{K^-} + \frac{\beta'}{K^- [HPB_f]}} \quad (3.50)$$

$$\gamma [HPB_f]^2 + [1 + \gamma C_T - \gamma [HPB_T]] [HPB_f] - [HPB_T] = 0 \quad (3.51)$$

where

$$\gamma = \frac{K^-}{\beta'} + \frac{K^u}{\beta} \quad (3.52)$$

HPB •HA Complex

$$C^{*u} = C_T - (C^u + C^- + C^{*-}) \quad (3.53)$$

The quadratic formula is applied to the solutions of the binomial equations. When the concentration ratio of $[HPB_T] / C_T$ is much greater than unity, say 100, $[HPB_i] \approx [HPB_T]$, which would simplify the calculations of the specific species concentrations. The fraction of each species is calculated using

$$F^u = C^u / C_T \quad (3.54)$$

$$F^- = C^- / C_T \quad (3.55)$$

$$F^{*u} = C^{*u} / C_T \quad (3.56)$$

$$F^{*-} = C^{*-} / C_T \quad (3.57)$$

3.9 Glossary

| <u>Notation</u> | <u>Definition</u> |
|-----------------------------|--|
| A^- | free caprate ion |
| A | membrane surface area |
| a | thermodynamic activity |
| ABL | aqueous boundary layer |
| $A^- \bullet \text{HPB}$ | caprate ion \bullet HPB complex |
| A^- / HPB | solution containing both caprate ion and HPB (pH 7.4) |
| $\Sigma A_{\text{imp,tot}}$ | the sum of impurity DPM over the 1500 minute run |
| $A_{\text{imp,100}}$ | the impurity DPM found in the 0-100 minute receiver sample |
| $A_{\text{imp,1500}}$ | the impurity DPM found in the 1400-1500 minute receiver sample |
| C | concentration |
| $C_{s,p}$ | concentration of capric acid in the silicone polymer membrane |
| C_{aq} | concentration of total caprate in the aqueous phase |
| $C_{\text{DPM,tot}}$ | total initial concentration of radioactivity in the donor chamber |
| $C_{\text{imp, init}}$ | initial concentration of impurity in the donor solution |
| C_T | total caprate concentration |
| C_D | concentration of solute in a donor solution |
| $C_{T,D}$ | concentration of total caprate in donor solution |
| $C_{T,S}$ | concentration of total caprate at the membrane surface |
| C^u | concentration of free capric acid |
| $C^u_{\text{sat soln}}$ | concentration of the saturated solution of X in pure water at low pH |
| C^- | concentration of free caprate ion |
| C^{*u} | concentration of capric acid \bullet HPB complex |
| C^{*-} | concentration of caprate ion \bullet HPB complex |
| D | diffusion coefficient |

| | |
|--------------|--|
| D_m | diffusion coefficient of capric acid in the silicone polymer membrane |
| D_X | diffusion coefficient of the permeant of interest |
| D_R | diffusion coefficient of the reference permeant |
| D^u | diffusion coefficient of the free capric acid species |
| D^- | diffusion coefficient of the free caprate ion species |
| D^{*u} | diffusion coefficient of the capric acid•HPB complex |
| D^{*-} | diffusion coefficient of the caprate ion•HPB complex |
| D^f | diffusion coefficient of free capric acid or of caprate ion |
| D^* | diffusion coefficient of capric acid•HPB complex or of the caprate ion•HPB complex |
| D^{eff} | effective diffusion coefficient |
| D_E | experimental diffusion coefficient |
| D_L | literature value of the diffusion coefficient |
| DPM | disintegrations per minute |
| F | fraction |
| F^u | fraction of the free capric acid species |
| F^- | fraction of the free caprate ion species |
| F^{*u} | fraction of the capric acid•HPB complex |
| F^{*-} | fraction of the caprate ion•HPB complex |
| F^f | sum of the fractions of the capric acid and the caprate ion species |
| F^* | sum of the fractions of the HA•HPB and the A ⁻ •HPB complexes |
| h | thickness |
| h_m | thickness of the silicone polymer membrane |
| h_{ABL} | aqueous boundary layer thickness |
| $h_{ABL,SM}$ | aqueous boundary layer thickness for the silicone membrane alone |

| | |
|------------------|---|
| $h_{ABL,SM-MM}$ | effective aqueous boundary layer thickness for the silicone membrane plus six Millipore membranes |
| h_{MM} | experimentally determined surrogate ABL thickness for the six millipore membrane assembly |
| $h_{MM,theo}$ | theoretically predicted surrogate ABL thickness of a six Millipore membrane assembly |
| $[H^+]$ | hydrogen ion concentration |
| HA | capric acid |
| HPB | 2-hydroxypropyl- β -cyclodextrin |
| HPB _f | free 2-hydroxypropyl- β -cyclodextrin |
| $[HPB_T]$ | the total concentration of all HPB species |
| HA•HPB | capric acid•HPB complex |
| HA/HPB | solution containing both capric acid and HPB (pH 3.0) |
| J | flux |
| J_m | flux across the membrane |
| J_{max} | maximum flux across the membrane system |
| $J_{max,f}$ | maximum flux of a test formulation containing drug X and HPB |
| $J_{max,o}$ | maximum flux of a test formulation in pure water at low pH |
| J_{ABL} | flux across the ABL |
| J_{imp} | impurity flux |
| K^u | capric acid•HPB binding constant |
| K^- | caprate ion•HPB binding constant |
| K_a | dissociation constant |
| $k_{p,i}$ | intrinsic partition coefficient |
| $k_{p,app}$ | apparent partition coefficient |
| P_T | total permeability coefficient |
| P_{MM} | permeability coefficient across six Millipore membranes |
| $P_{T,MM}$ | total permeability coefficient for the six Millipore membrane system |

| | |
|-------------------|--|
| P_i | intrinsic membrane permeability coefficient |
| P_m | effective membrane permeability coefficient |
| P_{ABL} | the ABL permeability coefficient in the absence of a carrier |
| $P_{ABL,SM}$ | the ABL permeability coefficient in the absence of a carrier in the SM experiments |
| $P_{ABL,SM-MM}$ | the ABL permeability coefficient in the absence of a carrier in the SM-MM experiments |
| $P_{T,X}$ | permeability coefficient of the permeant of interest |
| $P_{T,R}$ | permeability coefficient of the reference permeant |
| P_{imp} | impurity membrane permeability coefficient |
| P_{ABL}^{eff} | ABL permeability coefficient in the presence of a carrier |
| $R_{J,max}$ | ratio of $J_{max,f}$ to $J_{max,o}$ |
| SM | silicone membrane alone transport model |
| MM | six Millipore membranes alone transport model |
| SM-MM | silicone membrane plus six Millipore membranes transport model |
| T | absolute temperature |
| T_E | experimental absolute temperature |
| T_L | literature absolute temperature |
| V_D | volume in the donor chamber |
| X | hypothetical drug molecule with the same transport parameters as capric acid and a solubility of 0.05 mM |
| $X \bullet HPB$ | compound X•HPB complex |
| $X^- \bullet HPB$ | compound X anion•HPB complex |
| $\frac{dQ}{dt}$ | slope of the cumulative amount vs. time plot (permeant flux) |
| η_E | experimental viscosity |
| η_L | literature viscosity |
| ε | porosity |

3.10 References

1. Loftsson T 2002. Cyclodextrins and the biopharmaceutics classification system of drugs. *J Inclusion Phenom Macrocyclic Chem* 44(1-4):63-67.
2. Amidon GE, Higuchi WI, Ho NF 1982. Theoretical and experimental studies of transport of micelle-solubilized solutes. *J Pharm Sci* 71(1):77-84.
3. Cheng Y, Xu Z, Ma M, Xu T 2008. Dendrimers as drug carriers: applications in different routes of drug administration. *J Pharm Sci* 97(1):123-143.
4. Higuchi WI 1964. Effects of interacting colloids on transport rates. *J Pharm Sci* 53(5):532-535.
5. Gupta S, Moulik SP 2008. Biocompatible microemulsions and their prospective uses in drug delivery. *J Pharm Sci* 97(1):22-45.
6. Torchilin VP 2005. Recent advances with liposomes as pharmaceutical carriers. *Nat Rev Drug Discovery* 4(2):145-160.
7. Lukyanov AN, Torchilin VP 2004. Micelles from lipid derivatives of water-soluble polymers as delivery systems for poorly soluble drugs. *Adv Drug Del Rev* 56(9):1273-1289.
8. Brewster ME, Loftsson T 2007. Cyclodextrins as pharmaceutical solubilizers. *Adv Drug Del Rev* 59(7):645-666.
9. Brewster ME, Noppe M, Peeters J, Loftsson T 2007. Effect of the unstirred water layer on permeability enhancement by hydrophilic cyclodextrins. *Int J Pharm* 342(1-2):250-253.
10. Loftsson T, Duchene D 2007. Cyclodextrins and their pharmaceutical applications. *Int J Pharm* 329(1-2):1-11.
11. Loftsson T, Vogensen SB, Brewster ME, Konradsdottir F 2007. Effects of cyclodextrins on drug delivery through biological membranes. *J Pharm Sci* 96(10):2532-2546.
12. Rao VM, Stella VJ 2003. When can cyclodextrins be considered for solubilization purposes? *J Pharm Sci* 92(5):927-932.
13. Redenti E, Szente L, Szejtli J 2001. Cyclodextrin complexes of salts of acidic drugs. Thermodynamic properties, structural features, and pharmaceutical applications. *J Pharm Sci* 90(8):979-986.

14. Shaker DS, Ghanem AH, Li SK, Warner KS, Hashem FM, Higuchi WI 2003. Mechanistic studies of the effect of hydroxypropyl-beta-cyclodextrin on in vitro transdermal permeation of corticosterone through hairless mouse skin. *Int J Pharm* 253(1-2):1-11.
15. Stella VJ, Rajewski RA 1997. Cyclodextrins: their future in drug formulation and delivery. *Pharm Res* 14(5):556-567.
16. Uekama K 2004. Design and evaluation of cyclodextrin-based drug formulation. *Chem Pharm Bull* 52(8):900-915.
17. Roseman TJ, Higuchi WI 1970. Release of medroxyprogesterone acetate from a silicone polymer. *J Pharm Sci* 59(3):353-357.
18. Geinoz S, Rey S, Boss G, Bunge AL, Guy RH, Carrupt PA, Reist M, Testa B 2002. Quantitative structure-permeation relationships for solute transport across silicone membranes. *Pharm Res* 19(11):1622-1629.
19. Patel DC, Fox JL, Higuchi WI 1984. Physical model approach in the study of the transport of alkyl amines across a silicone rubber membrane in a two-chamber diffusion cell. *J Pharm Sci* 73(8):1028-1034.
20. Tsutsumi K, Li SK, Ghanem AH, Ho NF, Higuchi WI 2003. A systematic examination of the in vitro Ussing chamber and the in situ single-pass perfusion model systems in rat ileum permeation of model solutes. *J Pharm Sci* 92(2):344-359.
21. Tsutsumi K, Li SK, Hymas RV, Teng CL, Tillman LG, Hardee GE, Higuchi WI, Ho NFH 2008. Systematic studies on the paracellular permeation of model permeants and oligonucleotides in the rat small intestine with chenodeoxycholate as enhancer. *J Pharm Sci* 97(1):350-367.
22. Aungst BJ 2000. Intestinal permeation enhancers. *J Pharm Sci* 89(4):429-442.
23. Hayashi M, Tomita M 2007. Mechanistic analysis for drug permeation through intestinal membrane. *Drug Metab Pharmacokinet* 22(2):67-77.
24. Tillman LG, Geary RS, Hardee GE 2008. Oral delivery of antisense oligonucleotides in man. *J Pharm Sci* 97(1):225-236.
25. Peck KD, Ghanem AH, Higuchi WI 1994. Hindered diffusion of polar molecules through and effective pore radii estimates of intact and ethanol treated human epidermal membrane. *Pharm Res* 11(9):1306-1314.
26. Dippy JFJ 1938. Chemical constitution and dissociation constants of monocarboxylic acids. X. Saturated aliphatic acids. *J Chem Soc*:1222-1227.

27. Kielland J 1937. Individual activity coefficients of ions in aqueous solutions. *J Am Chem Soc* 59:1675-1678.
28. Butler JN. 1964. *Ionic equilibrium: a mathematical approach*. Reading, Mass: Addison-Wesley. p 547.
29. Okimoto K, Rajewski RA, Uekama K, Jona JA, Stella VJ 1996. The interaction of charged and uncharged drugs with neutral (HP-beta-CD) and anionically charged (SBE7-beta-CD) beta-cyclodextrins. *Pharm Res* 13(2):256-264.
30. Cussler EL. 1997. *Diffusion: mass transfer in fluid systems*. second edition ed., Cambridge, United Kingdom: Cambridge University Press. p 580.
31. Beck RE, Schultz JS 1972. Hindrance of solute diffusion within membranes as measured with microporous membranes of known pore geometry. *Biochim Biophys Acta* 255(1):273-303.
32. Ribeiro ACF, Ortona O, Simoes SMN, Santos CIAV, Prazeres PMRA, Valente AJM, Lobo VMM, Burrows HD 2006. Binary mutual diffusion coefficients of aqueous solutions of sucrose, lactose, glucose, and fructose in the temperature range from 298.15 to 328.15 K. *J Chem Eng Data* 51(5):1836-1840.
33. Deen WM 1987. Hindered transport of large molecules in liquid-filled pores. *AIChE Journal* 33(9):1409-1425.

CHAPTER 4

CAPRIC ACID ABSORPTION IN THE PRESENCE OF
HYDROXYPROPYL- β -CYCLODEXTRIN IN THE
RAT ILEUM USING THE IN SITU SINGLE
PASS PERFUSION TECHNIQUE

4.1 Introduction

While there has been much progress from the practical standpoint in the area of oral drug formulation development involving cyclodextrins,¹⁻⁵ there has been relatively little progress from the standpoint of obtaining a quantitative mechanistic understanding of the interplay of key variables involved in the intestinal absorption enhancement by cyclodextrins. In Chapter 3 we developed a physical model, which we called the flat surface model (FSM) that should represent an important step toward the mechanistic understanding of the transport of highly lipophilic, ionizable drug molecules between two aqueous compartments separated by a lipophilic membrane and where a carrier such as a cyclodextrin is present in the aqueous phase. Capric acid permeability coefficients predicted by the FSM equations describing the permeant transport behavior in the presence of a carrier were found to be in good agreement with the experimental results for capric acid transport between two aqueous compartments separated by a silicone polymer membrane over wide ranges of pH and the 2-hydroxypropyl- β -cyclodextrin (HPB) concentrations. The good agreement of experimental data with the FSM-

predictions over the range of conditions demonstrates the rigor of the model and the appropriateness of extending the applications of the FSM approach to other transport situations and conditions. The FSM was able to quantitatively demonstrate the interplay of key variables such as solution pH, capric acid pK_a , caprate species-HPB binding constants, aqueous boundary layer thickness, diffusion coefficients, and the capric acid lipophilicity and to demonstrate the relative importance of each of these variables for a given set of transport conditions.

A main purpose of establishing the FSM approach in Chapter 3 was to establish a sound physical model that could be used to probe the effects of HPB on the transport of lipophilic molecules across biological membranes, more specifically the intestinal membrane. One concern about using cyclodextrins in oral formulations is that of safety. As with any potential excipient, questions arise concerning possible adverse side effects. While unsubstituted cyclodextrins and cyclodextrins with lipophilic substitutions have been shown to cause damage to erythrocytes and biological membranes,^{6,7} the relatively high degree of safety of HPB in oral formulations has been well documented.⁸⁻¹³ It has been demonstrated that HPB concentrations up to 100 mM do not appear to extract relevant lipids from biological membranes or otherwise disrupt the integrity of epithelial cells.¹⁴⁻¹⁶ In addition to HPB being well tolerated, it is highly water soluble and not significantly absorbed in the gastrointestinal tract.^{1,2} These characteristics make HPB a good candidate for a solubilizing agent in oral dosage form design. Accordingly, the FDA has included HPB in its list of Inactive Pharmaceutical Ingredients.¹ In fact, HPB has already been used in approved and marketed drug formulations in Europe, Japan, and the United States, with several more formulations in clinical trials.¹⁷

The initial aim of the current study was to gain further insight into the role of cyclodextrin carriers in improving the oral bioavailability of highly lipophilic molecules by applying the FSM to results from intestinal absorption experiments involving the rat ileum. Capric acid and HPB are used to represent a typical, highly lipophilic weak acid molecule and a carrier molecule, respectively. The interplay of key variables, their relative importances under various experimental conditions, and the mechanism by which cyclodextrins may improve oral bioavailability were to be examined. An additional aim of this study was to adapt and extend the FSM to allow for a more detailed examination of the rat ileal intestinal absorption problem. Accordingly, a villus model (VM) that takes into account the villus architecture of the ileum is also presented. Each of the models are examined in light of the experimental data for capric acid absorption in the rat ileum at pH 7.4 in the presence of 0 – 50 mM HPB.

4.2 Strategy

4.2.1 The experimental method and the estimation of key FSM parameters

The technique of in situ single pass perfusion of an isolated rat ileal segment and local mesenteric venous blood collection is used.^{18,19} As the perfusing permeant (i.e., capric acid) solution flows down the rat ileum, taken as a cylinder with a smooth inner surface, at a constant rate, the permeant is absorbed across the epithelial cells into a blood sink. The perfusion flow rate is strictly controlled using a perfusion pump, and the exit concentration of the permeant and the osmolarity of the perfusate are assayed at regular time points. Mesenteric venous cannulation provides the means for the determination of

the permeant appearance rate in the blood draining the intestinal segment. This allows for a more sensitive determination of steady-state flux as compared with methods which determine the permeant flux from the disappearance kinetics in the lumen. The gut length and the inside diameter are measured for the flat surface area determination (flat surface area refers to treating the intestinal gut segment as a hollow smooth circular cylinder), and the mean permeant concentration in the lumen is determined from initial and exit concentrations of the permeant. With the mean luminal concentration, membrane surface area, and appearance rate of permeant in the blood, the permeant flux (J_b) and the total permeability coefficient (P_T) are directly determined. Further details are explained in the methods and data treatment sections.

Key parameters of the flat surface model (FSM) developed in Chapter 3 were intended for application in the intestinal perfusion studies. With the exception of the aqueous boundary layer thickness (h_{ABL}) and intrinsic membrane permeability coefficient (P_i), the previously determined parameters (Table 3.1) are applicable to the intestinal perfusion of capric acid in the presence of HPB and are listed, along with the appropriate h_{ABL} and P_i for the present study, in Table 4.1. The h_{ABL} is dependent upon the hydrodynamics and therefore must be determined experimentally under the same experimental conditions as those of the perfusion experiments in this study. The h_{ABL} was determined to be 0.117 cm by a best-fitting procedure (as described in detail in the results section) involving the experimental data over the range of HPB concentrations at pH 7.4. Taurocholate, which is actively absorbed in the rat ileum and which is completely aqueous boundary layer (ABL) controlled,¹⁸ was used to confirm the h_{ABL} thickness. A value of 0.102 cm was obtained using tracer levels of taurocholate, which

Table 4.1 Parameter values used in model calculations. Diffusion coefficients, binding constants, and pK_a are from Chapter 3. Intrinsic membrane permeability coefficient and aqueous boundary layer thickness were determined in the present study.

| Parameter | Symbol | Value |
|--|-------------|-----------------------------------|
| Effective aqueous boundary layer thickness (cm) | h_{ABL} | 0.117(± 0.02) |
| Capric acid intrinsic permeability coefficient (FSM case) (cm/s) | $P_{i,FSM}$ | 3.5(1.7-10) |
| Capric acid intrinsic permeability coefficient (VM case) (cm/s) | $P_{i,VM}$ | 0.48(0.15-2.1) |
| Capric acid (HA) or caprate ion (A^-) aqueous diffusion coefficient (cm^2/s) | D^f | 6.9(± 0.5) $\times 10^{-6}$ |
| A^- •HPB or HA•HPB diffusion coefficient (cm^2/s) | D^* | 2.9(± 0.2) $\times 10^{-6}$ |
| Taurocholate diffusion coefficient (cm^2/s) | | 5.6 $\times 10^{-6}$ ^a |
| HA•HPB binding constant (mM^{-1}) | K^u | 7.5(± 0.3) |
| A^- •HPB binding constant (mM^{-1}) | K^- | 2.5(± 0.2) |
| Buffer solution pH | pH | 7.40(± 0.01) |
| pK_a of capric acid | pK_a | 4.53(± 0.03) |

^a From reference¹⁸

was consistent with the h_{ABL} determined previously in our laboratory (0.109 cm) for the same perfusate flow rate.¹⁸ The best-fit h_{ABL} of 0.117 cm was chosen for the purposes of this study. The estimation of P_i was initially thought to be problematic. Although capric acid alone transport across the silicone polymer membrane was shown in Chapter 3 (the silicone membrane alone case experiments) to be essentially membrane-controlled at pH 7.4, preliminary intestinal perfusion experiments indicated that capric acid alone absorption was 100% ABL-controlled at pH 7.4 in the rat ileum and therefore P_i was thought to be insensitive to quantification. However, as will be seen, the HPB carrier investigation itself provided a means for obtaining a reasonably good estimate of P_i because, as was shown in Chapter 3, with increasing HPB concentration capric acid transport becomes increasingly membrane-controlled. Thus, the capric acid transport experiments in the presence of varying concentrations of HPB (0-50 mM) provided a means for determining both h_{ABL} and P_i by best fitting of both parameters to the entire range of experimental data.

In the present in situ perfusion experiments, the buffered condition of pH 7.4 was regarded to hold, not only in the bulk luminal solution, but also across the ABL and in the intervillus spaces, i.e., no significant pH gradients are expected to exist in the ileum for two reasons. Firstly, the buffer capacity (β) of 0.057 M sodium phosphate at pH 7.4 is 3.13×10^{-2} M.²⁰ Caprate (5×10^{-5} M cold and 0.4×10^{-5} M radiolabeled), correspond to a total caprate concentration (C_T) of 5.4×10^{-5} M). Therefore any pH gradient (ΔpH) should be insignificant:

$$\Delta pH = -\frac{[H^+]}{\beta} \cong -\frac{C_T}{\beta} = -0.0017 \quad (4.1)$$

Secondly, the microclimate pH about the rat ileal membrane surface, owing to the continuous flow of alkalinized secretions from intervillus secretory cells, has been found to be pH 7.3^{21,22}. In contrast, the secretory cells in the jejunum maintain a more acidic microclimate pH 6.0 environment; in the latter case there may be the potential to sustain pH gradients if the luminal solution pH was buffered at pH 7.4²³, and for this latter more complex situation, a physical model has yet to be written. On a somewhat different but related issue, the open-ended intraluminal perfusion of pH 7.4 buffered solution of capric acid and HPB mixtures from an infinite reservoir at 0.2 ml/min (or linear flow velocity of 1.6 cm/min) would also preclude the existence of any longitudinal pH gradient along the 10 cm ileal segment as well as any significant accumulation of secretions in the perfusate with time.

4.2.2 Flat surface versus villus surfaces

In addition to different FSM h_{ABL} and P_i parameter values when compared to the in vitro silicone polymer membrane transport system (Chapter 3), the in situ single pass perfusion system involves key fluid flow and geometry differences. The permeant solution flows into and out of the isolated ileal segment in the intestinal perfusion experiment, whereas the permeant solution is confined to a magnetically stirred donor compartment in the side-by-side diffusion cell experiment. Another key difference between the intestinal perfusion experiments and the silicone polymer membrane experiments is that the surface of the rat ileum is covered with villi which may significantly increase the effective surface area utilized for absorption compared to the smooth (flat) surface of the silicone polymer membrane. Accordingly, we also examine a modified physical model which should be more appropriate to the intestinal transport

experiments and is termed the villus model for intestinal absorption (VM). This villus model incorporates the height, diameter, and density of the villi as well as the mean intervillus space. Winne^{24,25} and Oliver et al.²⁶ have previously idealized the structure of the villi using a two-dimensional model with an intervillus space of given height and width that represents the villi as rectangular columns with a mean villus diameter. Using a similar approach, we idealize the villus structure using a 2D axial symmetry model (see Fig 4.1, Table 4.2, Fig 4.2, and Table 4.3) that represents the villi as circular-cylindrical columns of a given height and diameter with a defined intervillus space represented by an annular cylinder, coaxial with the villus, having a cross-sectional area of the average intervillus space per villus unit of $\pi(r_2^2 - r_1^2)$ where r_2 is the outer radius of this annular cylinder and r_1 is the villus radius. This model allows for diffusion of capric acid, the complexes, and HPB in the aqueous phase (ABL and intervillus space), rapid equilibrium between capric acid and HPB, and absorption of neutral free capric acid across the biomembrane at the various surfaces (i.e., tip, lateral surface, and crypt) of the villi into a blood sink. The villi density is the number of villus units per cm^2 of flat surface area and the cross-sectional area of the average intervillus space is the total intervillus cross-sectional area per cm^2 of flat surface divided by the villus density.

Although previous researchers have used similar villus models to demonstrate the effects of the villus geometry on drug absorption,²⁴⁻²⁶ this study was to examine for the first time the concept that including a cyclodextrin in the formulations may increase the effective epithelial surface area utilized for absorption of highly lipophilic molecules by providing a means for the permeant to diffuse further into the intervillus space than without a carrier. As will be seen, the extent to which the additional surface area is

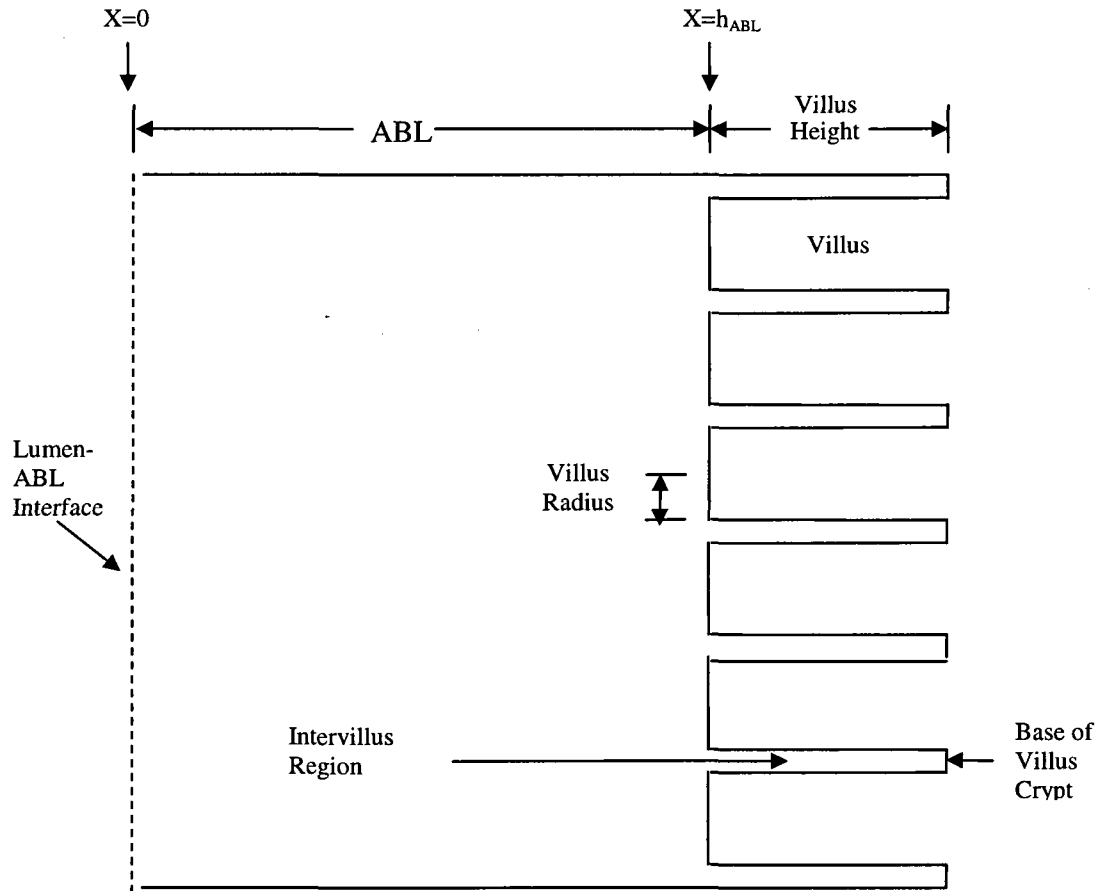


Fig 4.1 Schematic representation of the villus model (VM). Parameter values are listed in Table 4.2

Table 4.2 Parameters of the villus model

| | |
|--|--|
| Aqueous boundary layer thickness | 0.117 cm ^a |
| Villus height (h_v) | 0.0399 cm ^b |
| Villus radius (r_1) | 0.0037 cm ^b |
| Radius of villus plus intervillus space radius (r_2) | 0.0049 cm ^b |
| Villus density | 1.32×10^4 villi per cm ² of flat surface ^b |
| Cross-sectional area of average intervillus space ^c | 3.24×10^{-5} cm ² per villus; area= $\pi(r_2^2 - r_1^2)$ |

^a determined in the present study

^b taken from reference²⁶

^c calculated as (total cross-sectional area per cm² of flat surface) \div (villus density)

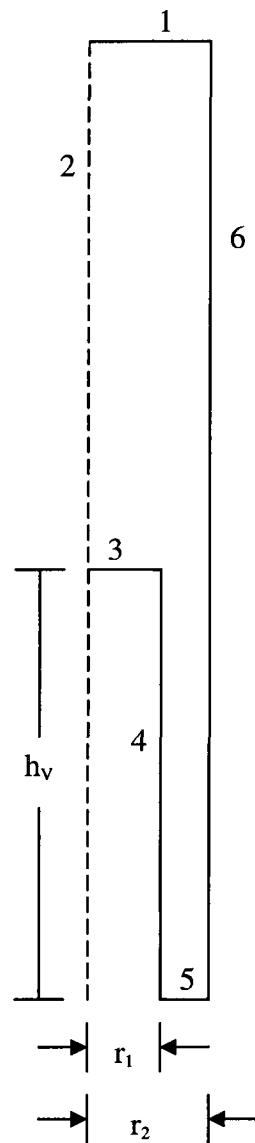


Fig 4.2 Boundary conditions for the COMSOL finite-element villus model simulations, where r_1 is the villus radius, r_2 is the radius of the villus plus the associated intervillus space, and h_v is the villus height.

Table 4.3 Definition of boundary conditions for Fig 4.2

| Site | Boundary conditions |
|---------|---|
| 1 | Luminal solution: caprate-HPB solution with total caprate at 0.054 mM and HPB from 0-50 mM |
| 2 | Axis of symmetry |
| 3, 4, 5 | The local capric acid flux, $j_i = P_i C_s^u$ where P_i ($P_i = P_{i,VM}$) is the intrinsic membrane permeability coefficient of capric acid and C_s^u is the villus surface site concentration of free capric acid species |
| 6 | Impenetrable boundary, capric acid flux, $j_i = 0$ |

effectively utilized is dependent on the various parameters (Table 4.1) and the experimental conditions, these including the intrinsic bio-membrane permeability coefficient ($P_{i,VM}$), the aqueous diffusion coefficients, the HPB concentration, and the binding affinity of the permeant to HPB.

To put the respective surface area contributions into proper context, we define the surface area ratio, $R_{VM/FSM}$, by

$$R_{VM/FSM} = A_{VM}/A_{FSM} \quad (4.2)$$

where A_{VM} and A_{FSM} are the surface areas of an ileal segment for the VM and the FSM cases, respectively. For an ileal segment of length (l) = 10 cm and radius (r) = 0.2 cm, A_{FSM} , is

$$A_{FSM} = 2\pi rl = 12.6 \text{ cm}^2 \quad (4.3)$$

A_{VM} for the same ileal segment is

$$A_{VM} = A_{tip} + A_{LS} + A_{crypt} \quad (4.4)$$

where A_{tip} , A_{LS} , and A_{crypt} are the area contributions from the villus tip, lateral surface, and the base of the crypt, respectively, and the values for these calculated from the parameters given in Table 4.2 are presented in Table 4.4 along with the $R_{VM/FSM}$ values. It is seen that full access to all area contributions in the VM may yield a maximal surface area advantage over the FSM by a factor of $R_{VM/FSM} = 13.3$.

Table 4.4 Maximal surface area contributions in the VM of the rat ileum

| Villus site | Surface area (cm²) | Percent of villus area | R_{VM/FSM} by location |
|--------------------|--------------------------------------|-------------------------------|---------------------------------------|
| Tip | 7.2 | 4.3% | 0.57 |
| Lateral surface | 154.5 | 92.4% | 12.30 |
| Bottom (crypt) | 5.4 | 3.3% | 0.43 |
| Total area | 167.1 | 100% | 13.30 |

4.3 Materials and Methods

4.3.1 Chemicals and reagents

For the in situ single pass perfusion system, the phosphate buffer solution consisted of 57 mM $\text{NaH}_2\text{PO}_4 \cdot \text{H}_2\text{O}$ and 79 mM Na_2SO_4 . The pH was adjusted to 7.4 with 10 M NaOH. Capric acid was obtained from Sigma-Aldrich (St. Louis, MO), [^{14}C]Mannitol, [^{14}C]capric acid, and [^{14}C]sodium taurocholate were purchased from Moravek Biochemicals Inc. (Brea, CA). Hydroxypropyl- β -cyclodextrin (Kleptose HPB) was obtained by a generous gift from Roquette America (Keokuk, IA). The purity of the radioisotopes was checked using high pressure liquid chromatography and found to be >97% pure. Solvable tissue solubilizer and Ultima Gold scintillation cocktail were obtained from PerkinElmer (Boston, MA). Other chemicals were of reagent grade.

4.3.2 In situ single pass perfusion experiments

The procedures used for the single pass perfusion experiments followed the procedures used by Tsutsumi et al.¹⁸ with some modifications. Male Sprague-Dawley rats weighing 300-400 g for intestinal perfusion, or retired breeders for blood donation, were obtained from Charles River (Wilmington, MA) and were used under the approval of the Institutional Animal Care and Use Committee at the University of Utah. The animals had free access to food and water prior to the experiment. The animal was placed in an anesthesia chamber and administered 5% halothane in oxygen at 1 L/min until unconscious. It was then transferred to a 37°C circulating water heating pad and administered 2% halothane in oxygen at a flow rate of 1 L/min through a small animal nose cone throughout the duration of the surgery and experimental setup. After testing

the animal for responsiveness using the foot pinch method, a 5 cm long silastic cannula was implanted into the jugular vein for blood collection or blood infusion as the case may be. In the case of blood donation rats, 1 ml of heparin solution (1000 U/ml) was infused into the animal via the jugular cannulation at a rate of 1ml/min. The pump was then reversed and the blood was withdrawn into a vial at the same rate until the animal expired. The vial was previously rinsed with dilute (100 U/ml) heparin, and 1ml of dilute heparin in saline was added to every 10 ml of blood to prevent clotting. The blood from these donor animals was used to replace the blood collected from the mesenteric vein of perfusion experiment animals. For the case of perfusion experiment rats, the jugular vein was cannulated as described above and the ileum was cannulated as follows. A 6 cm midline incision was made from the supralumbar to the sternum, and the distal ileum was located using the ileocecal junction as the point of reference. An approximately 10 cm segment of distal ileum was selected such that the entire mesenteric venous cascade from this intestinal segment drained into a single vein and all the blood from this segment could be collected by cannulating this vein. A semicircular incision was made at each end of the isolated segment of the ileum using electrocautery, and the luminal contents were removed by rinsing the lumen with isotonic saline at 37°C. A kynar reducing connector (from 3/32 inside diameter to 1/16 inside diameter, part number C1.5-1NK, Eldon James Corp., Loveland, CO) was then inserted into the incision at each end of the ileal segment and ligated using 4-0 silk suture. After testing to make certain there were no leaks of perfusion solution and then displacing any air bubbles trapped in the isolated ileal segment with saline, the proximal cannula was connected to a 60 ml syringe containing the perfusion solution and mounted in a perfusion pump. The distal cannula

was connected to tubing that was mounted 7 cm above the bench surface. This slight elevation prevented the lumen from collapsing but did not distend it. Following the intestinal cannulation, the connective tissue surrounding the previously selected mesenteric vein was gently removed using forceps. A 4-0 silk suture was carefully passed below the mesenteric vein, making sure the suture passed between the mesenteric artery and the mesenteric vein such that when the cannula to be placed in the mesenteric vein was ligated, the blood flow from the mesenteric artery was not disrupted. The mesenteric vein was cannulated using a 24 gauge Angeocath catheter (Beckton Dickenson, Sandy, UT), such that only the top 1cm tip remained in the vein. This cannula was then secured in place by the previously placed 4-0 silk suture. A 50 cm silastic tubing (.025 in. ID \times .047 in. OD) previously rinsed with dilute heparin was then carefully connected to the mesenteric vein cannula for blood collection. This tubing draped over the bench so that the end of the tubing was 20 cm below the bench surface. After blood collection from the mesenteric vein was established, previously collected donor blood (at 37°C) was infused into the jugular vein of the rat at a rate equal to the blood collection rate from the mesenteric vein cannulation. Then the intestinal perfusion was initiated (perfusion rate 0.2 ml/min) and the intestinal segment and venous cascade were covered with 2 pieces of 3-ply gauze (4 in. square). The halothane concentration was then reduced to 0.5% for the duration of the experiment. For capric acid with or without HPB, the perfusion solution consisted of 0.2-0.6 $\mu\text{Ci/ml}$ [^{14}C]capric acid, 0.05 mM cold capric acid, and an appropriate amount of HPB in the pH 7.4 buffer. The final osmolarity of the buffer was adjusted to 300 ± 10 mOsm/kg using reagent grade Na_2SO_4 , and the final ionic strength was 0.37. Taurocholate experimental buffer solutions were

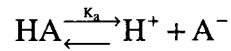
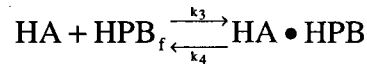
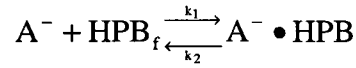
prepared in the same manner except the buffer contained only [^{14}C]taurocholate (no cold taurocholate or HPB). Each formulation was perfused through the rat ileum at 0.2 ml/min using a model 100 perfusion pump (KD Scientific, Holliston, MA). The animal was kept at $37 \pm 1^\circ\text{C}$ using a circulating water blanket, and the perfusate temperature was $30 \pm 2^\circ\text{C}$. The perfusate was collected at 10-minute intervals using preweighed 20 ml scintillation vials. Perfusate samples were weighed to determine the perfusion outflow rate, and a 100 μl sample of perfusate was assayed via scintillation counting to determine the permeant concentration in the perfusate. Water absorption/secretion was determined to be less than 5% by comparing the outflow of the perfusion solution with the inflow. The osmotic pressure change of the solution was found to be less than 5% from periodic osmolarity determinations using a micro osmometer (model 3300 Advanced Instruments Inc. Norwood, MA). Mesenteric blood flow from the isolated intestinal segment was collected at 10 minute intervals in preweighed 20 ml scintillation vials. The vials were weighed and the blood was analyzed using the following method. Exactly 500 μl of whole blood was pipetted into a fresh 20 ml scintillation vial along with 100 μl of heparin (5000 units/ml) and 550 μl of tissue solubilizer and incubated for 1 hour in a 50°C shaking water bath. Then 100 μl of 100 mM of EDTA at pH 7.4 and 300 μl 30% H_2O_2 were added to the sample and incubated at 50°C for another hour. The sample was then mixed with 10 ml scintillation cocktail and assayed by scintillation counting. For each experiment, an additional 500 μl sample of whole blood was taken from the 10 minute time point and spiked with 100 μl of donor solution and then analyzed as above as an internal standard to correct for any quenching due to the blood or reagents. The DPM of the 10-minute sample alone was subtracted from the internal standard and the remaining

DPM were compared to 100 μ l of donor solution in saline. The internal standard DPM was generally within 10% of the saline DPM. The blood samples were corrected by multiplying the blood DPM by the ratio of saline donor DPM to internal standard DPM. At the end of the transport experiment, the length of the intestinal segment was measured with silk thread. The outside diameter and intestinal wall thickness of the ileum were measured using a micrometer to determine the inside radius of the ileum. These measurements were used to calculate the flat surface area (A_{FSM}) of the ileum.

4.3.3 Villus model simulations

Finite-element simulations of permeant diffusion across the ABL and into the intervillus space with drug absorption into a sink at the villus surface sites were performed with computer software FEMLAB (v3.0a, COMSOL, Inc. Burlington, MA). The steady state diffusion analysis and 2D axial symmetry were used to model permeant absorption across the surfaces of a single villus in the rat ileum. Fig 4.1 depicts a schematic of the idealized villus structure. The villus height, radius, and intervillus space were obtained from Oliver et al.²⁶ and are listed in Table 4.2. The boundary conditions are described by Fig 4.2 and Table 4.3. Other parameters used in the VM calculations are listed in Table 4.2. As shown in the previous chapter, the diffusion coefficients of the free caprate ion (A^-) and the free capric acid (HA) species are essentially the same, as are the diffusion coefficients of the $A^- \bullet HPB$ and $HA \bullet HPB$ complexes. The diffusion coefficient of the free HPB (HPB_f), which was not experimentally determined in this study, was assumed to be the same as that of the complexes. The value for the diffusion coefficient of HPB_f was shown from model calculations to be inconsequential within a factor of ± 2 -fold because HPB_f is not absorbed and because the HPB_f concentration was

at least 10 times greater than those of either of the complexes. The axis of symmetry of the villus allows us to describe the system in two dimensions (height, z , and radius, r ,) such that for a given r and z the species concentrations at steady state are identical for all angles (ϕ). Free capric acid is absorbed into a sink at the top, sides, and bottom of the villus structure. The simulation assumes rapid equilibrium between all species (i.e., HA, A^- , HPB_f , $HA \bullet HPB$ and $A^- \bullet HPB$; pH constant at 7.4):



where the forward and reverse reaction rate constants k_1 , k_2 , k_3 , and k_4 are arbitrarily chosen high enough that all species are in rapid equilibrium (as examples $k_1 = 1 \times 10^6 \text{ mM}^{-1} \text{ s}^{-1}$, $k_2 = 4 \times 10^5 \text{ s}^{-1}$, and $K^- = \frac{k_1}{k_2} = 2.5 \text{ mM}^{-1}$; $k_3 = 7.5 \times 10^6 \text{ mM}^{-1} \text{ s}^{-1}$, $k_4 = 1 \times 10^6 \text{ s}^{-1}$, and $K^u = \frac{k_3}{k_4} = 7.5 \text{ mM}^{-1}$).

At steady state, the condition expressed by Eq (4.5) must apply simultaneously for all species.

$$\frac{\partial C_i}{\partial t} = \nabla \cdot (D_i \nabla C_i) + R = 0 \quad (4.5)$$

where C_i represents the concentration of each species and D_i represents the diffusion coefficient of each species. ∇ is the standard del (nabla) operator for cylindrical coordinates, and R is the rate of formation or disappearance of either complex and of either A^- or HA:

$$R = -k_1[A^-][HPB] + k_2[A^- \bullet HPB] \quad (4.6)$$

$$R = -k_3[HA][HPB] + k_4[HA \bullet HPB] \quad (4.7)$$

The local capric acid flux (j) at any villus site is expressed as

$$j = P_{i,VM} C_s^u \quad (4.8)$$

where $P_{i,VM}$ is the villus model intrinsic capric acid membrane permeability coefficient and C_s^u is the villus surface site free capric acid concentration. It is to be noted that, from here on, $P_{i,VM}$ will represent the P_i for the VM and $P_{i,FSM}$ that for the FSM.

4.3.4 Treatment of experimental data using the FSM

Here we describe the application of the flat surface model (FSM) in the analysis of ^{14}C -capric acid absorption in the in situ single pass perfusion experiment, following the method and conventions of Tsutsumi et al.¹⁸ The isolated ileum segment is taken as a smooth, hollow cylinder, with the perfusing solution from the reservoir entering the proximal intestinal segment at $x=0$ and exiting the segment at $x=l$. Fig 4.3 is a schematic representation of the intestinal perfusion experiment where r and l are the inside radius and the length of the isolated intestinal segment, respectively. As capric acid transports

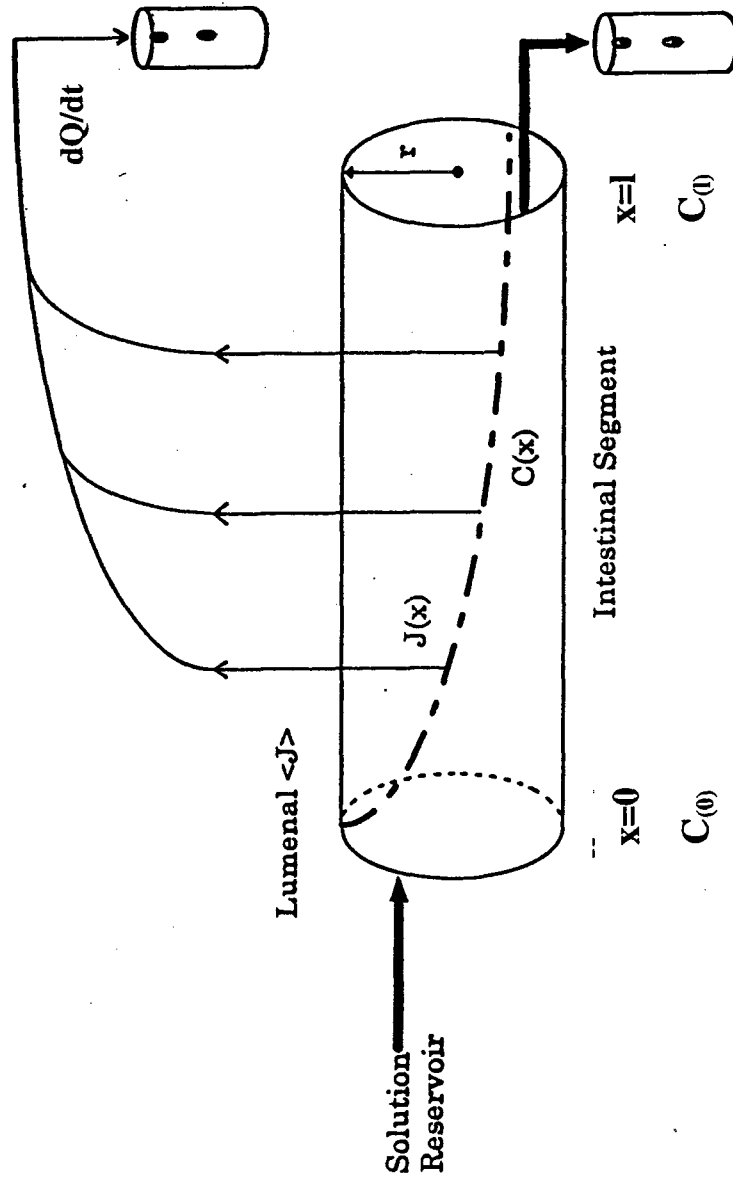


Fig 4.3 Schematics of the open-ended perfusion of rat intestinal segment from an infinite drug solution reservoir and concurrent mesenteric venous blood out-flow. The concentration gradient along the segment length and zero order flux into blood are shown.

across the absorptive surface of the ileum, there will be a steady-state longitudinal concentration gradient down the lumen of the isolated segment.²⁷ The logarithmic mean permeant concentration in the lumen, $\langle C \rangle$, is taken as the effective concentration of capric acid in the lumen.

$$\langle C \rangle = \frac{C_{(0)} [1 - C_{(1)} / C_{(0)}]}{\ln [C_{(0)} / C_{(1)}]} \quad (4.9)$$

where $C_{(0)}$ is the inflow total concentration of total caprate at $x=0$ and $C_{(1)}$ is the outflow total concentration of total caprate at $x=l$.

The total permeability coefficient (P_T) is then calculated from

$$P_T = \frac{J_b}{2\pi r l \langle C \rangle} \quad (4.10)$$

where J_b is the average steady-state flux of the permeant appearing in mesenteric blood.

P_T is expressed in terms of barriers in series:

$$P_T = \frac{1}{\frac{1}{P_{ABL}^{eff}} + \frac{1}{P_m}} \quad (4.11)$$

where P_m is the effective membrane permeability coefficient and P_{ABL}^{eff} is the effective permeability coefficient in the aqueous boundary layer. In the case of the present study, only free unionized capric acid (HA) is assumed to be absorbed; therefore, Eq (4.11) becomes:

$$P_T = \frac{1}{\frac{1}{P_{ABL}^{eff}} + \frac{1}{P_{i,FSM} F^u}} \quad (4.12)$$

where $P_{i,FSM}$ is the intrinsic membrane permeability coefficient of HA and F^u is the fraction of the total caprate in the HA form at the membrane-ABL interface. Since

$$P_{ABL}^{eff} = \frac{D^{eff}}{h_{ABL}}, \text{ Eq (4.12) becomes}$$

$$P_T = \frac{1}{\frac{h_{ABL}}{D^{eff}} + \frac{1}{P_{i,FSM} F^u}} \quad (4.13)$$

Also,

$$D^{eff} = D^f F^f + D^* F^* \quad (4.14)$$

where D^{eff} is the effective aqueous diffusion coefficient of total caprate in the caprate/HPB solution system, h_{ABL} is the thickness of the aqueous boundary layer (ABL), D^f is the diffusion coefficient of HA and A^- (6.9×10^{-6}), D^* is the diffusion coefficient of $HA \bullet HPB$ and $A^- \bullet HPB$ (2.9×10^{-6}), F^f is the fraction of free caprate ($HA + A^-$), and F^* is the HPB-bound fraction of caprate ($HA \bullet HPB$ and $A^- \bullet HPB$). It was previously validated that the diffusion coefficients of HA and A^- are essentially the same and that the diffusion coefficients of $HA \bullet HPB$ and $A^- \bullet HPB$ are the same within experimental error (Section 3.5.1.3).

It is of interest to point out that another method often used for calculating P_T from experiments such as in the present study involves the following equation^{23,28}

$$P_T = -\frac{Q}{2\pi r l} \ln[C_{(l)} / C_{(0)}] \quad (4.15)$$

where Q is the steady-state intestinal perfusate flow rate (cm^3/s) and the other terms are already defined. P_T calculated from Eq 4.15 is based on the fraction of permeant remaining in the intestinal segment at $x=l$. For the present in situ system we have a relatively short intestinal segment length, a relatively large ABL thickness, and relatively low diffusion coefficients. In this case, it is easy to anticipate that C_l/C_0 would be in the range of 0.7 to 0.9 with most of the results in the range of 0.8 to 0.9. For this situation, the uncertainties and errors in the calculation of P_T based on Eq 4.15 are expected to be up to 10 times greater than the P_T values calculated from Eq 4.10. For this reason, P_T results based on Eq 4.15 are not discussed here. A summary of an analysis of the P_T values based on Eq 4.15, however, is presented in Appendix A of this chapter.

4.4 Results and Discussion

4.4.1 Intestinal absorption

Fig 4.4 shows typical experimental results of the fractions of [^{14}C]-capric acid remaining in the ileal segment of length ~ 10 cm, $C_{(l)} / C_{(0)}$, in the absence and presence of 50 mM HPB. Here, in 20 minutes $C_{(l)} / C_{(0)}$ is seen to attain steady-state values of 0.7 and 0.9 in the absence and presence of 50 mM HPB, respectively. Fig 4.5 shows the cumulative amounts of [^{14}C]caprate transported into the blood for examples of caprate alone and caprate plus 50 mM HPB. Consistent with the results of Fig 4.4, these data also show steady-state of caprate absorption was generally attained in about 20 minutes

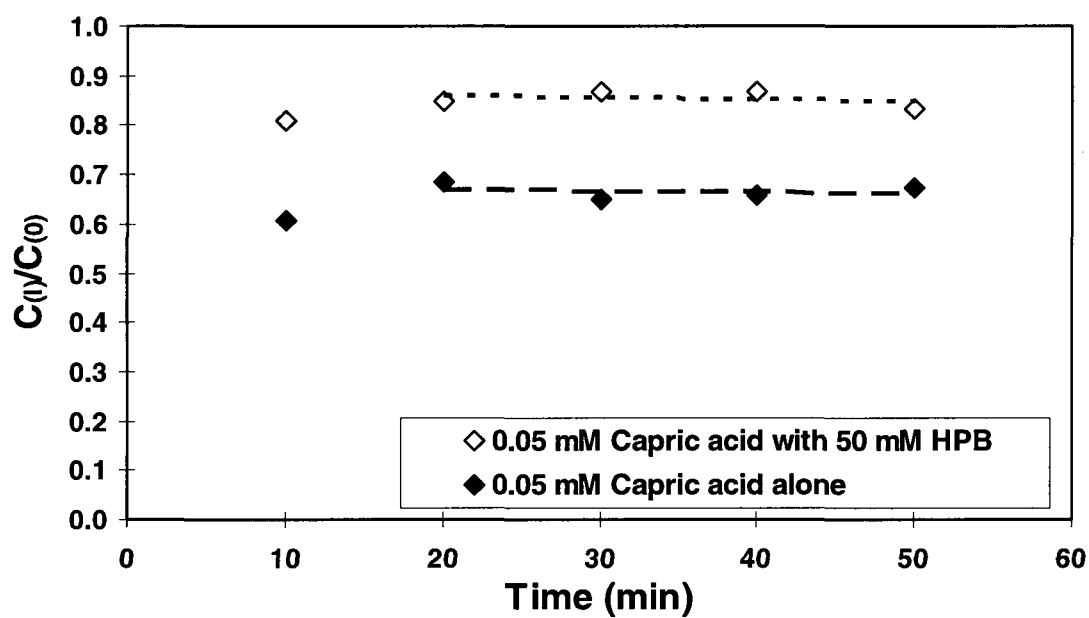


Fig 4.4 Representative plots of the fraction of caprate remaining in the intestinal lumen ($C(t)/C(0)$) for each 10 minute sample for capric acid alone (8.8 cm gut length) and capric acid in the presence of 50 mM HPB (10.0 cm gut length).

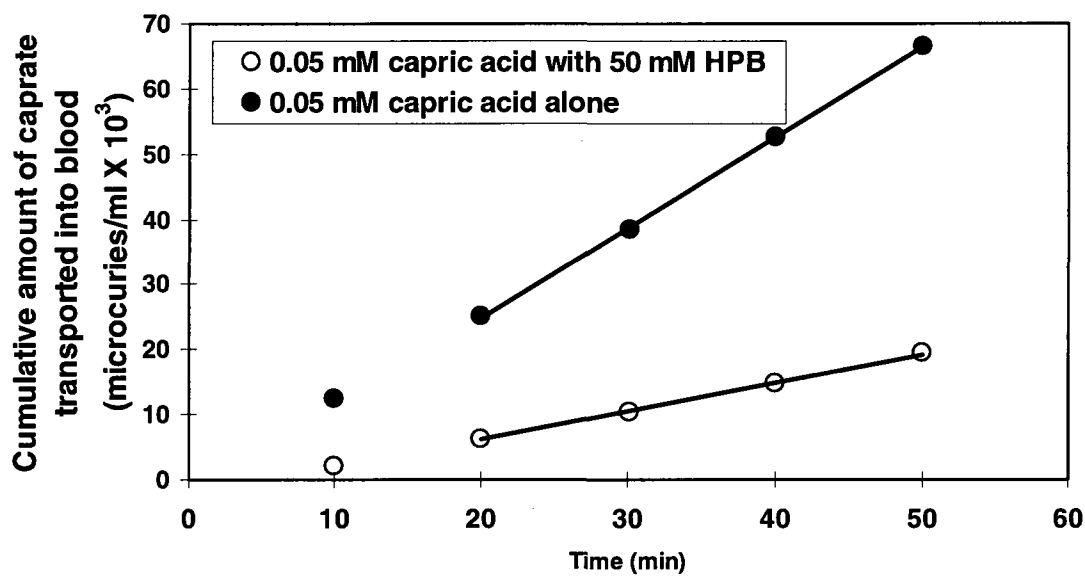


Fig 4.5 Representative plots of cumulative caprate appearance in blood as a function of time for capric acid alone and capric acid in the presence of 50 mM HPB. Note steady-state of absorption was reached in both cases in around 20 minutes.

and was essentially independent of the HPB concentration. The perfusion rate, the blood flow rate, and the osmotic pressure of the solution in the intestinal lumen were generally constant during an experiment and did not vary greatly from run to run (Figs 4.6 and 4.7). Water absorption/secretion was $\pm 5\%$ and inconsequential. Figs 4.4 to 4.7 represent typical displays from absorption studies conducted with 0.05 mM capric acid in HPB concentrations from 0 to 50 mM (i.e., molar ratios of [HPB]/[HA] ranging from 0 to 1000:1). Similar patterns as seen in Figs 4.4 through 4.7 were also observed in the [^{14}C]taurocholate experiments conducted with phosphate buffer at pH 7.4. Table 4.5 summarizes the flux of capric acid, the mean luminal concentration and the total permeability coefficient (calculated using Eq 4.10).

4.4.2 Analysis of the experimental P_T data **with the flat surface model (FSM)**

The principal outcomes of the FSM analysis of the experimental results are presented in Table 4.6 and Fig 4.8. The experimental P_T values (column 3 of Table 4.5) was best-fitted to Eq 4.12 in the following manner. As it was apparent from a preliminary analysis that, at low HPB concentrations (≤ 3.0 mM), capric acid absorption would be essentially 100% ABL controlled, a first approximation for the best h_{ABL} value was obtained based on this consideration. Then a first approximation of a best-fit value for $P_{i,FSM}$ was found using only the P_T results from the three highest HPB concentration experiments. Subsequent iterations employing all of the data did not significantly change these results. The best-fit h_{ABL} and $P_{i,FSM}$ values at the three lowest HPB concentrations, and the individual $P_{i,FSM}$ values at the three highest HPB concentrations are all presented in Table 4.6. The individual h_{ABL} values are in good agreement showing modest

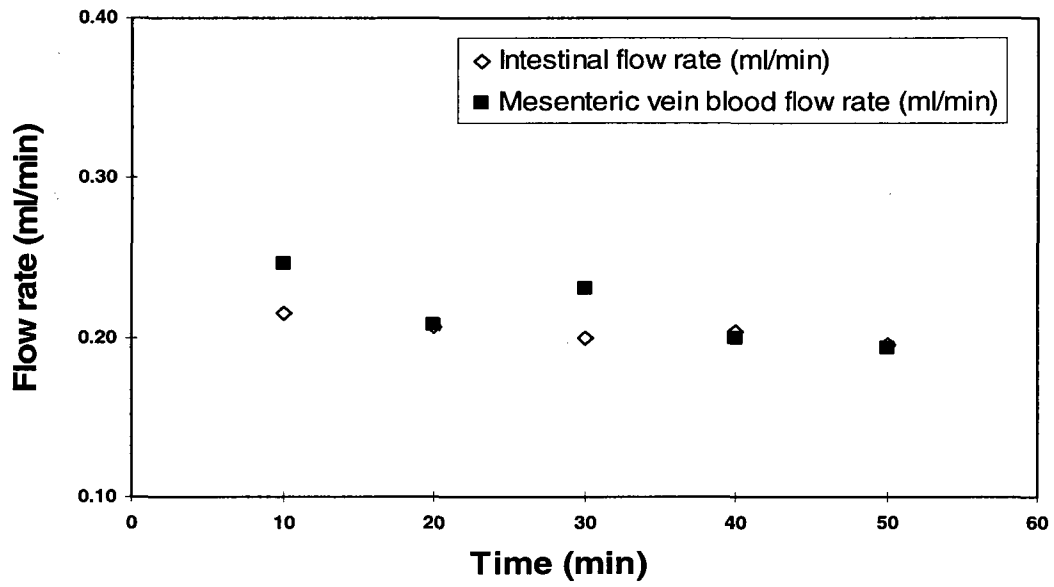


Fig 4.6 Intestinal perfusate flow rate of ^{14}C -caprate solution and blood flow rate out of the cannulated mesenteric vein for each 10 minute sample period. Data are from a typical experiment of 50 mM HPB.

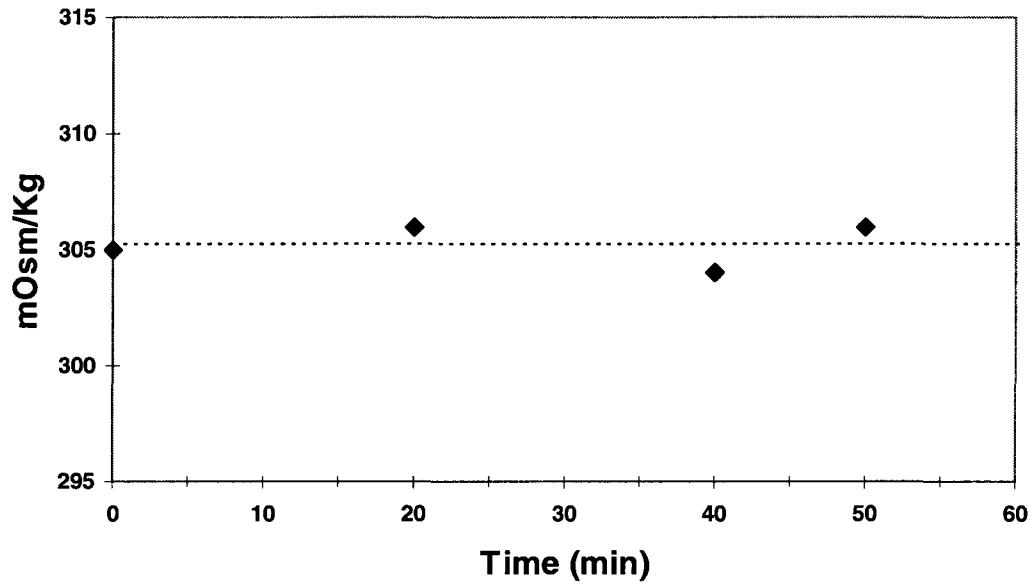


Fig 4.7 Representative plot of periodic determination of the osmolarity (mOsm/kg) of the perfusate from a typical experiment with caprate plus 50 mM HPB. The 0 minute time point represents the stock donor osmolarity.

Table 4.5 Experimentally determined flux (J_b) and total permeability coefficient (P_T) for caprate transport across the rat ileum in the presence or absence of hydroxypropyl- β -cyclodextrin (HPB), and for trace taurocholate alone. ($N \geq 3$)

| Species | HPB conc. | $J_b \times 10^9$ | $P_T \times 10^5$ |
|--------------|-----------|----------------------------|-------------------|
| | mM | moles/(cm ² ×s) | (cm/s) |
| Taurocholate | 0 | ***** | 5.50 (± 0.48) |
| Caprate | 0 | 2.88 (± 0.69) | 5.76 (± 1.37) |
| Caprate | 0.5 | 1.85 (± 0.35) | 3.69 (± 0.70) |
| Caprate | 3 | 1.45 (± 0.16) | 2.89 (± 0.31) |
| Caprate | 10 | 1.07 (± 0.24) | 2.14 (± 0.49) |
| Caprate | 30 | 1.01 (± 0.22) | 2.02 (± 0.43) |
| Caprate | 50 | 0.78 (± 0.25) | 1.56 (± 0.51) |

Table 4.6 Flat surface model (FSM) analysis of the influence of hydroxypropyl- β -cyclodextrin on the absorption of capric acid in the rat ileum at pH 7.4.

| Permeant | HPB conc. mM | $P_T \times 10^5$ (cm/s) ^a | F^u b | $D^{eff} \times 10^6$ cm ² /s ^b | h_{ABL} cm | $P_{i,FSM} F^u \times 10^5$ (cm/s) | $P_{i,FSM}$ (cm/s) | % ABL controlled ^{c,d} |
|--------------|-----------------|--|-----------------------|--|-----------------------|---------------------------------------|-----------------------|------------------------------------|
| Taurocholate | 0 | 5.5 (± 0.48) | 0 | 5.6 | 0.102 (± 0.010) | — | — | 100.0% |
| Capric acid | 0 | 5.8 (± 1.4) | 1.26×10^{-3} | 6.7 | 0.115 (± 0.027) | — | — | 98.9% |
| | 0.5 | 3.7 (± 0.7) | 5.75×10^{-4} | 4.7 | 0.126 (± 0.024) | — | — | 90.5% |
| | 3 | 2.9 (± 0.3) | 1.50×10^{-4} | 3.4 | 0.118 (± 0.013) | — | — | 96.7% |
| | 10 | 2.1 (± 0.5) | 4.85×10^{-5} | 3.1 | — | 9.8 | 2.0 (± 2.6) | 78.3% |
| | 30 | 2.0 (± 0.4) | 1.65×10^{-5} | 3.0 | — | 8.4 | 5.1 (± 3.5) | 76.3% |
| | 50 | 1.6 (± 0.5) | 1.26×10^{-5} | 3.0 | — | 4.6 | 3.7 (± 3.8) | 59.2% |
| | Best fit | — | — | — | 0.117 | — | 3.5 (1.7-10) | — |

a. $n=3$

b. F^u (fraction of free unionized capric acid) and D_{eff} (effective aqueous diffusion coefficient of capric acid-HPB systems) were calculated using experimentally-determined diffusion coefficients, pK_a and binding constants of capric- and caprate-HPB complex.

c. calculated $P_{ABL}^{eff} = D_{eff}/h_{ABL}$

d. Fraction ABL-controlled = P_T/P_{ABL}^{eff} where $P_{ABL}^{eff} = D_{eff}/h_{ABL}$

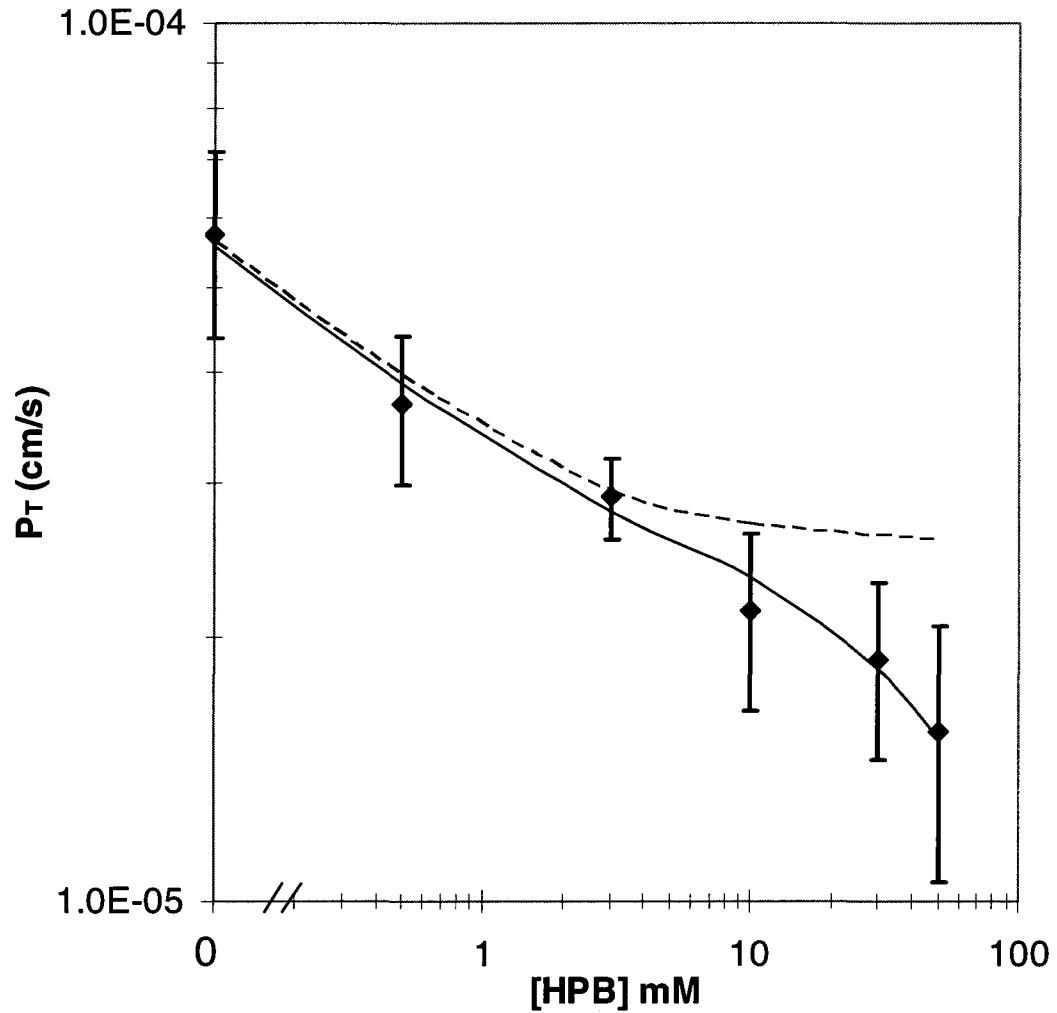


Fig 4.8 Comparison of experimental P_T values with FSM predictions. The solid curve depicts the best-fit FSM results employing the FSM-model parameters of Table 4.1. The dashed curve represents P_T values if 100 percent ABL-controlled over the entire range.

variability and good consistency with the reference value obtained with [^{14}C]taurocholate. The individual $P_{i,\text{FSM}}$ values show greater variability, as was expected. The capric acid absorption for the three highest HPB cases was still 78 to 59 percent ABL-controlled and was therefore still relatively insensitive to $P_{i,\text{FSM}}$. The large variability in the individual $P_{i,\text{FSM}}$ values also obscures any indication of a trend in $P_{i,\text{FSM}}$ with increasing membrane-controlled capric acid absorption (that would have been expected as discussed later in the villus model analysis). Nonetheless, the experimental P_T values correlate with the FSM deduced values reasonably well (see Fig. 4.8)

In applying the FSM it was assumed that the ABL can in fact be treated like a stagnant layer and that molecules cross the ABL by molecular diffusion only. It is important to note that all of the h_{ABL} values listed in column 6 of Table 4.6 are essentially the same within the data scatter while D_{eff} varied by almost a factor of two. This evidence supports the assumption implied in Eq (4.12) that the ABL can be treated as a stagnant diffusive layer for the molecules in the present study. If the ABL were to be characterized by a significant contribution from convective diffusion, the h_{ABL} determined would have been expected to have a dependence upon the diffusion coefficient to the n^{th} power (D^n)²⁹⁻³¹ where n may be a fraction greater than zero. Although the experimental error in the h_{ABL} values is too large to definitively state that there is no significant amount of convective diffusion in the ABL, the results suggest that transport across the ABL is predominantly diffusion-controlled and that convection does not contribute significantly to overall transport across the ABL, this supporting the appropriateness of the stagnant layer assumption inherent in Eq (4.12).

It is of interest to note that the $P_{i,FSM}$ for capric acid has been found to be 5-6 orders of magnitude larger than the P_{ABL} ; this is why absorption of capric acid from a solution of capric acid species alone would be essentially completely insensitive to $P_{i,FSM}$. At high HPB concentrations and a high pH of 7.4, however, F^u is sufficiently small that the product of $P_{i,FSM}$ and F^u is comparable to P_{ABL} ; this then affords reasonable sensitivity to $P_{i,FSM}$ (see Eq 4.12). This example illustrates that, although lipophilic weak acid molecules can have a very high intrinsic membrane permeability coefficient compared to the aqueous boundary layer permeability coefficient, by reducing F^u sufficiently (i.e., high HPB and high pH) an accurate $P_{i,FSM}$ determination may be possible. This also illustrates the important role played by HPB in obtaining $P_{i,FSM}$ values under experimental conditions that otherwise would have been insensitive to $P_{i,FSM}$. This role of cyclodextrins and other carriers to improve sensitivity of the determination of $P_{i,FSM}$ for lipophilic molecules has not, to our knowledge, been previously reported.

At this point it should be helpful to comment on the reasonableness of the intrinsic permeability coefficient deduced from the FSM ($P_{i,FSM}$), particularly in light of the large error bars (see Fig 4.8). An attempt can be made to examine the consistency of the $P_{i,FSM}$ value of 3.5 in Table 4.6, column 8 with data from the work of Ho et. al. who had obtained permeability coefficients of a series of n-alkanoic acids up to n-octanoic acid employing a modified Doluisio in situ technique using rat jejunal segments. By extrapolation of the shorter chain fatty acids, N. Ho has deduced a $P_{i,FSM}$ value for capric acid absorption in the rat jejunum (unpublished results) that appears to be within a factor of two of the $P_{i,FSM}$ value for capric acid transport in the ileum after the above 3.5 cm/s value is corrected for a) the effect of the presence of HPB and b) the effect of the

differences between the ileum and jejunum villus architecture. Details are presented in Appendix B. The closeness of the $P_{i,FSM}$ values for the ileum and the jejunum seems reasonable in light of the known constituent compositions of the ileum and the jejunum, especially those components associated with the lipoidal structures.

A final point of interest is that the goodness of fit of the FSM to experimental data (see Fig 4.8) provides an opportunity to examine the effects of HPB on the transport behavior of capric acid for equal thermodynamic activity of capric acid in the lumen (for example, as would be the case for considering saturated solutions of capric acid in the lumen; this consideration should be important in the formulation optimization of very low solubility lipophilic drugs). Fig 4.9 shows that the capric acid activity would drop by 98.9% across the ABL for the capric acid alone case compared to a 59.2% drop for the capric acid plus 50 mM HPB case. This would translate into a 37-fold increase in the surface thermodynamic activity (and therefore the flux) of capric acid in the presence of 50 mM HPB compared to the capric acid alone condition for equal capric acid thermodynamic activity conditions in the lumen. Fig 4.9 demonstrates that the HPB as a drug carrier can improve bioavailability for lipophilic permeants by increasing the surface thermodynamic activity of the permeant at the membrane surface by reducing the permeant concentration gradient across the ABL (See also Fig 3.8).

4.4.3 Analysis of the experimental results

with the villus model (VM)

The villus $P_{i,VM}$ values were deduced using the database of the fluxes of capric acid at 10, 30 and 50 mM: the kinetics are partially membrane-controlled, the effective permeability coefficients of the ABL, where h_{ABL} is 0.117, and the parameter values and

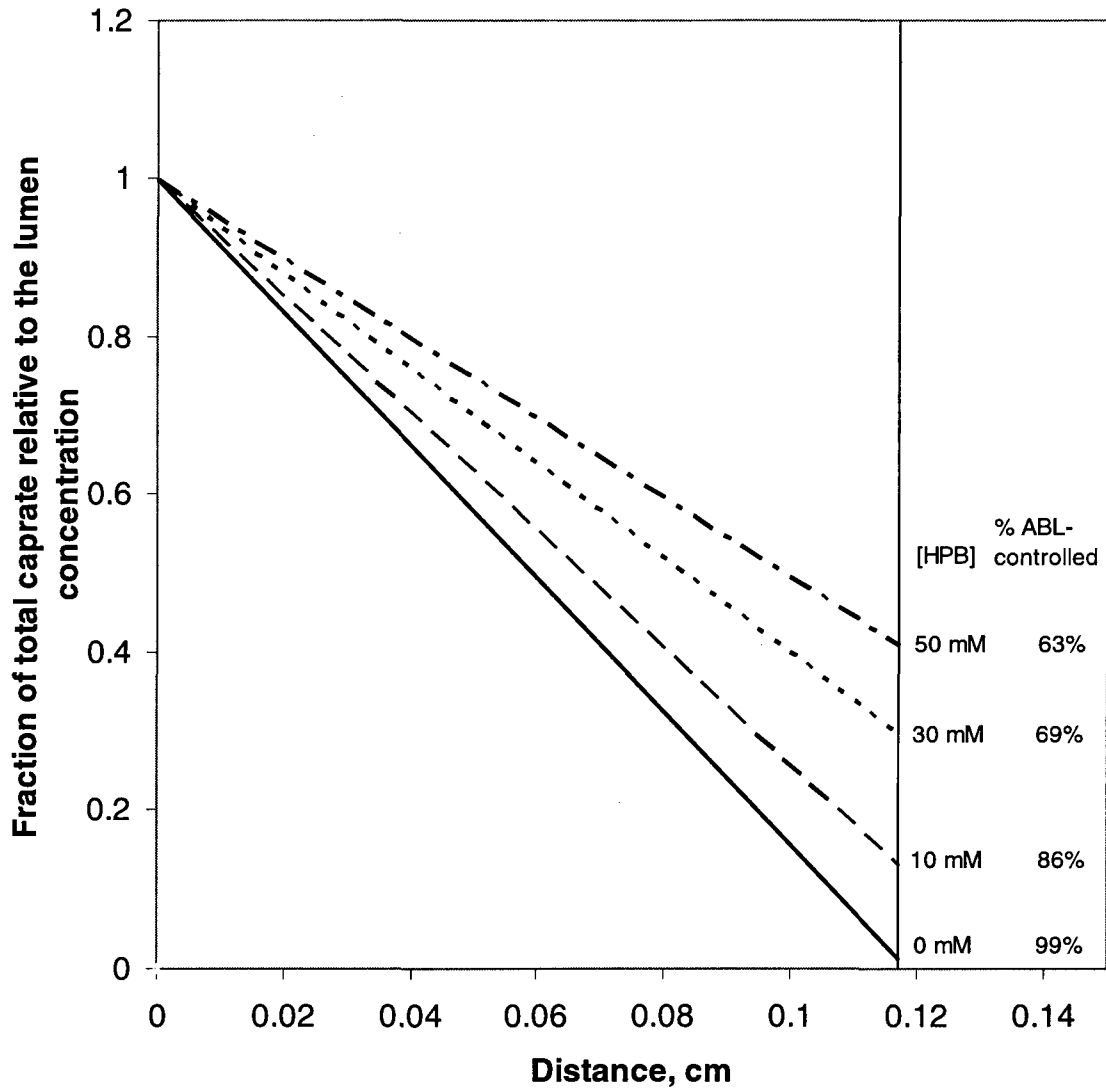


Fig 4.9 Relative concentration of total capric acid, expressed as a fraction of the luminal concentration, as a function of position in the ABL.

the conditions are given in Tables 4.1 – 4.3. The estimates of $P_{i,VM}$ ranged from 0.39 to 0.89 cm/s in the various cases (Table 4.7). The $P_{i,VM}$ by least squares fitting was found to be 0.48 cm/s which is 7-fold smaller than the $P_{i,FSM}$ of 3.5 cm/s because of the differences in the effective absorptive surface areas utilized. The VM-deduced P_T values are compared to experimentally determined values, and are presented in Fig 4.10. Model-deduced P_T values are found to be in good agreement with experimental P_T values for capric acid over the range of HPB concentrations studied with the model-deduced values falling within experimental error for all conditions. While the VM and the FSM both offer good predictability of P_T for capric acid at pH 7.4 over the range of HPB concentrations studied, the following discussion presents some important insights that are revealed from the VM analysis that would not be discernable from the FSM. The surface area based on the VM parameters (see Table 4.4) is 13.3 times greater than the inside surface area of a smooth, hollow cylinder (the FSM). The extent to which capric acid may utilize this surface area in the presence and absence of HPB is illustrated in the concentration-distance profiles in Fig 4.11. It has been previously demonstrated^{25,26} and is widely understood that highly permeable compounds are absorbed primarily at the villus tips. As can be seen in Fig 4.11, the VM demonstrates that capric acid alone behaves like other rapidly absorbed, highly lipophilic compounds. For this case the concentration gradient of capric acid decays rapidly across the ABL, with only about 5% of the original lumen concentration remaining at the tips of the villi; as the capric acid reaches the villi it is rapidly absorbed at the villi tips, and the concentration decays rapidly to zero in the initial portion of the intervillus space. Because of the rapid absorption at the tips, capric acid is not able to diffuse more than approximately

Table 4.7 VM analysis of the influence of HPB upon the absorption of capric acid in the rat ileum at pH 7.4

| [HPB] mM | $P_T \times 10^5$ (cm/s) | $P_{ABL} \times 10^5$ (cm/s) | $P_{T,VM}$ (cm/s) | %ABL-controlled from experimental P_T | Accessibility | Accessibility/accessibility at 0 mM HPB |
|-------------|-----------------------------|---------------------------------|----------------------|--|---------------|--|
| 0 | 5.76 | 4.64 | — | 102.1% | 0.126 | 1.00 |
| 0.5 | 3.69 | 3.97 | — | 92.9% | 0.147 | 1.17 |
| 3 | 2.89 | 2.93 | — | 98.6% | 0.227 | 1.81 |
| 10 | 2.14 | 2.66 | 0.39 (± 0.41) | 79.6% | 0.328 | 2.61 |
| 30 | 2.02 | 2.85 | 0.89 (± 0.79) | 72.2% | 0.508 | 4.04 |
| 50 | 1.56 | 2.56 | 0.48 (± 0.38) | 60.1% | 0.563 | 4.48 |
| Best fit | | | 0.48 (± 0.38) | | | |

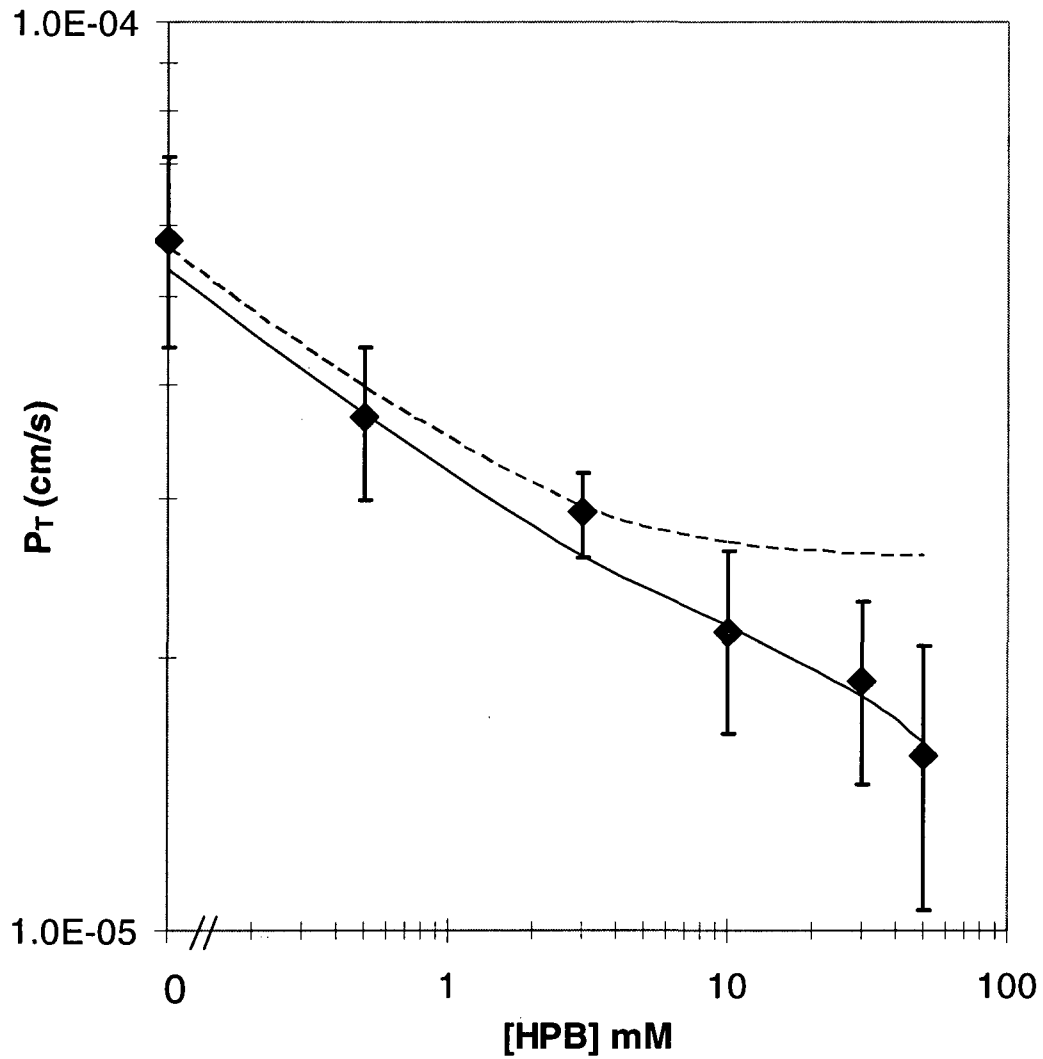


Fig 4.10 Log plot of experimentally determined permeability coefficients (P_T) for capric acid in the presence of 0-50 mM HPB. The solid line represents the best-fit VM results employing the VM-model parameters of Table 4.1. The dashed lines represent the P_{ABL} over the same range of HPB concentrations.

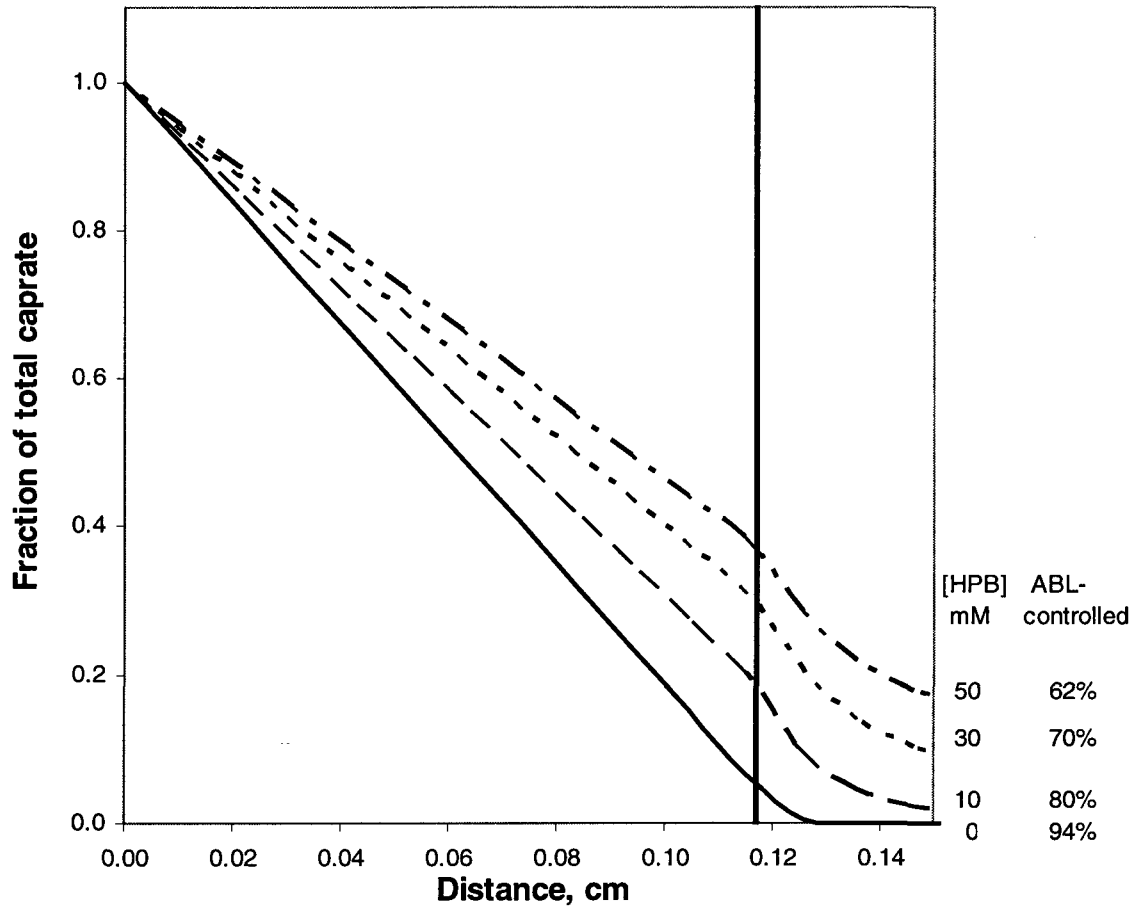


Fig 4.11 Fraction of total capric acid concentration versus distance across ABL and intervillus space. ABL thickness is 0.117 cm and villus height is 0.04 cm. Vertical line is ABL/villus tip interface, with the caprate concentration determined along a vertical line at the lateral villus surface extending upward to the ABL/lumen interface.

10% into the intervillus space, leaving the majority of the crypt cells un-utilized for absorption. With increasing HPB concentrations, however, the concentration gradient across the ABL is decreased. Additionally, more capric acid is able to penetrate further into the villus crypts. For the capric acid plus 50 mM HPB formulation, the total capric acid concentration at the tips is approximately 40% of that in the bulk, and the concentration at the bottom of the crypts is approximately one-half of the concentration at the tips of the villi.

A comparison of the capric acid concentration distributions for capric acid alone and capric acid plus 50 mM HPB using iso-concentration profiles (representing total caprate, with a constant incremental concentration change between successive curves within the villus unit) provides further insight into the absorption characteristics of capric acid in the rat ileum (see Figs 4.12 and 4.13). The comparison of the two figures is striking with respect to the differences in the slopes of the iso-concentration lines at and around the villus tips. For the case of the capric acid alone conditions, one can see that the caprate iso-concentration lines for the 0 mM HPB case are much more horizontally parallel than those of the 50 mM HPB case just above the villus tip, demonstrating much more vertical diffusion, with a significant fraction of the caprate being absorbed by the villus tip; this is due to the higher P_m in the absence of HPB. For the 50 mM HPB case (Fig 4.13), the lines are more curved (more vertically inclined) just above the villus tip, demonstrating that the flux is directed more laterally (toward the intervillus space), resulting in a greater fraction of the caprate entering and diffusing down the villus crypt, this due to the lower P_m for the 50 mM HPB case. The result is more caprate in the villus crypt, allowing the HPB conditions to take fuller advantage of the available absorptive

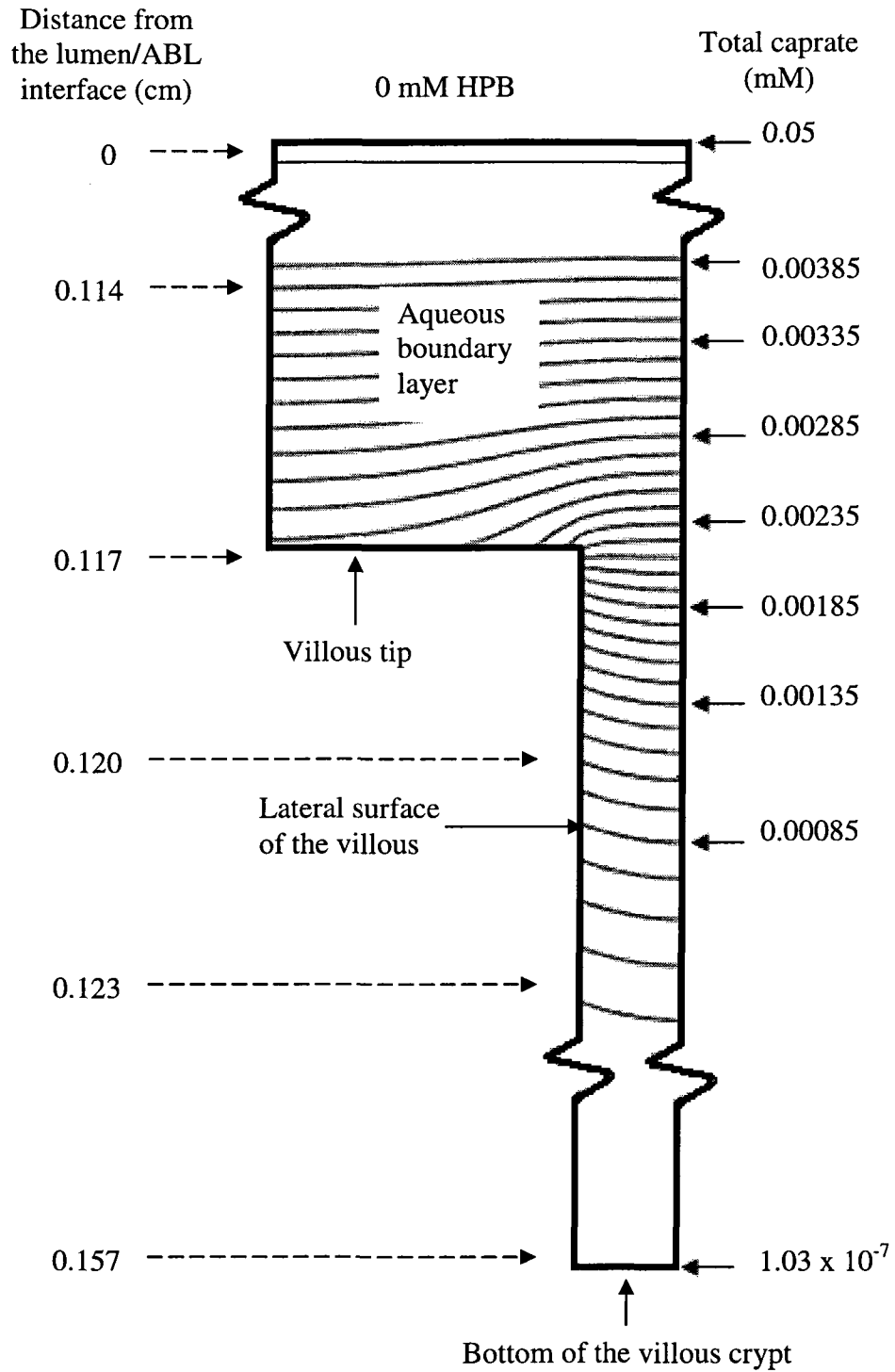


Fig 4.12 Iso-concentration profiles of caprate in the aqueous boundary layer and in the intervillus space for the 0.05 mM caprate alone condition.

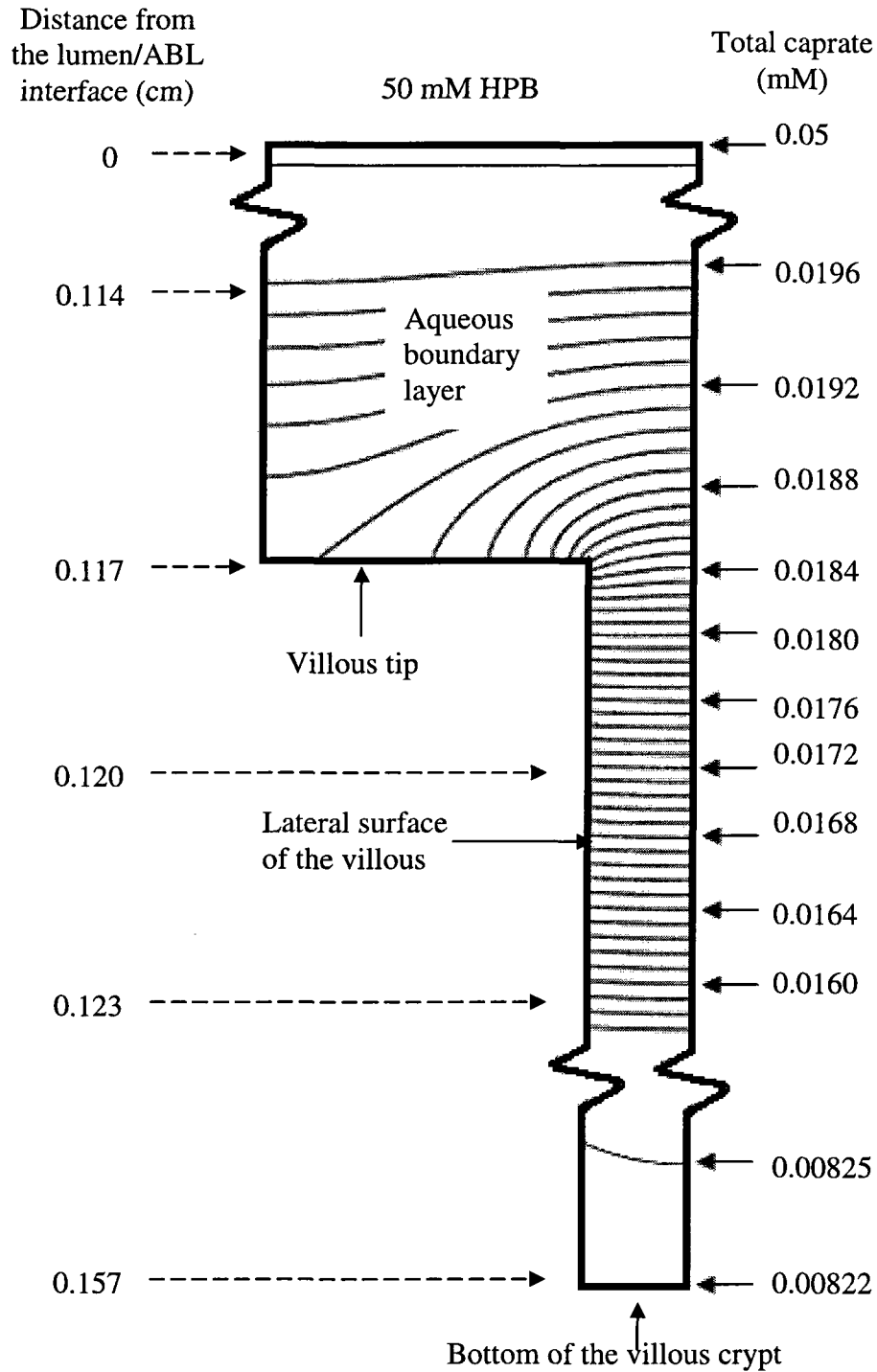


Fig 4.13 Iso-concentration profiles of caprate in the aqueous boundary layer and in the intervillus space for the 0.05 mM caprate + 50 mM HPB condition.

surface area at the lateral surface of the villus. Also of note is the flux and concentration gradient within the intervillus space. For the case of the 0 mM HPB (Fig 4.12), the flux decays rapidly as demonstrated by the rapidly increasing space between successive iso-concentration lines. This is consistent with the rapidly decaying caprate concentration seen in Fig 4.11 for the 0 mM case. Additionally, in the 0 mM HPB case there is an observable lateral concentration gradient within the intervillus space of about 5% from the middle of the intervillus space (far right side of the figure) to the lateral surface of the villus, this due to the absorptive surface of the villus. For the 50 mM HPB case, however, the flux decay in the intervillus space and the lateral concentration gradients are much less pronounced. This result was expected due to the carrier effect of the HPB present in the intervillus space, this providing the means for greater access of caprate to the lateral surfaces of the villus. Taken together with the VM, Figs 4.12 and 4.13 demonstrate that HPB acts as a carrier molecule for caprate not only across the ABL, but also into the intervillus space, allowing capric acid to more effectively access and utilize the surface area available for absorption.

A permeant's ability to access the various surface sites of the villi has been defined by Winne²⁵ and applied by Oliver et al.,²⁶ and it has been given the term accessibility. Accessibility is a means to quantify the extent to which a permeant utilizes the surface area available and is calculated by dividing the actual flux (J_{actual}) of the permeant by the flux that would occur if the surface concentration of the permeant was constant for all regions of the villi i.e., tip, lateral surface, and crypt ($J_{\text{SC,constant}}$). $J_{\text{SC,constant}}$ is determined by:

$$J_{SC, constant} = A_{vm} P_{i, VM} C_{s, tip}^u \quad (4.16)$$

where A_{VM} is the villus surface area (see Eq 4.4), $C_{s, tip}^u$ is the free capric acid species concentration at the villus tip, and $P_{i, VM}$ has been already defined. J_{actual} is the VM calculated flux. Accessibility was calculated for all the capric acid/HPB solutions using the VM (see Table 4.7, column 6). A comparison of the accessibilities for the different capric acid formulations quantitatively demonstrates what is already qualitatively understood from Figs 4.11, 4.12, and 4.13: that HPB improves the access of capric acid to the surface area in the villus crypts. For the case of the 50 mM HPB formulation, capric acid is able to access 4.5-fold more surface area than the capric acid alone formulation. It should be noted that accessibility increases with increasing concentration of HPB, and that 50 mM HPB allowed access of capric acid to slightly more than one-half of the total surface area available for absorption.

Additional insight is available from the accessibility value when we compare the VM to the FSM. The VM has 13.3 times more surface area than the FSM. Therefore, if we multiply the accessibility value determined from the VM by its surface area amplification factor (13.3), we can see how much surface area is effectively utilized for absorption as compared to the flat model (see Table 4.7). Making this comparison demonstrates why the $P_{i, VM}$ values obtained from the VM and the FSM differ by a factor of approximately 6. Column 7 in Table 4.7 shows that the more membrane-controlled conditions utilize much more surface area than would be predicted from the flat model.

Several investigators³²⁻³⁴ have pointed out that the effective ABL thickness in anesthetized animals may be much thicker than in unanesthetized animals due to the

influence of the anesthesia upon the intestinal motility. Yuasa et al.³⁵ reported a 2- to 3-fold thicker ABL thickness in anesthetized rats compared to unanesthetized rats in studies using a single pass perfusion technique with a flow rate of 0.16 ml/min in the rat jejunum. In order to examine how this may impact upon the principal conclusions of this chapter, caprate transport was also modeled with the VM under the condition where the h_{ABL} value was reduced 10-fold from 0.117 cm to 0.0117 cm (10-fold is much greater than that indicated in the study by Yuasa et al.³⁵). The VM simulation of capric acid concentration as a function of distance as with varying concentrations of HPB demonstrated that, as expected, each condition was more membrane-controlled than its counterpart with the thicker h_{ABL} (compare Figs 4.14 and 4.11). It is quite noteworthy that even for a very thin h_{ABL} condition the intervillus concentration of caprate and the accessibility of caprate to the membrane surface sites also increased significantly with increasing concentration of HPB. This exercise of comparing the thicker h_{ABL} results encountered in in situ experiments (Fig 4.11) to a thinner h_{ABL} expected in vivo (Fig 4.14) demonstrates that even for in vivo conditions the h_{ABL} is likely a significant transport barrier for highly permeable molecules such as capric acid. Additionally, this exercise shows that a carrier molecule such as HPB can markedly improve the membrane accessibility of rapidly absorbed compounds under in vivo conditions. This increased accessibility may become particularly useful when the molecule of interest is a membrane permeability enhancer (see Chapter 5).

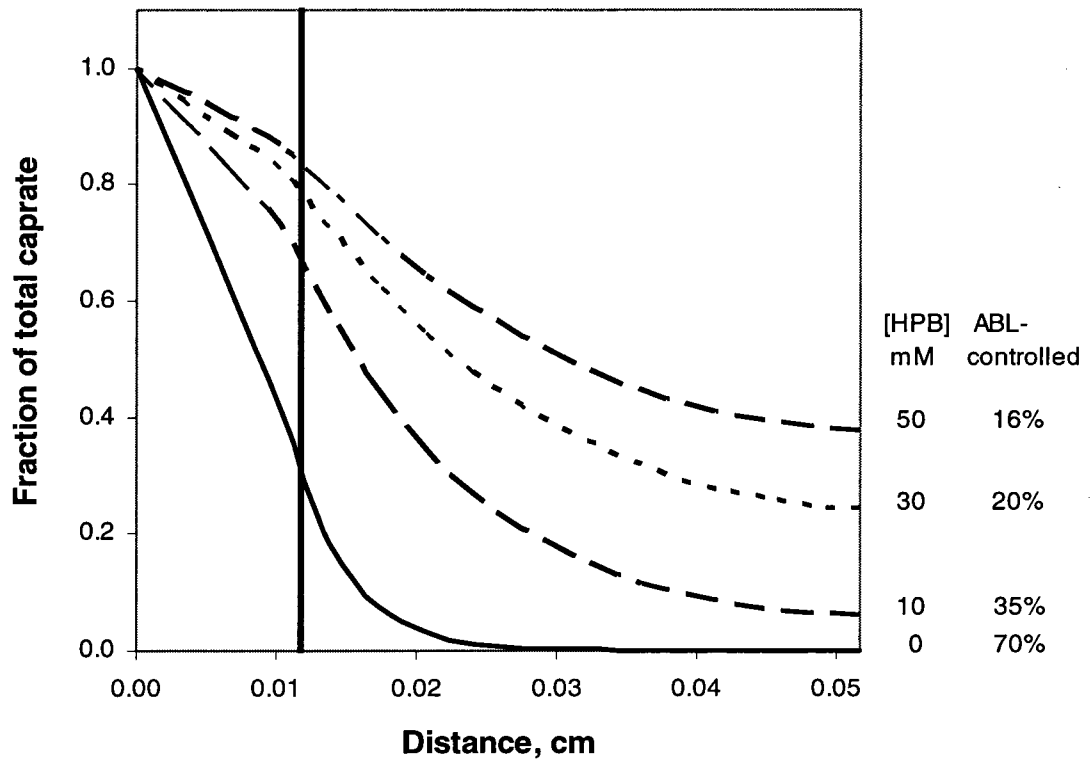


Fig 4.14 Fraction of total caprate concentration versus distance across the ABL and in the intervillus space, when $h_{ABL} = 0.0117$ cm ; all other parameter values are the same as in Fig 4.11. The vertical line is the ABL/villus tip interface.

4.4.4 A comparison of the villus model

(VM) to the flat surface model (FSM)

With respect to the goodness of fit of experimental data to model-predicted P_T values, the VM and the FSM models both predict P_T equally well. In light of the discussion above, however, the VM clearly provides additional valuable information concerning the intrinsic permeability coefficient values, effective surface area utilized for absorption, and extent of permeant penetration into the villus crypts. Although it is well understood that the small intestine contains villi which significantly increase the effective surface area available for absorption³⁶, the common approach for predicting permeability across the membranes of the small intestines simplify the gut as a hollow, smooth cylinder. The VM, however, utilizes a better first approximation to the morphology of the absorptive surface of the small intestine than does the FSM. In addition to the visually apparent differences between a smooth cylinder and the small intestine, there is also experimental evidence that the villus structure can play an important role in the presentation of chemical absorption enhancers to the absorptive surfaces of the small intestine. Utilizing capric acid as an enhancer for mannitol absorption in the rat ileum, it was found (see Chapter 5) that in the presence of 30 mM HPB a three- to four-fold higher capric acid flux is observed before any indication of mannitol permeability enhancement is seen as compared to capric acid alone. This experimental evidence suggests that a significantly greater surface area is effectively utilized for capric acid absorption in the presence of 30 mM HPB; this is consistent with the VM, but not with the FSM. For the above stated reasons, the VM appears to be a more useful model for quantitatively

investigating the effects of carrier molecules on the effectiveness of chemical enhancers, such as capric acid, on absorption rates of polar molecules in the small intestine.

4.5 Significance

The effects of HPB upon the absorption of a lipophilic permeant in the rat ileum were observed in this study, and the means for a quantitative interpretation of these effects have been presented. The VM and FSM demonstrated that HPB reduces the concentration gradient of the permeant across the ABL from the lumen to the membrane surface and increases the small intestinal membrane surface area utilized for absorption by allowing the permeant to penetrate deeper into the intervillus space and access additional surface area within the villus crypt that would otherwise would not have been available for absorption. Taking both of these effects into consideration, HPB has the potential to significantly increase the permeant flux in the ileum (for constant free permeant lumen concentration comparisons). That cyclodextrins can be effective absorption enhancers through their roles as carriers for high lipophilicity low solubility (BCS class 2) compounds has been previously demonstrated by others on a qualitative basis. The contribution of the present study has been to demonstrate the mechanism of absorption enhancement using the physical model approach and to experimentally test the model predictions employing capric acid as the highly lipophilic, ionizable permeant and HPB representing a cyclodextrin carrier molecule. The physical model approach utilized in this study has also demonstrated the complex interplay of key parameters and their relative contributions to overall permeant flux. An obvious practical application of this study would be in the use of the VM for predicting the optimum composition of

cyclodextrin-containing formulations for the oral administration of highly lipophilic drug molecules.

4.6 Appendix A

4.6.1 Analysis of the P_T results based on Eq 4.15

For reasons given in Section 4.3.4, no attempt has been made to include P_T values ($P_T=P_{T,e}$) deduced from Eq 4.15 for discussion. Here, we present the $P_{T,e}$ results and a brief summary of the impact of these results upon the conclusions in this chapter. It is to be noted that, for this appendix, $P_{T,e}$ is to represent P_T deduced from Eq 4.15 and $P_{T,b}$ that deduced from Eq 4.10

Table 4.8 shows all of the relevant experimental data and the results of the analysis. An initial concern was the large differences between the $P_{T,b}$ and $P_{T,e}$ values (column 9). It was apparent, however, that an approximately 10% adjustment in the ratio, $C_{(t)}/C_{(0)}$, was sufficient to yield P_T values for which $P_{T,b} = P_{T,e}$. Importantly, this adjustment corresponded to an average change in $P_{T,b}$ of only 7%, which is well within the data scatter and would not significantly impact upon the conclusions of this chapter.

Because these discrepancies, though small, appeared to be systematic, further tests were conducted with the syringe and polymer tubing system to determine whether any significant unexpected time dependences of glass or tubing adsorption might have occurred. It was determined from these additional experiments that there was no significant change in solution inflow concentration ($C_{(0)}$) as a function of time during the steady state absorption time frame (20-50 minutes) for any of the HA/HPB solutions.

Table 4.8 Analysis of P_T results calculated from Eq 4.15

| 1 | 2 | 3 | 4 | 5 | 6 | 7 | 8 | 9 | 10 | 11 |
|--------------------|-------------|----------------------------|----------------------------|-------------------------------------|---|--------------------------|--------------------------|------------------------------------|----------------------------------|--|
| Exp # | [HPB] mM | C ₍₀₎ DPM/ml | C _(t) DPM/ml | 2πr _l cm ² | J _b mol/min/cm ² ×10 ¹¹ | P _{T,b} cm/s | P _{T,e} cm/s | P _{T,e} /P _{T,b} | C _{(t)/C₍₀₎} | [C _{(t)/C₍₀₎]^{1/2}} |
| 261 | 0 | 78460 | 51760 | 11.1 | 17.9 | 7.30E-05 | 1.21E-04 | 1.66 | 0.66 | 0.77 |
| 279 | 0 | 65815 | 54376 | 7.5 | 18.5 | 6.17E-05 | 8.38E-05 | 1.36 | 0.83 | 0.87 |
| 401 | 0 | 80480 | 52806 | 8.8 | 10.3 | 4.20E-05 | 2.04E-04 | 4.86 | 0.66 | 0.88 |
| 403 | 0 | 70190 | 56053 | 8.8 | 13.7 | 5.12E-05 | 8.72E-05 | 1.70 | 0.8 | 0.87 |
| 360 | 0.5 | 52720 | 35993 | 14.5 | 10.9 | 4.35E-05 | 8.92E-05 | 2.05 | 0.68 | 0.81 |
| 361 | 0.5 | 53550 | 45060 | 7.5 | 8.1 | 2.95E-05 | 7.86E-05 | 2.66 | 0.84 | 0.93 |
| 362 | 0.5 | 53550 | 43776 | 8.3 | 10.2 | 3.77E-05 | 8.01E-05 | 2.12 | 0.82 | 0.91 |
| 405 | 3 | 65000 | 54296 | 8.8 | 8.5 | 3.11E-05 | 6.81E-05 | 2.19 | 0.84 | 0.92 |
| 406 | 3 | 64570 | 49653 | 12.6 | 7.0 | 2.67E-05 | 6.85E-05 | 2.57 | 0.77 | 0.90 |
| 354 | 10 | 55360 | 47870 | 8.2 | 5.2 | 1.85E-05 | 5.75E-05 | 3.11 | 0.87 | 0.95 |
| 355 | 10 | 55360 | 44263 | 13.8 | 7.3 | 2.70E-05 | 4.59E-05 | 1.70 | 0.8 | 0.89 |
| 356 | 10 | 55360 | 49536 | 7.5 | 5.3 | 1.86E-05 | 5.08E-05 | 2.73 | 0.9 | 0.96 |
| 339 | 30 | 61080 | 51333 | 15.1 | 6.1 | 2.16E-05 | 3.75E-05 | 1.74 | 0.84 | 0.90 |
| 340 | 30 | 61065 | 54255 | 10.7 | 6.4 | 2.08E-05 | 3.64E-05 | 1.75 | 0.89 | 0.93 |
| 349 | 30 | 76850 | 60010 | 11.8 | 3.9 | 1.43E-05 | 8.10E-05 | 5.66 | 0.78 | 0.94 |
| 350 | 30 | 76850 | 60193 | 13.2 | 7.1 | 2.72E-05 | 6.13E-05 | 2.25 | 0.78 | 0.89 |
| 351 | 30 | 135610 | 114656 | 10.1 | 5.2 | 1.81E-05 | 5.84E-05 | 3.23 | 0.85 | 0.94 |
| 352 | 30 | 131730 | 109883 | 11.6 | 6.0 | 1.90E-05 | 5.29E-05 | 2.78 | 0.83 | 0.92 |
| 353 | 30 | 80960 | 71030 | 10.6 | 3.2 | 1.05E-05 | 4.14E-05 | 3.94 | 0.88 | 0.96 |
| 262 | 50 | 174130 | 149153 | 12.6 | 2.7 | 9.79E-06 | 4.33E-05 | 4.42 | 0.86 | 0.96 |
| 363 | 50 | 52180 | 46451 | 9.2 | 5.0 | 1.77E-05 | 4.51E-05 | 2.55 | 0.89 | 0.95 |
| 364 | 50 | 52180 | 45300 | 9.2 | 5.4 | 1.92E-05 | 5.74E-05 | 2.99 | 0.87 | 0.95 |
| Average | | | | | | | | 2.73 | 0.82 | 0.91 |
| Standard Deviation | | | | | | | | 1.12 | 0.07 | 0.05 |

Table 4.8 Cont.

| 1 | 12 | 13 | 14 | 15 |
|--------------------|--------------------------------------|-----------------------|-----------------------|--|
| Exp # | $P'_T = P'_{T,b} = P'_{T,e}$ cm/s | % change in $P_{T,b}$ | % change in $P_{T,e}$ | % difference between $C_{(t)}/C_{(0)}$ and $[C_{(t)}/C_{(0)}]'$ |
| 261 | 7.89E-05 | -7% | 53% | 14% |
| 279 | 6.35E-05 | -3% | 32% | 4% |
| 401 | 4.89E-05 | -14% | 317% | 25% |
| 403 | 5.34E-05 | -4% | 63% | 8% |
| 360 | 4.75E-05 | -9% | 88% | 16% |
| 361 | 3.13E-05 | -6% | 151% | 10% |
| 362 | 3.97E-05 | -5% | 102% | 9% |
| 405 | 3.26E-05 | -5% | 109% | 8% |
| 406 | 2.88E-05 | -7% | 138% | 14% |
| 354 | 1.94E-05 | -4% | 197% | 9% |
| 355 | 2.86E-05 | -5% | 61% | 10% |
| 356 | 1.93E-05 | -4% | 163% | 6% |
| 339 | 2.32E-05 | -7% | 62% | 7% |
| 340 | 2.31E-05 | -10% | 58% | 4% |
| 349 | 1.63E-05 | -13% | 395% | 17% |
| 350 | 2.85E-05 | -5% | 115% | 13% |
| 351 | 1.98E-05 | -8% | 196% | 10% |
| 352 | 2.28E-05 | -17% | 132% | 10% |
| 353 | 1.19E-05 | -12% | 246% | 9% |
| 262 | 1.03E-05 | -5% | 318% | 11% |
| 363 | 1.82E-05 | -3% | 148% | 6% |
| 364 | 2.00E-05 | -4% | 188% | 8% |
| Average | | | | 10% |
| Standard Deviation | | | | 5% |

Table 4.8 Cont.

| Symbols | |
|-----------------------------|--|
| HPB | concentration of cyclodextrin |
| $C_{(0)}$ | the initial concentration of capric acid |
| $C_{(l)}$ | the exit concentration of capric acid from the lumen of the rat gut |
| $P_{T,b}$ | P_T based on Eq 4.10 |
| $P_{T,e}$ | P_T based on Eq 4.15 |
| $[C_{(l)}/C_{(0)}]'$ | is the adjusted $C_{(l)}/C_{(0)}$ ratio that will give $P_T = P'_{T,b} = P'_{T,e}$ where $P'_{T,b}$ and $P'_{T,e}$ are the adjusted new values for P_T based on Eq 4.10 and for Eq 4.15, respectively. |
| $P_T = P'_{T,b} = P'_{T,e}$ | the new permeability coefficient obtained from $[C_{(l)}/C_{(0)}]'$. |
| % change in $P_{T,b}$ | this represents the % difference between $P'_{T,b}$ and $P_{T,b}$ |
| % change in $P_{T,e}$ | this represents the % difference between $P_{T,e}$ and $P'_{T,e}$ |

4.7 Appendix B

4.7.1 Calculation permitting the comparison of capric acid absorption data in the ileum with jejunum data from Ho et al.³⁷

The purpose of this appendix is to examine whether the capric acid value of 3.5 cm/s deduced with the FSM in the present study is consistent with a $P_{i,FSM}$ value of 1.2 cm/s obtained by Ho et al. for capric acid absorption in the rat jejunum. Ho et al. investigated a series of n-alkanoic acids (butanoic to octanoic) employing a modified Doluisio in situ technique and deduced the capric acid $P_{i,FSM}$ value for the jejunum by extrapolating the $P_{i,FSM}$ data of the shorter chain fatty acids to carbon number of ten. The authors also showed that P_{pore} , the pore pathway (paracellular pathway) permeability coefficient was negligible in the pH range 6-7, for the longer chain fatty acids (including capric acid); therefore, $P_{i,FSM}$ of the longer chain fatty acids should be predominantly a measure of the transepithelial transport (lipoidal pathway).

A) to make this comparison, because in the present study the $P_{i,FSM}$ value of 3.5 was deduced in the presence of HPB, a correction for the effect of HPB upon $P_{i,FSM}$ must be considered. This correction is simply correcting for the accessibility ratio corresponding to the particular HPB concentration relative to the 0mM HPB concentration using the villus model (see Table 4.7). Let us take the specific case of 50 mM HPB, for which the accessibility ratio is 4.48. Hence

$$P_{i,FSM} = \frac{3.7}{4.48} \approx 0.8 \text{ cm/s}$$

for 0 mM HPB. Let us call this $P_{i,FSM,ileum}$.

B) Secondly, a “correction” for the differences in the villus unit geometry between that of the ileum and that of the jejunum must be considered in order to obtain the corresponding $P_{i,FSM}$ value for the jejunum (i.e., the $P_{i,FSM,jejunum}$) from $P_{i,FSM,ileum}$. This will require the use of the villus model. The geometrical dimensional values for the jejunum and the ileum are given by Table 4.9 and the areas corresponding to the various sites of the villus architecture are presented in Table 4.10. The strategy entails using the $P_{i,VM}$ value obtained for the ileum in the present study together with the geometrical parameters of the jejunum (Table 4.9 and Table 4.10) to calculate the “corrected” $P_{i,FSM,jejunum}$ value and then to see how close this value is to the $P_{i,FSM,jejunum}$ value of Ho et al. Several calculational steps are involved. 1) The ileum $P_{i,VM}$ (0.48 cm/s; see Table 4.1) is used in the VM together with the jejunum parameters (Tables 4.9 and 4.10) to obtain a model-calculated flux (J') of capric acid in the jejunum and a model-calculated free capric acid species concentration at the villus tip ($C_{s,tip}^u$) that together gives $J_{SC,constant}$ (Eq 4.16). 2) Using the $J_{SC,constant}$ and the J' , we then calculate the accessibility (0.10) for capric acid in the jejunum from

$$\text{accessibility} = \frac{J'}{J_{SC,constant}} \quad (4.17)$$

3) We now may calculate $P_{i,FSM,jejunum}$ using the following equation,

$$P_{i,FSM,jejunum} = (\text{accessibility})(A_{VM})(P_{i,VM}) \quad (4.18)$$

Table 4.9 Geometric villus parameters of the ileum and the jejunum.
From Oliver et al.

| Parameter | Jejunum (μm) | Ileum (μm) |
|---------------------------------|---------------------------|-------------------------|
| villus radius (tip radius) | 75 | 37 |
| radius of the intervillus space | 7-20 (use 12) | 12 |
| channel depth (villus height) | 577 | 399 |

values are in μm

Table 4.10 Intrinsic surface area (cm^2) per cm^2 of intestine.
From Oliver et al.

| Area | Jejunum | Ileum |
|--------------------|---------|-------|
| tip | 0.74 | 0.57 |
| lateral surface | 11.43 | 12.30 |
| crypt | 0.26 | 0.43 |
| total (A_{VM}) | 12.43 | 13.30 |

where accessibility = 0.10, AVM = 12.43 (Table 4.10), and $P_{i,VM} = 0.48$ (Table 4.1). Eq 4.18 gives a $P_{i,FSM,jejunum}$ value of 0.6 cm/s. This compares well with the $P_{i,FSM,jejunum}$ value of 1.2 cm/s of Ho et al.

4.8 Glossary

| <u>Notation</u> | <u>Definition</u> |
|----------------------|--|
| ABL | aqueous boundary layer |
| A_{FSM} | area of a smooth hollow cylinder for an ileal segment |
| A_{VM} | surface area of the villi ($13.3 \times$ the area of a smooth cylinder) |
| A_{tip} | area of the villus tip |
| A_{LS} | area of the villus lateral surface |
| A_{crypt} | area of the villus crypt |
| A^- | free caprate ion |
| $\langle C \rangle$ | logarithmic mean concentration in the ileal segment |
| $C_{(0)}$ | inflow permeant concentration |
| $C_{(l)}$ | outflow permeant concentration |
| C_i | concentration of the i^{th} species |
| C_T | total caprate concentration |
| $C_{s,tip}^u$ | total free caprate concentration at the villus tip |
| $C(x)$ | donor concentration at position X |
| C_S^u | the villus surface site concentration of free capric acid |
| $[C_{(l)}/C_{(0)}]'$ | the adjusted $C_{(l)}/C_{(0)}$ ratio that will give $P_T = P'_{T,b} = P'_{T,e}$ where $P'_{T,b}$ and $P'_{T,e}$ are the adjusted new values for P_T based on Eq 4.9 and for Eq 4.15, respectively. |
| D_i | diffusion coefficient of the i^{th} species |
| D^f | diffusion coefficient of free capric acid or of caprate ion |
| D^* | diffusion coefficient of capric acid•HPB complex or of the caprate ion•HPB complex |
| D^{eff} | effective diffusion coefficient |
| F^u | fraction of the free capric acid species |
| F^f | sum of the fractions of the capric acid and the caprate ion species |
| F^* | sum of the fractions of the HA•HPB and the A^- •HPB |

| | |
|--------------------------|---|
| | complexes |
| FSM | flat surface model |
| HA | capric acid |
| HPB | 2-hydroxypropyl- β -cyclodextrin |
| HPB _f | free 2-hydroxypropyl- β -cyclodextrin |
| HA•HPB | capric acid•2-hydroxypropyl- β -cyclodextrin complex |
| A ⁻ •HPB | caprate ion•2-hydroxypropyl- β -cyclodextrin complex |
| h _{ABL} | aqueous boundary layer thickness |
| h _v | villus height |
| J | flux |
| j | local flux |
| J _b | flux into blood |
| J(x) | flux at position X |
| J _{actual} | actual flux of the permeant |
| J _{SC,constant} | constant surface concentration of permeant at the tip, lateral surface, and crypt of the villi. |
| k ₁ | A ⁻ + HPB association rate constant, $1 \times 10^6 \text{ mM}^{-1} \text{ s}^{-1}$ |
| k ₂ | A ⁻ •HPB dissociation rate constant, $4 \times 10^5 \text{ s}^{-1}$ |
| k ₃ | HA + HPB association rate constant, $7.5 \times 10^6 \text{ mM}^{-1} \text{ s}^{-1}$ |
| k ₄ | HA•HPB dissociation rate constant, $1 \times 10^6 \text{ s}^{-1}$ |
| K ⁻ | caprate ion•HPB binding constant |
| K ^u | HA•HPB binding constant |
| l | length of the ileal segment |
| n | some fraction greater than zero |
| P _T | total permeability coefficient |
| P _i | intrinsic membrane permeability coefficient |
| P _{i,FSM} | P _i as determined from the FSM |
| P _{i,VM} | P _i as determined from the VM |
| P _{T,b} | the permeability coefficient determined by appearance into blood |

| | |
|---------------------------|---|
| $P'_{T,b}$ | is the adjusted $P_{T,b}$ that gives $P'_{T,b} = P'_{T,e}$ |
| $P_{T,e}$ | the permeability coefficient determined by the disappearance from the lumen |
| $P'_{T,e}$ | is the adjusted $P_{T,e}$ that gives $P'_{T,b} = P'_{T,e}$ |
| P_{ABL} | the ABL permeability coefficient in the absence of a carrier |
| P_{ABL}^{eff} | ABL permeability coefficient in the presence of a carrier |
| P_m | effective membrane permeability coefficient |
| Q | steady-state intestinal perfusate flow rate |
| r | inside radius of the intestinal segment |
| r_1 | villus radius |
| r_2 | radius of the villus and associated intervillus space |
| R | rate of formation of caprate or the disappearance rate of the caprate•HPB complex |
| $R_{VM/FSM}$ | surface area ratio of the VM to the FSM |
| VM | villus model |
| x | position in the lumen (0-1) |
| ΔpH | pH gradient |
| ∇ | the standard del (nabla) operator for cylindrical coordinates |
| β | buffer capacity |
| $\partial Q / \partial t$ | slope of cumulative amount vs. time (permeant flux) |
| ϕ | the angle in 3D cylindrical coordinates |

4.9 References

1. Brewster ME, Loftsson T 2007. Cyclodextrins as pharmaceutical solubilizers. *Adv Drug Deliv Rev* 59(7):645-666.
2. Loftsson T, Duchene D 2007. Cyclodextrins and their pharmaceutical applications. *Int J Pharm* 329(1-2):1-11.
3. Loftsson T, Vogensen SB, Brewster ME, Konradsdottir F 2007. Effects of cyclodextrins on drug delivery through biological membranes. *J Pharm Sci* 96(10):2532-2546.
4. Stella VJ, Rajewski RA 1997. Cyclodextrins: their future in drug formulation and delivery. *Pharm Res* 14(5):556-567.
5. Uekama K 2004. Design and evaluation of cyclodextrin-based drug formulation. *Chem Pharm Bull (Tokyo)* 52(8):900-915.
6. Arima H, Yunomae K, Hirayama F, Uekama K 2001. Contribution of P-glycoprotein to the enhancing effects of dimethyl-beta-cyclodextrin on oral bioavailability of tacrolimus. *J Pharmacol Exp Ther* 297(2):547-555.
7. Arima H, Yunomae K, Morikawa T, Hirayama F, Uekama K 2004. Contribution of cholesterol and phospholipids to inhibitory effect of dimethyl-beta-cyclodextrin on efflux function of P-glycoprotein and multidrug resistance-associated protein 2 in vinblastine-resistant Caco-2 cell monolayers. *Pharm Res* 21(4):625-634.
8. Matsubara K, Irie T, Uekama K 1997. Spectroscopic characterization of the inclusion complex of a luteinizing hormone-releasing hormone agonist, buserelin acetate, with dimethyl-beta-cyclodextrin. *Chem Pharm Bull (Tokyo)* 45(2):378-383.
9. Nagase Y, Arima H, Wada K, Sugawara T, Satoh H, Hirayama F, Uekama K 2003. Inhibitory effect of sulfobutyl ether beta-cyclodextrin on DY-9760e-induced cellular damage: In vitro and in vivo studies. *J Pharm Sci* 92(12):2466-2474.
10. Nagase Y, Hirata M, Wada K, Arima H, Hirayama F, Irie T, Kikuchi M, Uekama K 2001. Improvement of some pharmaceutical properties of DY-9760e by sulfobutyl ether beta-cyclodextrin. *Int J Pharm* 229(1-2):163-172.
11. Ono N, Arima H, Hirayama F, Uekama K 2001. A moderate interaction of maltosyl-alpha-cyclodextrin with Caco-2 cells in comparison with the parent cyclodextrin. *Biol Pharm Bull* 24(4):395-402.

12. Tokihiro K, Arima H, Tajiri S, Irie T, Hirayama F, Uekama K 2000. Improvement of subcutaneous bioavailability of insulin by sulphobutyl ether beta-cyclodextrin in rats. *J Pharm Pharmacol* 52(8):911-917.
13. Tokihiro K, Irie T, Uekama K 1997. Varying effects of cyclodextrin derivatives on aggregation and thermal behavior of insulin in aqueous solution. *Chem Pharm Bull (Tokyo)* 45(3):525-531.
14. Irie T, Uekama K 1997. Pharmaceutical applications of cyclodextrins. III. Toxicological issues and safety evaluation. *J Pharm Sci* 86(2):147-162.
15. Irie T, Uekama K 1999. Cyclodextrins in peptide and protein delivery. *Adv Drug Deliv Rev* 36(1):101-123.
16. Piel G, Piette M, Barillaro V, Castagne D, Evrard B, Delattre L 2007. Study of the relationship between lipid binding properties of cyclodextrins and their effect on the integrity of liposomes. *Int J Pharm* 338(1-2):35-42.
17. Davis ME, Brewster ME 2004. Cyclodextrin-based pharmaceuticals: past, present and future. *Nat Rev Drug Discov* 3(12):1023-1035.
18. Tsutsumi K, Li SK, Ghanem AH, Ho NF, Higuchi WI 2003. A systematic examination of the in vitro Ussing chamber and the in situ single-pass perfusion model systems in rat ileum permeation of model solutes. *J Pharm Sci* 92(2):344-359.
19. Tsutsumi K, Li SK, Hymas RV, Teng CL, Tillman LG, Hardee GE, Higuchi WI, Ho NFH 2008. Systematic studies on the paracellular permeation of model permeants and Oligonucleotides in the rat small intestine with chenodeoxycholate as enhancer. *J Pharm Sci* 97(1):350-367.
20. Butler JN. 1964. *Ionic Equilibrium: a Mathematical Approach*. Reading, Mass: Addison-Wesley. p 547.
21. Lucas M 1983. Determination of acid surface pH in vivo in rat proximal jejunum. *Gut* 24:734-739.
22. Podesta RB, Mettrick DF 1977. HCO_3^- and H^+ secretion in rat ileum in vivo. *Am J Physiol* 232(6):E574-579.
23. Ho NFH, Park JY, Ni PF, Higuchi WI 1983. Advancing quantitative and mechanistic approaches in interfacing gastrointestinal drug absorption studies in animals and humans. *Animal Models Oral Drug Delivery Man: In Situ In Vivo Approaches, [Symp]:27-106*.
24. Winne D 1978. The permeability coefficient of the wall of a villous membrane. *J Math Biol* 6(1):95-108.

25. Winne D 1989. Effect of villosity and distension on the absorptive and secretory flux in the small intestine. *J Theor Biol* 139(2):155-186.
26. Oliver RE, Jones AF, Rowland M 1998. What surface of the intestinal epithelium is effectively available to permeating drugs? *J Pharm Sci* 87(5):634-639.
27. Winne D, Markgraf I 1979. The longitudinal intraluminal concentration gradient in the perfused rat jejunum and the appropriate mean concentration for calculation of the absorption rate. *Naunyn Schmiedebergs Arch Pharmacol* 309(3):271-279.
28. Singhal D, Ho NF, Anderson BD 1998. Absorption and intestinal metabolism of purine dideoxynucleosides and an adenosine deaminase-activated prodrug of 2',3'-dideoxyinosine in the mesenteric vein cannulated rat ileum. *J Pharm Sci* 87(5):569-577.
29. Komiya I, Park JY, Kamani A, Ho NFH, Higuchi WI 1980. Quantitative mechanistic studies in simultaneous fluid flow and intestinal absorption using steroids as model solutes. *Int J Pharm* 4:249-262.
30. Levich VG. 1962. *Physicochemical hydrodynamics*. In Prentice-Hall EC, N.J.
31. Schlichting H. 1955. *Boundary layer theory*. In McGraw-Hill NY, N.Y.
32. Anderson BW, Levine AS, Levitt DG, Kneip JM, Levitt MD 1988. Physiological measurement of luminal stirring in perfused rat jejunum. *Am J Physiol* 254(6 Pt 1):G843-848.
33. Fagerholm U, Lennernäs H 1995. Experimental estimation of the effective unstirred water layer thickness in the human jejunum, and its importance in oral drug absorption. *Eur J of Pharm Sci* 3(5):247-253.
34. Levitt MD, Strocchi A, Levitt DG 1992. Human jejunal unstirred layer: evidence for extremely efficient luminal stirring. *Am J Physiol* 262(3 Pt 1):G593-596.
35. Yuasa H, Iga T, Hanano M, Watanabe J 1988. Comparative assessment of the resistance of the unstirred water layer to solute transport between two different intestinal perfusion systems. *Biochim Biophys Acta* 938(2):189-198.
36. DeSesso JM, Jacobson CF 2001. Anatomical and physiological parameters affecting gastrointestinal absorption in humans and rats. *Food and Chemical Toxicology* 39(3):209-228.
37. Ho NF, Park JY, Morozowich W, Higuchi WI. 1977. Physical model approach to the design of drugs with improved intestinal absorption. In Roche EB, editor *Design of biopharmaceutical properties through prodrugs and analogs*, Washington D.C.: APhA. p 147-156.

CHAPTER 5

EXPLORATORY STUDY OF THE ROLE OF CYCLODEXTRINS IN PRESENTING CHEMICAL ENHANCERS TO THE SURFACE OF THE RAT ILEUM USING THE IN SITU SINGLE PASS PERFUSION TECHNIQUE

5.1 Introduction

Effective gastrointestinal absorption of highly polar molecules is frequently limited by poor intestinal membrane permeability. Because high solubility, low permeability (BCS class III) molecules generally have low bioavailability, oral dosing formulations of such molecules are frequently not only inefficient, but generally have much higher inter- and intrasubject variability.¹⁻³ Recent efforts to improve intestinal membrane permeability, and therefore bioavailability, of BCS class III compounds have included, among other approaches, the use of membrane permeation-enhancing excipients. Compounds that have been studied for their membrane permeation-enhancing effects include ionic and non-ionic surfactants,⁴⁻¹³ bile salts,¹³⁻²⁴ fatty acids,²⁵⁻³³ glycerides,³⁴⁻⁴⁰ and others.^{4-7,41-43} Intestinal membrane permeation enhancers consist of a wide range of molecules with a variety of structures and mechanisms of action. Aungst et al.⁴⁴ believe that the three most important criteria for evaluating permeation enhancers are (1) how effective the permeation enhancer is for the drug of interest, (2) the potential

to cause toxicity, and (3) the mechanisms by which absorption is enhanced. Frequently, the toxicity of the enhancers themselves is the limiting factor in successful application of the permeation enhancer.^{6,45,46} The application of materials or methods that would limit enhancer toxicity and/or improve the enhancer's effectiveness would certainly improve the formulation characteristics and increase the likelihood that the formulation could become a marketable product. The present author proposes that the inclusion of cyclodextrin carrier molecules in enhancer formulations may provide a means of reducing the toxicity and increasing the effectiveness of the permeation enhancer. This chapter presents exploratory studies examining the hypothesis that including cyclodextrins in permeation-enhancing solutions for delivering BCS class III molecules can improve the characteristics of the system. Sulfobutyl ether- β -cyclodextrin (SBE), hydroxypropyl- β -cyclodextrin (HPB), and hydroxypropyl- γ -cyclodextrin (HPG) will be used to represent model cyclodextrin carriers; chenodeoxycholic acid (CDC), a typical un-conjugated bile acid, and capric acid (HA), a typical fatty acid, are the chemical enhancers; and mannitol is the surrogate for typical BCS class III drug molecules for the present study. We have believed there are at least two possible ways in which solubilizing agents/carriers like the cyclodextrins may be able to improve the performance of lipophilic enhancers such as CDC and capric acid. Firstly, lipophilic enhancers such as CDC and capric acid are absorbed rapidly in the intestinal tract because they possess very high values of membrane intrinsic permeability coefficients, and their transport would likely be close to being aqueous-boundary-layer-controlled. Thus, such compounds would have a relatively short half-life in the intestinal fluids (30 minutes) and this would limit their time of action as an enhancer in the intestinal tract.

Cyclodextrins that possess appropriate binding constant(s) for such enhancers may prolong their time of action in the intestinal tract by acting to provide a reservoir for the enhancer. In this way a larger total dose of enhancer can be administered, with the delivery of that dose to the surface being spread out over a longer period of time. It is expected that this behavior could potentially increase the enhancers overall effectiveness and utility. The second way in which cyclodextrins may aid in the performance of an enhancer is by permitting deeper penetration of the enhancer into the crypts (i.e., the space between the villi) of the villus structures. In Chapter 4 of this thesis we have already noted based on model calculations that penetration of capric acid into the crypt regions increases significantly with increasing HPB concentration (see Fig 4.11). Deeper penetration into the crypts is expected to permit more effective utilization of the total surface area of the intestinal membrane (due to increasing accessibility). This would likely mean having the same enhancer performance but with less membrane damage because lower steady-state concentrations would be required in the relevant microenvironments to obtain the same overall flux of the molecule of interest. Alternatively, this could mean having greater enhancer performance at the same steady-state enhancer concentrations in the villus tip environment. The combination of increased half-life and increased surface area accessibility of the enhancing agent due to cyclodextrin are hypothesized to provide synergistically beneficial effects on the presentation of the enhancing molecule to the surface, with the expectation of increased bioavailability of the BCS class III permeant at equal or less enhancer toxicity. The purpose of the present study was to experimentally explore several combinations of the above mentioned cyclodextrins and enhancers, to interpret the results employing the

physical model approach, and to assess the possibilities of this approach in formulation development of enhancer systems.

5.2 Overview

In order for the reader to more fully understand the author's approach and the evolution of thought that went into the design of the experiments presented in this study, we present here a chronology of research to date. This study occurred in parallel with the studies presented in Chapter 3 and Chapter 4. As such, the physical models developed in the previous chapters were not available at the time these studies were designed and carried out. Accordingly, these experiments should be considered to be exploratory in nature, designed to seek out appropriate enhancer-carrier combinations and concentrations that would be suitable for future more systematic, quantitative studies. Near the end of the experimental portions of the present study, the physical model results presented in Chapter 3 and Chapter 4 were completed and became available to aid in the interpretation of the experimental mannitol transport enhancement experiments.

Mannitol, a compound that is transported across the rat intestinal membrane via the paracellular route, was selected to be the permeant in the present study. The mannitol flux enhancement range-finding experiments in this study were designed with the approach of combining a cyclodextrin carrier with a permeation enhancer to find an enhancer-carrier combination that would be effective at enhancing mannitol flux in rat ileum. The three cyclodextrin carriers chosen for this study are 1) sulfobutyl ether- β -cyclodextrin (SBE), 2) hydroxypropyl- β -cyclodextrin (HPB), and 3) hydroxypropyl- γ -cyclodextrin (HPG). These three carriers were chosen because they have been shown by

others as likely not to cause rat intestinal membrane damage.⁴⁷⁻⁴⁹ It was important for the present study that the carrier would not damage the membrane so that the chemical enhancers used would be permitted to demonstrate their effect on mannitol transport without the results being compromised by membrane alteration/damage due to the carrier itself. The two enhancers chosen for this investigation, chenodeoxycholic acid (CDC) and capric acid (HA), were chosen because they had been previously studied by others as permeation enhancers for class III compounds. Additionally, because these enhancers are naturally occurring, they may have potential for future biological applications. The first combination studied was the CDC/SBE system. The second combination, selected based upon the findings with the CDC/SBE system, was the HA/HPB system. The third combination studied was the HA/HPG system, its selection based on the results of both the SBE/CDC and the HA/HPB studies.

As will be seen, the ability to utilize the physical model results to interpret the experimental results of these enhancer-carrier systems greatly aided in understanding the mechanistic aspect of the influence of carriers in the presentation of the enhancers to the intestinal surface. The complexity of the enhancer-carrier systems necessitated the use of an appropriate physical model to properly interpret the physical meaning of the experimental results.

5.3 Materials and Methods

5.3.1 Chemicals and reagents

For the in situ single pass perfusion system, the phosphate buffer solution consisted of 57 mM $\text{NaH}_2\text{PO}_4 \cdot \text{H}_2\text{O}$ in distilled water. The pH was adjusted to 7.4 with

NaOH and the final osmolarity was adjusted to 300 mOsm/Kg using Na₂SO₄. Capric acid, chenodeoxycolic acid, mannitol, and hydroxypropyl- γ -cyclodextrin were obtained from Sigma-Aldrich (St. Louis, MO). Sulfobutyl ether- β -cyclodextrin (Trade name Captisol) was obtained from CyDex Inc. (Lenexa, Kansas), and hydroxypropyl- β -cyclodextrin (Trade name Kleptose HPB) was obtained by a generous gift from Roquette America (Keokuk, IA). [¹⁴C]Mannitol, [¹⁴C]capric acid, and [¹⁴C]chenodeoxycholic acid were purchased from Moravek Biochemicals Inc. (Brea, CA). The purity of the radioisotopes was checked using high pressure liquid chromatography and found to be >97% pure. Solvable tissue solubilizer and Ultima Gold scintillation cocktail were obtained from PerkinElmer (Boston, MA). Other chemicals were \geq 98% pure.

5.3.2 Intestinal and mesenteric cannulation

The procedures used for the single pass perfusion experiments follow the procedures used by Tsutsumi et al.⁵⁰ with some modifications. Male Sprague-Dawley rats weighing 300-400 g for intestinal perfusion, or retired breeders for blood donation, were obtained from Charles River (Wilmington, MA) and were used under the approval of the Institutional Animal Care and Use Committee at the University of Utah. Rats had free access to food and water prior to the experiment. Details of the techniques involved in the intestinal cannulation, the mesenteric vein cannulation, and blood replacement from donor rats are described in detail in Chapter 4 of this thesis.

5.3.3 Intestinal perfusion

Perfusion of the solution through the intestinal segment was carried out at 0.2 ml/min. The perfusate and mesenteric venous blood samples were collected at 10 minute

intervals. Typical blood flow rates, perfusion outflow rates, and assay procedures were the same as those described in Chapter 4. Flux (J) and permeability coefficient (P_T) were determined using the employing the same methods described in Chapter 4.

5.3.3.1 CDC/SBE system

CDC/SBE solutions were prepared using 57 mM $\text{NaH}_2\text{PO}_4 \cdot \text{H}_2\text{O}$ and either 0 or 7.5 mM SBE. To this was added 0, 1.5, 2.5, 3, 5, 7.5, 10, 12.5, 13.75, or 15 mM cold CDC. The pH was then adjusted to 7.4 using NaOH and the osmotic pressure was adjusted to 300 ± 10 Osm/Kg using Na_2SO_4 . For mannitol permeability coefficient studies, 1-2 $\mu\text{Ci/ml}$ [^{14}C]mannitol and 0.05 mM cold mannitol were added to the solution, or for the CDC flux determination, 0.2-0.6 $\mu\text{Ci/ml}$ [^{14}C]CDC was added to the solution.

5.3.3.2 HA/HPB solution preparation

HA/HPB solutions were prepared using 57 mM $\text{NaH}_2\text{PO}_4 \cdot \text{H}_2\text{O}$ and either 0 or 30 mM HPB. To this was added 0, 2, 10, 12, 15, 20, 30, 35, 40, or 50 mM cold capric acid. The pH was then adjusted to 7.4 using NaOH and the osmotic pressure was adjusted to 300 ± 10 Osm/Kg using Na_2SO_4 . For mannitol permeability coefficient studies, 1-2 μCi [^{14}C]mannitol and 0.05 mM cold mannitol were added to the system, or for the capric acid flux determination, 0.2-0.6 μCi [^{14}C]capric acid was added to the system.

5.3.3.3 HA/HPG solution preparation

HA/HPG solutions were prepared using 57 mM $\text{NaH}_2\text{PO}_4 \cdot \text{H}_2\text{O}$ and either 0 or 30 mM HPG. To this was added 0, 2, 10, 12, 15, 20, 30, 35, 40, or 50 mM cold capric acid. The pH was then adjusted to 7.4 using NaOH and the osmotic pressure was adjusted to

300 \pm 10 Osm/Kg using Na₂SO₄. For mannitol permeability coefficient studies, 1-2 μ Ci/ml [¹⁴C]mannitol and 0.05 mM cold mannitol were added to the system, or for the capric acid flux determination, 0.2-0.6 μ Ci/ml [¹⁴C]capric acid was added to the system.

5.3.3.4 Villus model (VM) simulations

Finite-element simulations of permeant diffusion across the ABL and into the inter-villus space with drug absorption into a sink at the villus surface were performed with computer software FEMLAB (v3.0a, Comsol, Inc. Burlington, MA). The steady state diffusion analysis and 2D axial symmetry were used to model permeant absorption across the various sites of a single villus in the rat ileum. The idealized villus structure was based on previous work by Winne⁵¹, and the model parameters were obtained from Oliver et al.⁵² The villus model (VM) simulations were performed in the same manner and with the same parameters as in Chapter 4.

5.4 Results and Discussion

Because of the exploratory, range-finding nature of the present studies, many of the conditions represent only n=1 experiments. For those cases where multiple experiments were performed, error bars represent the standard deviation of those experiments. The experimental results for all enhancer-cyclodextrin systems are listed in Tables 5.1 and 5.2.

5.4.1 Enhancement of mannitol transport in the CDC/SBE system

SBE was chosen as a carrier to be investigated because it has been suggested^{47-49,53-55} to be the most likely among cyclodextrins not to cause membrane alteration or

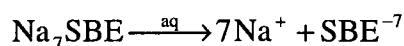
Table 5.1 Experimental results for chenodeoxycholate (CDC) alone and CDC plus sulfobutyl ether- β -cyclodextrin (CDC/SBE)

| System | [CDC] _{Total} (mM) | [Cyclodextrin] mM | [CDC] _{Free} (mM) | CDC flux (J) (moles/min/cm ²) | Mannitol P _T (cm/s) |
|---------|-----------------------------|-------------------|----------------------------|---|---|
| CDC | 0 | 0 | 0 | | $7.3 \times 10^{-7} \pm 3.8 \times 10^{-7}$ |
| CDC | 1.5 | 0 | 1.5 | $5.4 \times 10^{-9} \pm 1.1 \times 10^{-9}$ | $1.2 \times 10^{-6} \pm 7.6 \times 10^{-7}$ |
| CDC | 2.5 | 0 | 2.5 | $8.7 \times 10^{-9} \pm 1.7 \times 10^{-9}$ | $2.9 \times 10^{-6} \pm 5.6 \times 10^{-7}$ |
| CDC | 3 | 0 | 3 | $1.1 \times 10^{-8} \pm 2.6 \times 10^{-9}$ | $5.4 \times 10^{-6} \pm 1.9 \times 10^{-6}$ |
| CDC | 5 | 0 | 5 | $1.2 \times 10^{-8} \pm 2.3 \times 10^{-9}$ | $7.8 \times 10^{-6} \pm 1.7 \times 10^{-6}$ |
| CDC | 7.5 | 0 | 7.5 | $1.4 \times 10^{-8} \pm 3.4 \times 10^{-9}$ | $1.5 \times 10^{-5} \pm 2.4 \times 10^{-6}$ |
| CDC | 10 | 0 | 10 | $1.3 \times 10^{-8} \pm 3.4 \times 10^{-9}$ | $1.5 \times 10^{-5} \pm 3.4 \times 10^{-6}$ |
| CDC | 12.5 | 0 | 12.5 | $1.7 \times 10^{-8} \pm 3.8 \times 10^{-9}$ | $2.3 \times 10^{-5} \pm 8.3 \times 10^{-6}$ |
| CDC | 15 | 0 | 15 | $1.7 \times 10^{-8} \pm 4.8 \times 10^{-9}$ | $2.4 \times 10^{-5} \pm 1.8 \times 10^{-6}$ |
| CDC/SBE | 0 | 7.5 | | | $6.3 \times 10^{-7} \pm 2.7 \times 10^{-7}$ |
| CDC/SBE | 7.5 | 7.5 | 0.48 | $5.1 \times 10^{-9} \pm 1.3 \times 10^{-9}$ | $1.5 \times 10^{-6} \pm 9.9 \times 10^{-7}$ |
| CDC/SBE | 10 | 7.5 | 2.59 | $9.1 \times 10^{-9} \pm 2.1 \times 10^{-9}$ | $9.6 \times 10^{-6} \pm 3.6 \times 10^{-7}$ |
| CDC/SBE | 12.5 | 7.5 | 5.05 | $1.4 \times 10^{-8} \pm 2.1 \times 10^{-9}$ | $6.8 \times 10^{-6} \pm 4.4 \times 10^{-6}$ |
| CDC/SBE | 13.75 | 7.5 | 6.29 | $1.7 \times 10^{-8} \pm 1.2 \times 10^{-9}$ | $7.3 \times 10^{-6} \pm 2.7 \times 10^{-7}$ |
| CDC/SBE | 15 | 7.5 | 7.53 | $1.6 \times 10^{-8} \pm 3.6 \times 10^{-9}$ | $2.0 \times 10^{-5} \pm 8.9 \times 10^{-6}$ |

Table 5.2 Experimental results for capric acid (HA) alone, capric acid plus hydroxypropyl- β -cyclodextrin (HA/HPB), and capric acid plus hydroxypropyl- γ -cyclodextrin (HA/HPG).

| Condition | [Capric acid] _{Total} (mM) | [Cyclodextrin] mM | [Capric acid] _{Free} (mM) | Capric acid flux (J) (moles/min/cm ²) | Mannitol P _T (cm/s) |
|-----------|--|----------------------|---------------------------------------|--|---|
| HA | 0.05 | 0 | 0.05 | 1.8×10^{-10} | $7.3 \times 10^{-7} \pm 3.8 \times 10^{-7}$ |
| HA | 1 | 0 | 1 | 3.6×10^{-9} | |
| HA | 2 | 0 | 2 | 6.8×10^{-9} | 1.0×10^{-6} |
| HA | 5 | 0 | 5 | 2.0×10^{-8} | |
| HA | 10 | 0 | 10 | $4.3 \times 10^{-8} \pm 6.0 \times 10^{-9}$ | $2.6 \times 10^{-6} \pm 6.9 \times 10^{-7}$ |
| HA | 12 | 0 | 12 | 5.4×10^{-8} | $4.9 \times 10^{-6} \pm 1.5 \times 10^{-6}$ |
| HA | 15 | 0 | 15 | $5.1 \times 10^{-8} \pm 3.8 \times 10^{-9}$ | 8.1×10^{-6} |
| HA | 20 | 0 | 20 | 5.6×10^{-8} | 1.1×10^{-5} |
| HA | 50 | 0 | 50 | | 1.8×10^{-5} |
| HA/HPB | 0.05 | 30 | 0.00066 | | $7.2 \times 10^{-7} \pm 6.5 \times 10^{-7}$ |
| HA/HPB | 30 | 30 | 3.27 | $3.7 \times 10^{-8} \pm 1.9 \times 10^{-9}$ | $3.6 \times 10^{-6} \pm 2.8 \times 10^{-6}$ |
| HA/HPB | 35 | 30 | 6.69 | $6.7 \times 10^{-8} \pm 2.0 \times 10^{-9}$ | $9.9 \times 10^{-7} \pm 6.4 \times 10^{-7}$ |
| HA/HPB | 40 | 30 | 11.05 | $7.2 \times 10^{-8} \pm 3.2 \times 10^{-9}$ | 1.6×10^{-6} |
| HA/HPG | 0.05 | 30 | 0.0031 | | 8.3×10^{-7} |
| HA/HPG | 10 | 30 | 0.89 | $9.7 \times 10^{-9} \pm 3.2 \times 10^{-10}$ | |
| HA/HPG | 30 | 30 | 6.81 | $6.8 \times 10^{-8} \pm 5.4 \times 10^{-9}$ | $3.7 \times 10^{-6} \pm 2.6 \times 10^{-6}$ |
| HA/HPG | 35 | 30 | 10 | $7.7 \times 10^{-8} \pm 6.4 \times 10^{-9}$ | $6.5 \times 10^{-6} \pm 3.6 \times 10^{-6}$ |
| HA/HPG | 40 | 30 | 13.8 | $7.7 \times 10^{-8} \pm 4.3 \times 10^{-9}$ | $1.2 \times 10^{-5} \pm 7.1 \times 10^{-7}$ |
| HA/HPG | 50 | 30 | 22.45 | $7.9 \times 10^{-8} \pm 3.5 \times 10^{-9}$ | $1.7 \times 10^{-5} \pm 5.9 \times 10^{-6}$ |

damage. The seven negative charges (on average) of SBE were expected to help prevent lipid extraction from the surface of the ileal membrane. The dissociation of SBE in solution is demonstrated as follows.



Although the poly-anionic nature of SBE was expected to help prevent any significant membrane damage, the associated sodium ions contribute significantly to the overall osmolarity of the solution, which limits the SBE concentration that can be studied in iso-osmotic buffer solutions. CDC was chosen as an enhancer because it was previously shown to enhance mannitol transport in rat ileum without serious membrane damage for lumen CDC concentrations up to at least 12 mM.²⁴ It should be noted that the critical micelle concentration (CMC) for CDC is approximately 2.5 mM. SBE/CDC solutions with free concentrations of CDC above 2.5 mM would be a mixture of free monomeric CDC, micellar CDC, and/or the CDC•SBE complex, this increasing the complexity of the system.

The results of the mannitol transport studies as a function of CDC concentration for the CDC alone solution and the CDC plus 7.5 mM SBE solution are shown in Fig 5.1. The baseline mannitol transport rate was determined to be 7.3×10^{-7} cm/s. In the presence of 7.5 mM SBE, the mannitol transport rate was determined to be 6.3×10^{-7} , which was within experimental error of the baseline mannitol alone transport rate (see Table 5.1). These results support the conclusions of others that SBE does not cause membrane damage.^{47-49,53-55} They are also consistent with previous studies by the author that have

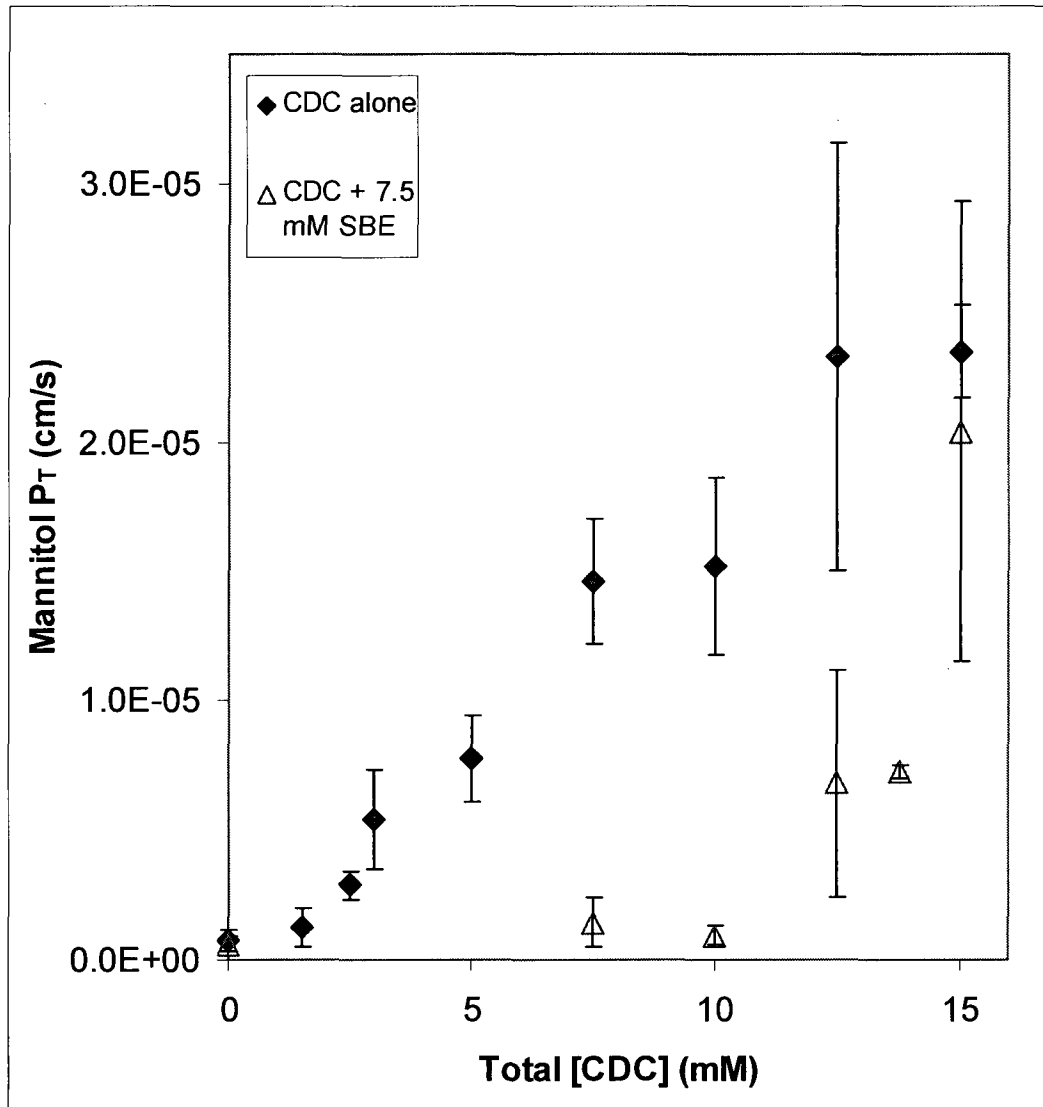


Fig 5.1 Mannitol permeability coefficients (P_T) for the rat ileum as a function of total sodium chenodeoxycholate (CDC) concentration in the presence and absence of 7.5 mM sulfobutyl ether- β -cyclodextrin (SBE).

demonstrated mannitol does not bind significantly with HPB cyclodextrin (see Chapter 3). All of this information taken together support the assumption that the mannitol enhancement observed from the various CDC/SBE solutions is a result of the enhancer action of CDC and not from any kind of direct SBE involvement in the mannitol transport across the rat ileum.

With respect to the enhancement of mannitol transport by CDC, it can be seen in Fig 5.1 that the presence of 7.5 mM SBE in the solution has resulted in the need to have a significantly higher concentration of CDC to achieve enhancement of mannitol transport across the rat ileum. Although SBE was expected to reduce the activity of CDC in solution due to the formation of the CDC• SBE complex, and therefore a greater concentration of total CDC in solution would be required to obtain a given mannitol enhancement factor, it was initially hoped that some degree of significant mannitol enhancement could be achieved using CDC concentrations at or below the SBE concentration of 7.5 mM. It was anticipated that the carrier effect of SBE would reduce the concentration gradient of CDC across the aqueous boundary layer (ABL) to some extent and this would partially offset the negative effect of decreased CDC activity (as observed with capric acid in the presence of HPB in Chapter 3 and Chapter 4). That 10 mM CDC in the presence of 7.5 mM SBE did not produce significant mannitol enhancement suggests that the binding constant between CDC and SBE was too great to allow for an effective enhancer concentration at the surface of the membrane. Experiments involving the transport of CDC across a perm-selective membrane⁵⁶ determined that the CDC• SBE binding constant was approximately 30 mM^{-1} (data not shown). This binding constant was much higher than anticipated and was believed to be

the reason CDC did not significantly enhance mannitol transport in the presence of 7.5 mM SBE for conditions below 12.5 mM CDC. As can be seen in Fig 5.1, significant mannitol enhancement did not occur until the CDC concentration exceeds the SBE concentration by 5 mM. Furthermore, because of the high CDC•SBE binding constant, it was suspected that the observed mannitol enhancement at the 12.5 mM and higher CDC concentrations in the presence of 7.5 mM SBE was induced by the CDC in excess of the CDC needed to form a one-to-one complex with all of the SBE present rather than by any contribution involving SBE as a carrier. Insight into this can be obtained from Fig 5.2, which presents mannitol enhancement as a function of the lumen concentration of free (i.e., uncomplexed) CDC. Based on this plot of the data, mannitol enhancement by CDC appears to be merely a function of free CDC concentration in the lumen, demonstrating that SBE offered no significant improvement of mannitol enhancement over the CDC alone system. Based on this interpretation of the data, it was believed that the CDC transport and the enhancing effects of CDC on the mannitol transport rate were governed primarily by the excess free CDC, and that the CDC•SBE complex was not contributing significantly to the presentation of CDC to the surface for mannitol enhancement. Fig 5.3 presents the mannitol permeability coefficient as a function of CDC flux. As can be seen, the CDC/SBE results are essentially superposed with the CDC alone results. These results were to be expected if one assumed that a flat membrane adequately represented the surface of the rat ileum (FSM of Chapter 4). It has been shown, however, that when taking the villus model (VM) into consideration, it was expected that the CDC alone and the CDC/SBE results presented in Fig 5.3 may not coincide if the surface area accessibility of CDC was significantly different (See Chapter

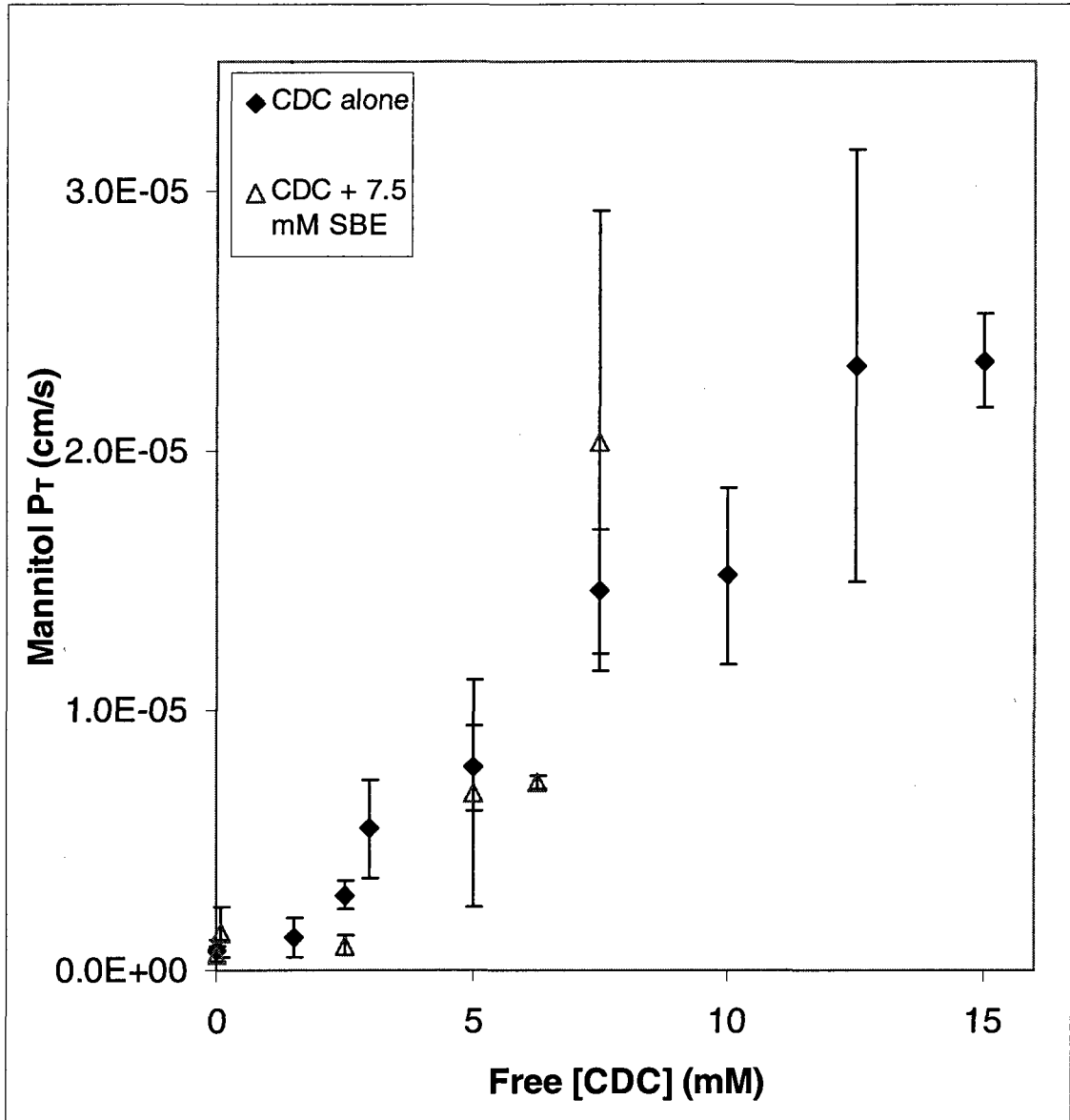


Fig 5.2 Mannitol permeability coefficients (P_T) for the rat ileum as a function of free sodium chenodeoxycholate (CDC) concentration in the lumen in the presence and absence of 7.5 mM sulfobutyl ether- β -cyclodextrin (SBE).

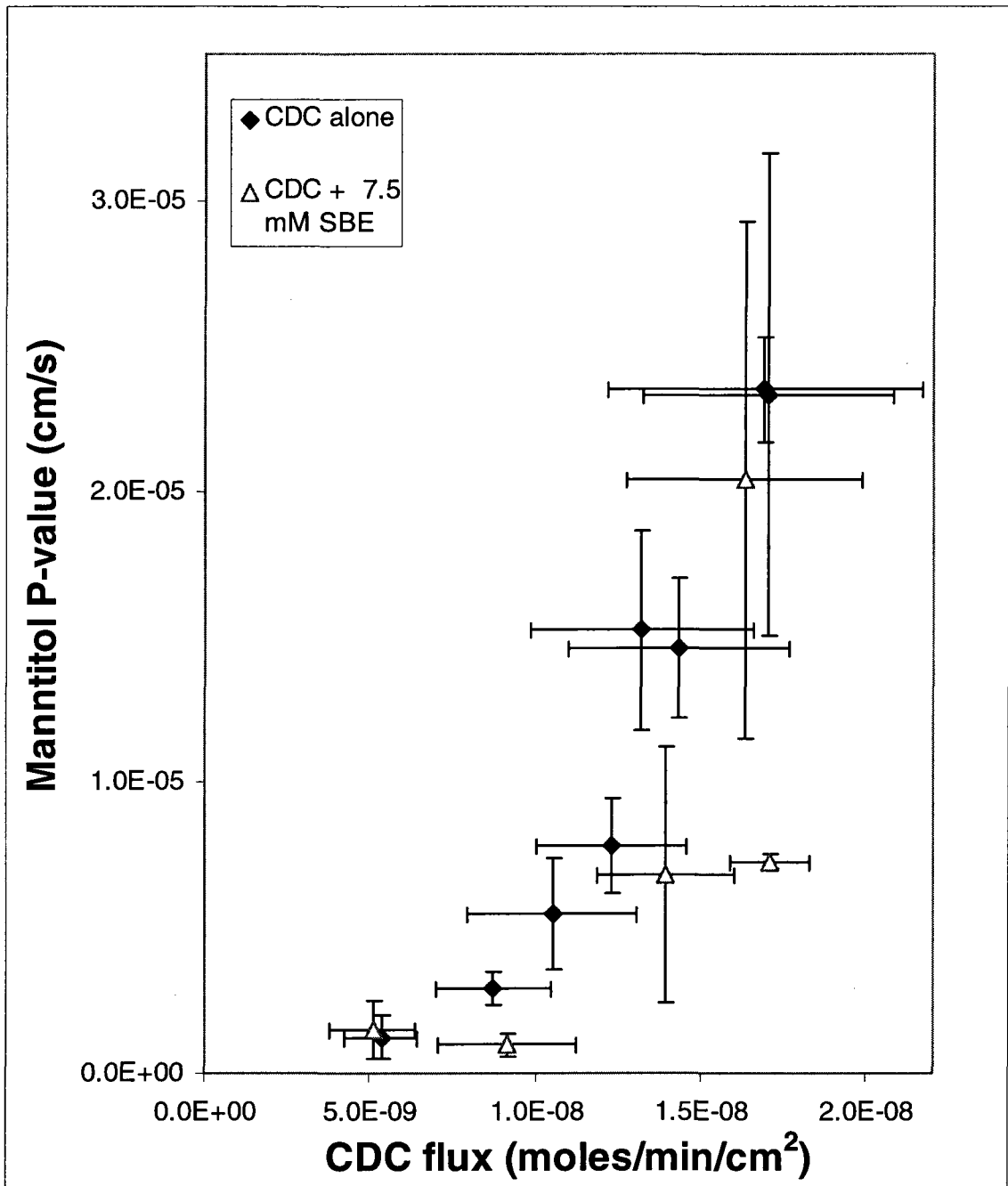


Fig 5.3 Mannitol permeability coefficients (P_T) as a function of sodium chenodeoxycholate (CDC) flux across the rat ileum in the presence and absence of 7.5 mM sulfobutyl ether- β -cyclodextrin (SBE).

4). In light of the villus model, the fact that the data points on Fig 5.3 for CDC alone and those for CDC/SBE are essentially superposed suggest that CDC is utilizing essentially the same amount of surface area for transport in both systems. Fig 5.4 demonstrates that the CDC flux vs. free CDC lumen concentration (bulk activity) data for the two solutions being compared again superpose in the data plots. These results suggest that including 7.5 mM SBE in a formulation does not increase the CDC flux for constant activity comparisons. This interpretation of the data presented in Fig 5.4 is consistent with the interpretation of the data presented in Figs 5.1-5.3: that the very high binding constant of the CDC•SBE complex prevented effective concentrations of the enhancer from being presented to the membrane surface for 7.5 mM SBE systems with CDC concentrations below 12.5 mM. The mannitol enhancement observed for the 12.5, 13.75, and 15 mM CDC conditions in the presence of 7.5 mM SBE has likely resulted primarily from the excess CDC in the solution rather than from any advantageous effect of including SBE in the solution. In theory, one could foresee using equal concentrations of CDC and SBE that were high enough to present effective enhancer concentrations at the surface of the ileum, but such concentrations of CDC and SBE required to achieve this result are likely to be very high. Due to the significant influence the poly-anionic SBE on the osmolarity of the solution, practical constraints prevent us from increasing the concentration much higher than 7.5 mM without sustaining detrimental consequences to the buffer capacity and/or the isotonicity of the system. Accordingly, at this point in the research, an enhancer-cyclodextrin system was sought that did not have the concentration constraints of the CDC/SBE system and that possessed a lower binding constant.

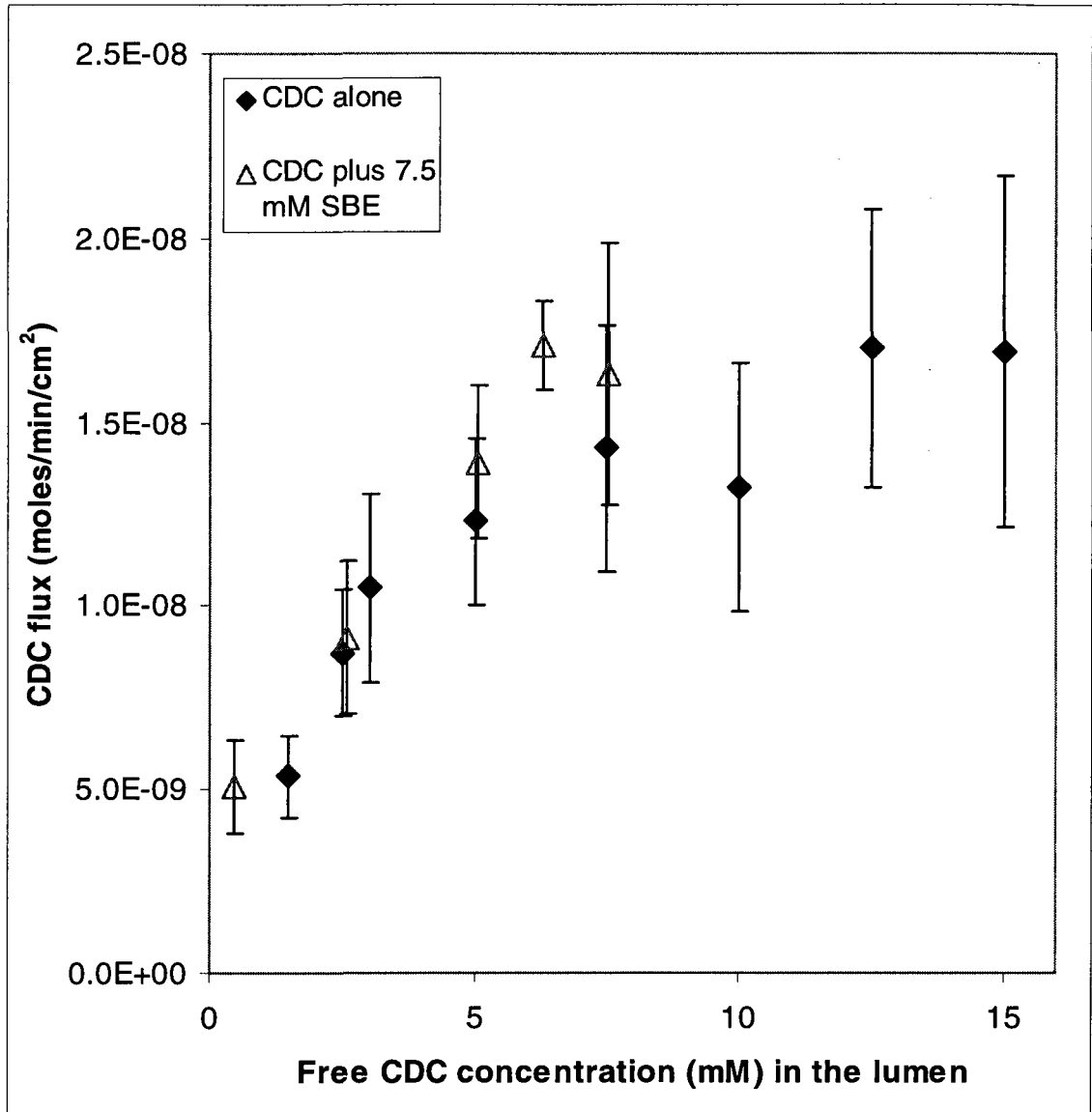


Fig 5.4 Sodium chenodeoxycholate (CDC) flux across the rat ileum as a function of free CDC concentration in the lumen in the presence and absence of 7.5 mM sulfobutyl ether- β -cyclodextrin (SBE).

With respect to interpreting the CDC/SBE system with the VM, unfortunately a reliable intrinsic permeability coefficient value for CDC was not attainable because the actively transported CDC was ABL controlled and, therefore, not sensitive to an accurate determination of the CDC intrinsic permeability coefficient from membrane transport experiments. Unfortunately, therefore, the VM discussion in Section 5.4.4 are limited to the HA/HPB and the HA/HPG systems.

5.4.2 HA/HPB enhancer-carrier system for

the enhancement of mannitol transport

The second cyclodextrin carrier selected for enhancer-carrier studies was hydroxypropyl- β -cyclodextrin (HPB). This carrier was selected because it has been demonstrated by others not likely to cause membrane damage⁴⁷⁻⁴⁹ and because solutions containing the neutral but highly polar HPB would be less osmotically constrained than the poly-anionic SBE carrier. Capric acid (HA) was selected as the second enhancer to study because we anticipated that HA•HPB would have a lower binding constant than the SBE•CDC complex. Preliminary binding constant experiments using the perm-selective membrane transport method confirmed that the HA•HPB binding constant was approximately 10 times lower than the SBE•CDC binding constant (this was thought to be encouraging). The CMC of capric acid was experimentally determined using the perm-selective membrane transport experiments⁵⁶ and found to be approximately 35 mM (data not shown), which allowed for significantly high free capric acid concentrations in buffer without forming micelles. Additionally, the capric acid half-life in the rat ileum for the HA/HPB system was determined to be 2.9 times longer than capric acid alone

case (see Table 5.3). Based on the characteristics of capric acid and HPB, we anticipated more interesting results with this enhancer-carrier system than with the CDC/SBE system. The mannitol permeability coefficients as a function of capric acid concentration in the presence and absence of 30 mM HPB are presented in Fig 5.5. As can be seen, capric acid alone enhanced mannitol transport for concentrations above 10 mM capric acid. For the mannitol transport enhancement experiments involving 30 mM HPB, significant enhancement did not occur with up to 40 mM capric acid. Drawing your attention to the 30 mM capric acid plus 30 mM HPB data point in Fig 5.5, there was evidence of some mannitol transport enhancement for this situation. This experiment was repeated $n=4$, with two experiments yielding baseline mannitol transport results and two experiments yielding enhanced mannitol transport results (as demonstrated by the large error bars). This leaves the interpretation of the results for this particular situation somewhat inconclusive; however the lack of enhancement for the higher capric acid concentrations in the presence of 30 mM HPB suggests that the two experiments resulting in elevated mannitol transport may have been outliers rather than representative experiments. Capric acid concentrations higher than 30 mM HPB were not studied. This decision not to examine higher capric acid concentrations in the presence of 30 mM HPB was unfortunate as can be understood from the discussion to follow. Fig 5.6 presents an examination of the relationship of mannitol permeability coefficients to capric acid flux. Unlike the CDC/SBE system (see Fig 5.3) the results with the HA/HPB system do not superpose. Based on the results in Chapters 3 and 4, in the case of a smooth surface (FSM), the capric acid flux should be proportional to the capric acid species surface concentration; and also because it is reasonable to expect that enhancer action may be a

Table 5.3 Relative half-life in rat ileum for capric acid (HA) alone, in the presence of 30 mM hydroxypropyl- β -cyclodextrin (HPB) and in the presence of 30 mM hydroxypropyl- γ -cyclodextrin (HPG). The relative half-life was determined by dividing the HA alone P_T value by P_T value for the situation of interest.

| Condition | P_T (cm/s) | Relative half-life ($t_{1/2}$) (for trace HA conditions) |
|-----------|----------------------|---|
| HA alone | 5.8×10^{-5} | 1.0 |
| 30 mM HPG | 2.4×10^{-5} | 2.4 |
| 30 mM HPB | 2.0×10^{-5} | 2.9 |

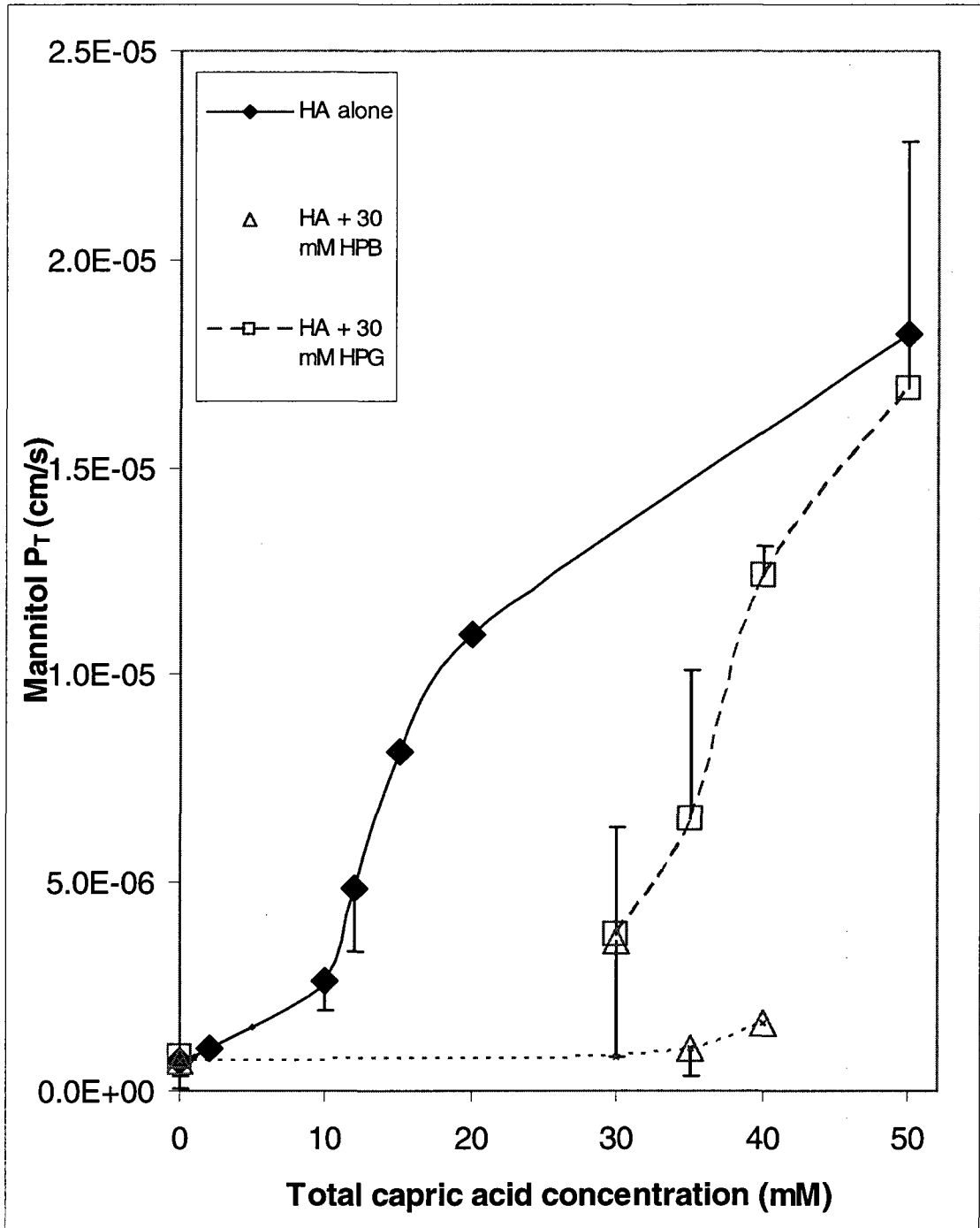


Fig 5.5 Mannitol permeability coefficients (P_T) for the rat ileum as a function of total capric acid (HA) concentration for capric acid alone and capric acid plus 30 mM hydroxypropyl- β -cyclodextrin (HPB) or 30 mM hydroxypropyl- γ -cyclodextrin (HPG).

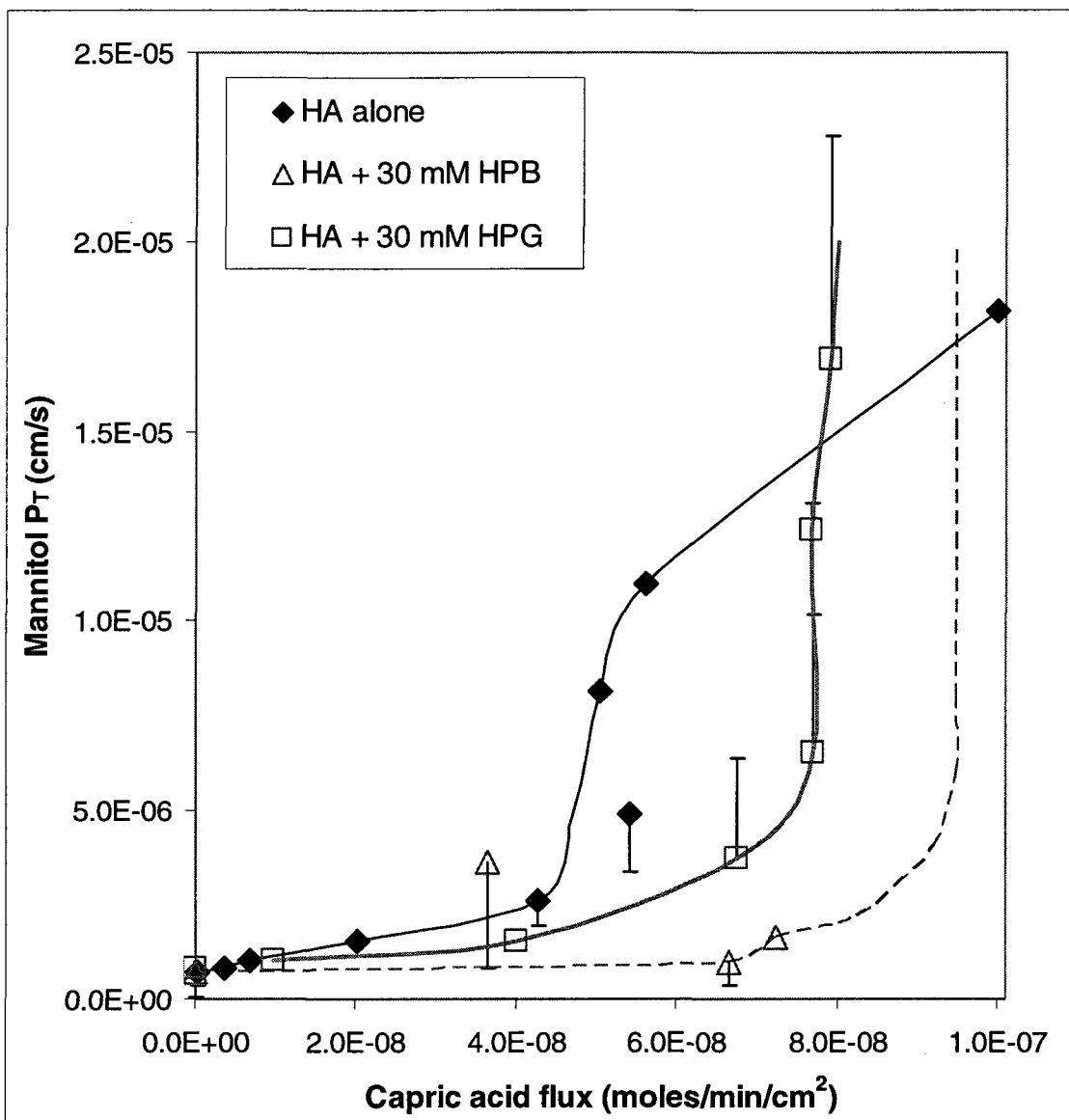


Fig 5.6 Mannitol permeability coefficients (P_T) for the rat ileum as a function of capric acid (HA) flux for capric acid alone and for capric acid plus 30 mM hydroxypropyl- β -cyclodextrin (HPB) or 30 mM hydroxypropyl- γ -cyclodextrin (HPG). Dashed line for HA + 30 mM HPB is speculation but illustrates a reasonable possibility.

single valued function of the surface enhancer concentration, it is reasonable to propose that superpositioning of the results of Fig 5.3 suggests no significant carrier effect arising from the presence of SBE that may give rise to a higher capric acid species surface concentration. The HA alone and the HA + 30 mM HPB results (Fig 5.6) however do not superpose and the latter data are rightwardly displaced relative to the HA alone data. A reasonable explanation for this is the following: As discussed in Chapter 4, for the HA/HPB system, there is likely an increased effective area for absorption due to a more extensive penetration of HA into the villus crypts that can permit yielding the same mannitol P_T value as for HA alone but at a higher capric acid flux and at a lower average surface capric acid species concentration.

Fig 5.7 presents the capric acid flux as a function of free capric acid concentration in the lumen. This plot demonstrates clearly that HPB provides significantly greater capric acid flux than the capric acid alone solutions for a given lumen activity of free capric acid. This was in contrast to the CDC/SBE behavior seen in Fig 5.4 where the CDC/SBE data and the CDC alone data essentially superposed. The increased capric acid flux in the presence of HPB is clear from the data presented in Fig 5.7; however, the mechanism for the increased flux remained unclear. As will be discussed later, using the villus model (VM) reveals that HPB significantly reduced the concentration gradient of capric acid activity across the ABL and allowed the capric acid to utilize up to four-fold more surface area for absorption than in the absence of HPB.

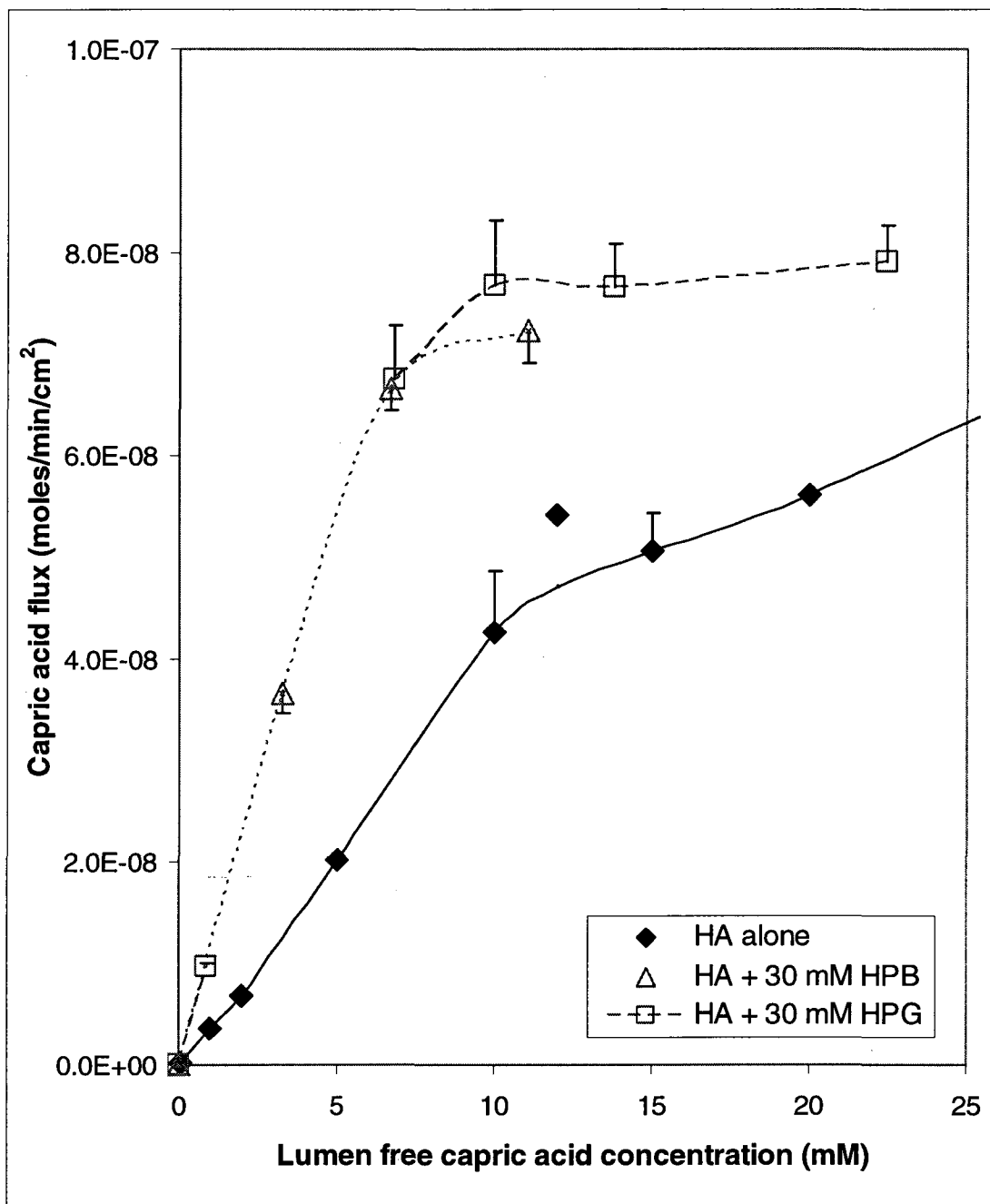


Fig 5.7 Capric acid (HA) flux across the rat ileum as a function of free capric acid concentration for capric acid alone and for capric acid plus 30 mM hydroxypropyl- β -cyclodextrin (HPB) or 30 mM hydroxypropyl- γ -cyclodextrin (HPG).

5.4.3 HA/HPG enhancer-carrier system for the enhancement of mannitol transport

Based on the initial interpretation of the results of the HA/HPB studies, it was thought that a still smaller capric acid-cyclodextrin binding constant was required for a system that would yield mannitol enhancement with more reasonable concentrations of enhancer and carrier. HPG was investigated because it was expected to bind more weakly to capric acid due to the larger cavity size of HPG as compared to HPB. Permselective membrane transport experiments⁵⁶ determined that binding constant between capric acid and HPG was 0.5 mM^{-1} . Accordingly, we expected the highest concentration of free enhancer and, therefore, the highest probability of attaining mannitol enhancement at reasonable concentrations of capric acid and HPG. Additionally, the capric acid half-life in the rat ileum for the HA/HPG system was determined to be 2.4 times longer than capric acid alone case (see Table 5.3). The mannitol and capric acid transport data for the HA/HPG system are presented in Figs 5.5-5.7 along side the capric acid alone data and the HA/HPB data.

In Fig 5.5 we see that mannitol transport enhancement occurred in the presence of 30 mM HPG for capric acid concentrations at and above 30 mM, with higher capric acid concentrations resulting in greater mannitol permeability coefficients. While most of the HA/HPG conditions were composed of a higher concentration of total capric acid than of HPG, the behavior of the HA/HPG system (as was the HA/HPB system), is clearly different from the CDC/SBE system, which involved very strong CDC•SBE complexes (Section 5.4.1.) For the CDC/SBE case, CDC transport and mannitol enhancement behaved as if the bound CDC did not contribute at all to the CDC flux or the mannitol

enhancement, and that the CDC/SBE solutions appeared to behave the same as CDC alone at the same free CDC concentration in the lumen. The relationship between the mannitol permeability coefficient and capric acid flux for the HA/HPG solutions, on the other hand, differed with the CDC/SBE system but was similar to the HA/HPB system (compare Fig 5.3 with Fig 5.6; Compare Fig 5.4 with Fig 5.7).

Fig 5.6 demonstrates that the capric acid plus HPG solutions require a higher capric acid flux than capric acid alone before mannitol enhancement is observed. It appears, however, that when a critical capric acid flux is reached, the mannitol permeability coefficient can increase rapidly. This behavior would be difficult to explain assuming a flat surface membrane (the FSM model of Chapter 4). With the villus structure in mind however as in the case for the HA/HPB system, a reasonable hypothesis explaining the Fig 5.6 results may be presented as follows. As demonstrated in Chapter 4, capric acid is absorbed almost exclusively at the tips for capric acid alone. This suggests that, in this case, the only region of the villi that can be enhanced is the region near the villus tips. In the presence of HPG, however, capric acid may access regions of the villus crypts that capric acid alone may not. Higher capric acid flux may, therefore, be reached without attaining significant mannitol flux enhancement at any point along the surface sites of the villi. This can mean, also, that when high enough capric acid concentrations are used in HA/HPG solutions, mannitol transport enhancement may occur over a greater villus surface area.

The significantly greater capric acid flux for the HA/HPG solutions as compared to capric acid alone at equal free capric acid concentration in the lumen (Fig 5.7) deserves a comment. It was initially suspected that was due only to the carrier effect across the

ABL (as demonstrated in Chapter 3); however, the VM suggests that this increased capric acid flux is caused by both the ABL carrier effect and the increased surface area utilized for absorption due to deeper penetration of capric acid into the villus crypts. As with the HA/HPB system, the physical model is required to distinguish the relative importance of the ABL carrier effect and the increased surface area effect in accounting for the overall increase in capric acid flux for the cyclodextrin-containing systems as compared to the capric acid alone case.

Taken as a whole, Figs 5.1-5.7 suggest that cyclodextrin carriers may provide the means by which the concentration gradient of enhancers across the ABL can be reduced and more of the membrane surface can be effectively enhanced and utilized for absorption. The net result of these effects may include increased duration of action for the enhancer and reduced toxicity caused by the enhancer, (as a consequence of the greater accessibility of the total surface area resulting in lower average microenvironmental concentration of the enhancer to achieve the same net enhancement) as well as a potentially higher maximum flux of the target permeant (mannitol in this case). In order to better understand the relationship that exists between the parameters that govern the presentation of chemical enhancers to the membrane surface by cyclodextrin carriers, the VM is required. Accordingly, the capric acid experimental data from this study is interpreted in the following discussion using the VM.

5.4.4 Insights obtained from examining the capric acid experimental results using the villus model

The villus model (VM) described in Chapter 4 may be used to obtain information on increased effective surface area for capric acid absorption in the presence of the carriers HPB and HPG. Accessibility represents the fraction of available surface area utilized for absorption as defined in Chapter 4. Table 5.4 presents the accessibility of capric acid for several HPB and HPG solutions relative to trace capric acid alone calculated using the VM. These accessibility values were calculated using a constant intrinsic membrane permeability coefficient ($P_{i,VM}$) value for capric acid based on experimental results described in Chapter 4. This assumes that capric acid does not enhance its own flux. As can be seen, HPB increases the capric acid accessibility to a somewhat greater extent than HPG. For both cases, the accessibility decreases with increasing capric acid concentration due to the non-linear binding behavior (i.e. partial saturation effects) of the enhancer and cyclodextrin for the higher capric acid concentration conditions. For both cases, the greater penetration of capric acid into the villus crypts provides opportunities for enhancing mannitol transport across a greater fraction of the total intestinal surface area. Fig 5.8 presents results of VM calculations showing the concentration profiles of free capric acid across the ABL and within the intervillus space for the three cases where the capric acid activity is normalized to be equal at the villus tips. These plots suggest that, when comparing the three cases, for a given free capric acid concentration at the villus tips (and therefore, presumably, at a given level of epithelial cell toxicity) the HPB system will gain the greatest access to

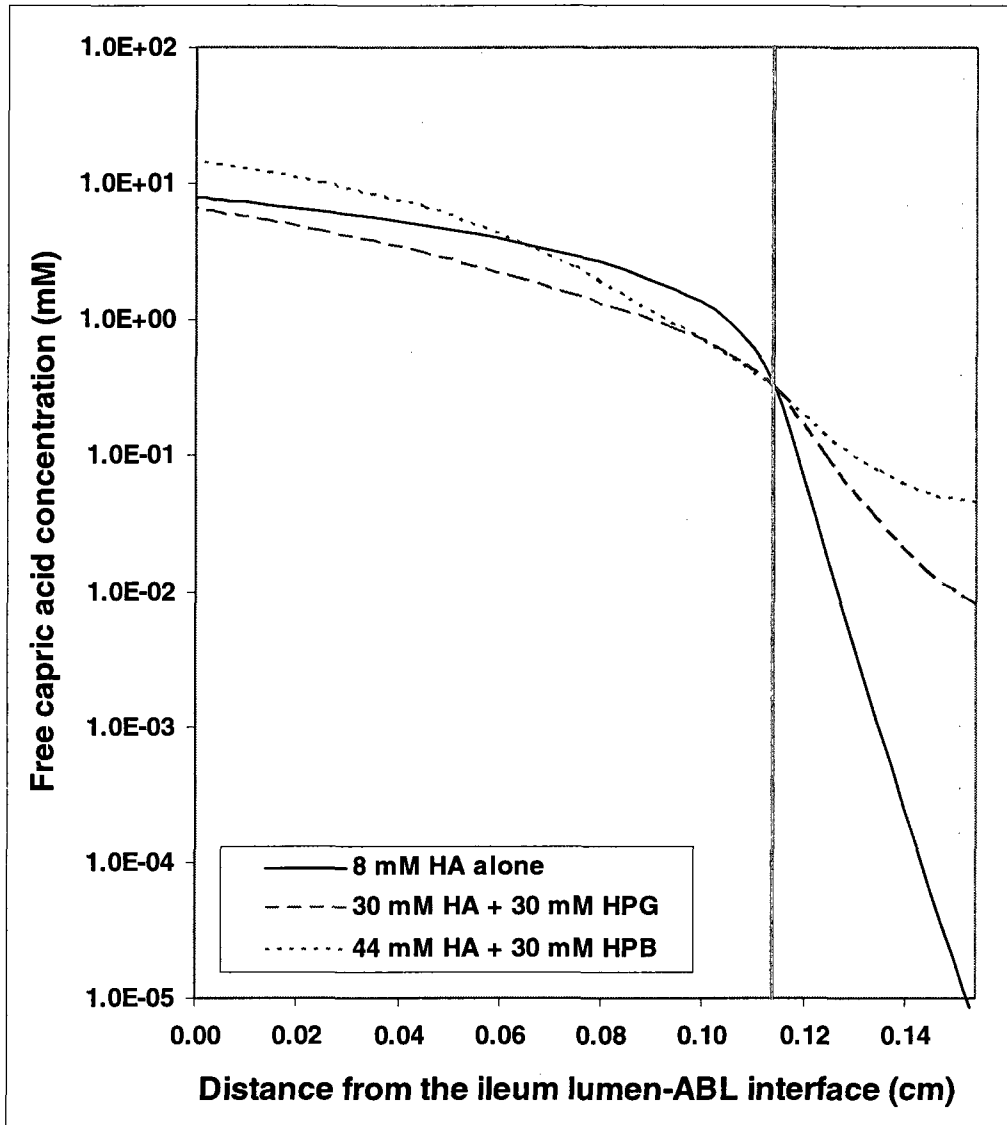


Fig 5.8 Free total capric acid (HA) concentration profiles for the three cases: 8 mM HA alone; 30 mM HA + 30 mM HPG; 44 mM HA + 30 mM HPB. The capric acid concentrations in the ileum lumen were chosen so that, for all three cases, the free caprate concentration at the villus tips would be equal to that for the 30 mM HA + 30 mM HPG case. The vertical line represents the location of the villus tips.

available surface area and thus provide the greatest potential increase in mannitol bioavailability.

It is instructive at this point to examine how well the results of Table 5.4 are consistent with the actual experimental data of Fig 5.6. We shall take three examples. 1) An HA/HPB case. First, take data point 40 mM HA/30 mM HPB, where the capric acid flux is 7.2×10^{-8} and the mannitol P_T value is 1.6×10^{-6} (see Table 5.2). The increased accessibility for this case relative to capric acid alone is 3.0 (Table 5.4). Therefore the predicted capric acid flux for capric acid alone would be $7.2 \times 10^{-8} / 3.0 = 2.4 \times 10^{-8}$. As can be seen in Fig 5.9, this prediction is in very good agreement with the experimental value and supports the validity of the hypothesis. This is a good example because we have selected a data point for which the mannitol enhancement is quite modest (around a factor of 2). 2) An HA/HPG case. Similar to the calculation for the HA/HPB case we may select a data point from the HA/HPG data set. It seems that the data point with the least mannitol enhancement but clearly higher than baseline mannitol P_T value is the case of 30 mM HA/30 mM HPG, where the capric acid flux is 6.7×10^{-8} and the mannitol P_T value is 3.7×10^{-6} (see Table 5.2). The increased accessibility for this case relative to capric acid alone is 2.0 (Table 5.4). Therefore the predicted capric acid flux for the capric acid alone for this case would be 3.3×10^{-8} (see Fig 5.9). The predicted value is around 73% of the experimental capric acid flux value (interpolated from a smooth curve) for capric acid alone. In light of the large experimental data scatter, the agreement should be considered satisfactory. Also, the experimental P_T for mannitol ($\sim 3.7 \times 10^{-6}$) is around five times larger than that of the baseline P_T for mannitol of around 7.2×10^{-6} .

Table 5.4 Increase in accessibility (Acc) compared to the capric acid (HA) alone case. HPB and HPG concentrations are 30 mM.

| Enhancer•carrier complex | Binding constant (K) of complex | Increase in accessibility (Acc) relative to capric acid alone (Acc=1.0) | | | | |
|--------------------------|---------------------------------|---|----------|----------|----------|----------|
| | | 0.05 mM HA | 30 mM HA | 35 mM HA | 40 mM HA | 50 mM HA |
| HA•HPB | 2.5 mM ⁻¹ | 4.0 | 3.5 | 3.2 | 3.0 | 2.7 |
| HA•HPG | 0.5 mM ⁻¹ | 2.2 | 2.0 | 2.0 | 2.0 | 1.9 |

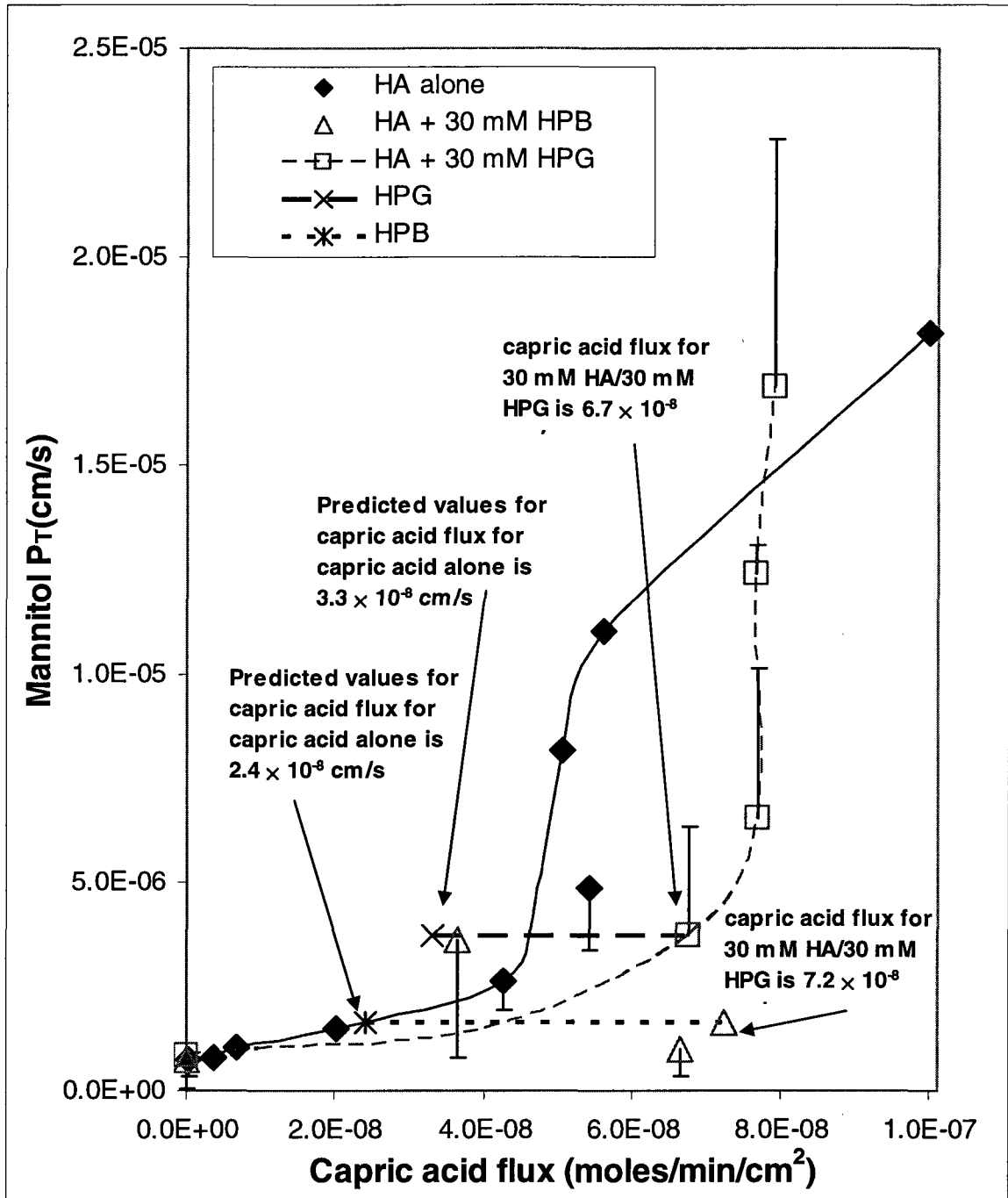


Fig 5.9 Mannitol permeability coefficients (P_T) for the rat ileum as a function of capric acid (HA) flux for capric acid alone and for capric acid plus 30 mM hydroxypropyl- β -cyclodextrin (HPB) or 30 mM hydroxypropyl- γ -cyclodextrin (HPG).

Likely, this will impact somewhat on the assumption that the baseline P_i values of capric acid may be used in the calculations, while this consideration would be less important for HA/30 mM HPG solution have similar free concentrations of capric acid at the villus tips (0.42 mM and 0.43 mM, respectively) according to VM calculations. Their relative HA flux and mannitol enhancement factors are given in Table 5.5. A comparison of the experimental results demonstrates that the solution containing HPG provided a 2.5-fold greater mannitol enhancement than the capric acid alone solution for the given tip concentration. This comparison illustrates the potential for cyclodextrin carriers to provide greater enhancement for a given free tip concentration of enhancer (a measure of the membrane toxicity). An examination of these three examples demonstrates that, although these studies were exploratory in nature, the experimental results are found to be quantitatively consistent with the VM.

5.5 Implications

This range-finding study and the interpretation of the experimental results using the VM provide significant insight into the optimum characteristics for ideal combinations of permeation enhancers and cyclodextrin carriers for improving the bioavailability of BCS class III compounds. The VM clearly demonstrates that enhancer/cyclodextrin combinations with higher binding constants provide increased enhancer accessibility to the villus surface (Table 5.4) and increased duration of action due to an increased half-life (Table 5.3). The increased binding constant, however, also decreases F^U at the surface. Therefore, an ideal enhancer/cyclodextrin combination would consist of a cyclodextrin molecule with a high enough enhancer binding constant to

Table 5.5 A comparison of capric acid (HA) flux and mannitol enhancement factor for two conditions with similar capric acid (HA) tip concentrations.

| Condition | $[\text{HA}]_{\text{free,tip}}$ (mM) | HA flux (moles/min/cm ²) | Enhancement factor |
|----------------------|---|---|-----------------------|
| 10 mM HA | 0.42 | 4.3×10^{-8} | 3.6 |
| 35 mM HA + 30 mM HPG | 0.43 | 7.7×10^{-8} | 9.0 |

achieve near-maximum accessibility and provide an optimum enhancer half-life in the lumen, combined with an enhancer that was potent enough to cause enhancement at very low surface concentrations without causing an unacceptable level of toxicity at therapeutic concentrations. As long as the enhancer is potent enough to cause membrane permeation enhancement in the presence of the cyclodextrin at practical concentrations, the formulation could be fine-tuned to provide optimum surface free concentrations of the enhancer and appropriate duration of action by simply adjusting the enhancer and/or carrier concentrations accordingly. The increased half-life and decreased concentration gradient resulting from including cyclodextrins in enhancer formulations is expected to facilitate safer and more effective enhancer delivery by presenting a greater intestinal surface area with a more narrow range of enhancer concentrations for a longer duration. These effects are expected to increase the likelihood that safe and effective permeation-enhancing formulations may someday be developed for commercial application.

5.6 References

1. Aungst BJ 2000. Intestinal permeation enhancers. *J Pharm Sci* 89(4):429-442.
2. Aungst BJ 1993. Novel formulation strategies for improving oral bioavailability of drugs with poor membrane permeation or presystemic metabolism. *J Pharm Sci* 82(10):979-987.
3. Hellriegel ET, Bjornsson TD, Hauck WW 1996. Interpatient variability in bioavailability is related to the extent of absorption: implications for bioavailability and bioequivalence studies. *Clin Pharmacol Ther* 60(6):601-607.
4. Lee VHL, Yamamoto A 1990. Penetration and enzymatic barriers to peptide and protein absorption. *Adv Drug Del Rev* 4:171-207.
5. Muranishi S 1990. Absorption enhancers. *Crit Rev Ther Drug Carrier Syst* 7(1):1-33.
6. Swenson ES, Curatolo W 1992. Intestinal Permeability enhancement for proteins, peptides, and other polar drugs: mechanisms and potential toxicity. *Adv Drug Del Rev* 8:39-92.
7. van Hoogdalem EJ, de Boer AG, Breimer DD 1989. Intestinal drug absorption enhancement: an overview. *Pharmacol Ther* 44(3):407-443.
8. Drewe J, Fricker G, Vonderscher J, Beglinger C 1993. Enteral absorption of octreotide: absorption enhancement by polyoxyethylene-24-cholesterol ether. *Br J Pharmacol* 108(2):298-303.
9. Kreutler CJ, Davis WW 1971. Normal and promoted GI absorption of water-soluble substances. 3. Absorption of antibiotics from stomach and intestine of the rat. *J Pharm Sci* 60(12):1835-1838.
10. Malik SN, Canaham DH, Gouda MW 1975. Effect of surfactants on absorption through membranes III: effects of dioctyl sodium sulfosuccinate and poloxalene on absorption of a poorly absorbable drug, phenolsulfonphthalein, in rats. *J Pharm Sci* 64(6):987-990.
11. Ichikawa K, Ohata I, Mitomi M, Kawamura S, Maeno H, Kawata H 1980. Rectal absorption of insulin suppositories in rabbits. *J Pharm Pharmacol* 32(5):314-318.
12. Walters KA, Dugard PH, Florence AT 1981. Non-ionic surfactants and gastric mucosal transport of paraquat. *J Pharm Pharmacol* 33(4):207-213.

13. Guarini S, Ferrari W 1984. Structural restriction in bile acids and non-ionic detergents for promotion of heparin absorption from rat gastro-intestinal tract. *Arch Int Pharmacodyn Ther* 271(1):4-10.
14. Feldman S, Gibaldi M 1969. Physiologic surface-active agents and drug absorption. I. Effect of sodium taurodeoxycholate on salicylate transfer across the everted rat intestine. *J Pharm Sci* 58(4):425-431.
15. Feldman S, Gibaldi M 1969. Physiologic surface-active agents and drug absorption II. Comparison of the effect of sodium taurodeoxycholate and ethylenediaminetetraacetic acid on salicylamide and salicylate transfer across the everted rat small intestine. *J Pharm Sci* 58(8):967-970.
16. Freel RW, Hatch M, Earnest DL, Goldner AM 1983. Dihydroxy bile salt-induced alterations in NaCl transport across the rabbit colon. *Am J Physiol* 245(6):G808-815.
17. Freel RW, Hatch M, Earnest DL, Goldner AM 1983. Role of tight-junctional pathways in bile salt-induced increases in colonic permeability. *Am J Physiol* 245(6):G816-823.
18. Kakemi K, Sezaki H, Konishi R, Kimura T, Murakami M 1970. Effect of bile salts on the gastrointestinal absorption of drugs. I. *Chem Pharm Bull (Tokyo)* 18(2):275-280.
19. Kakemi K, Sezaki H, Konishi R, Kimura T, Okita A 1970. Effect of bile salts on the gastrointestinal absorption of drugs. II. Mechanism of the enhancement of the intestinal absorption of sulfaguanidine by bile salts. *Chem Pharm Bull (Tokyo)* 18(5):1034-1039.
20. Kidron M, Bar-On H, Berry EM, Ziv E 1982. The absorption of insulin from various regions of the rat intestine. *Life Sci* 31(25):2837-2841.
21. Rafter JJ, Eng VW, Furrer R, Medline A, Bruce WR 1986. Effects of calcium and pH on the mucosal damage produced by deoxycholic acid in the rat colon. *Gut* 27(11):1320-1329.
22. Teichberg S, McGarvey E, Bayne MA, Lifshitz F 1983. Altered jejunal macromolecular barrier induced by alpha-dihydroxy deconjugated bile salts. *Am J Physiol* 245(1):G122-132.
23. Ziv E, Eldor A, Kleinman Y, Bar-On H, Kidron M 1983. Bile salts facilitate the absorption of heparin from the intestine. *Biochem Pharmacol* 32(5):773-776.
24. Tsutsumi K, Li SK, Hymas RV, Teng CL, Tillman LG, Hardee GE, Higuchi WI, Ho NF 2008. Systematic studies on the paracellular permeation of model permeants and

oligonucleotides in the rat small intestine with chenodeoxycholate as enhancer. *J Pharm Sci* 97(1):350-367.

25. Anderberg EK, Lindmark T, Artursson P 1993. Sodium caprate elicits dilatations in human intestinal tight junctions and enhances drug absorption by the paracellular route. *Pharm Res* 10(6):857-864.

26. Ramakrishna BS, Mathan M, Mathan VI 1994. Alteration of colonic absorption by long-chain unsaturated fatty acids. Influence of hydroxylation and degree of unsaturation. *Scand J Gastroenterol* 29(1):54-58.

27. Sawada T, Ogawa T, Tomita M, Hayashi M, Awazu S 1991. Role of paracellular pathway in nonelectrolyte permeation across rat colon epithelium enhanced by sodium caprate and sodium caprylate. *Pharm Res* 8(11):1365-1371.

28. Tomita M, Hayashi M, Awazu S 1995. Absorption-enhancing mechanism of sodium caprate and decanoylcarnitine in Caco-2 cells. *J Pharmacol Exp Ther* 272(2):739-743.

29. Tomita M, Hayashi M, Horie T, Ishizawa T, Awazu S 1988. Enhancement of colonic drug absorption by the transcellular permeation route. *Pharm Res* 5(12):786-789.

30. Tomita M, Sawada T, Ogawa T, Ouchi H, Hayashi M, Awazu S 1992. Differences in the enhancing effects of sodium caprate on colonic and jejunal drug absorption. *Pharm Res* 9(5):648-653.

31. Tomita M, Shiga M, Hayashi M, Awazu S 1988. Enhancement of colonic drug absorption by the paracellular permeation route. *Pharm Res* 5(6):341-346.

32. Raoof AA, Chiu P, Ramtoola Z, Cumming IK, Teng C, Weinbach SP, Hardee GE, Levin AA, Geary RS 2004. Oral bioavailability and multiple dose tolerability of an antisense oligonucleotide tablet formulated with sodium caprate. *J Pharm Sci* 93(6):1431-1439.

33. Raoof AA, Ramtoola Z, McKenna B, Yu RZ, Hardee G, Geary RS 2002. Effect of sodium caprate on the intestinal absorption of two modified antisense oligonucleotides in pigs. *Eur J Pharm Sci* 17(3):131-138.

34. Beskid G, Unowsky J, Behl CR, Siebelist J, Tossounian JL, McGarry CM, Shah NH, Cleeland R 1988. Enteral, oral, and rectal absorption of ceftriaxone using glyceride enhancers. *Chemotherapy* 34(2):77-84.

35. Sekine M, Maeda E, Sasahara K, Okada R, Kimura K, Fukami M, Awazu S 1985. Improvement of bioavailability of poorly absorbed drugs. III. Oral acute toxicity and local irritation of medium chain glyceride. *J Pharmacobiodyn* 8(8):633-644.

36. Sekine M, Sasahara K, Hasegawa K, Okada R, Awazu S 1985. Improvement of bioavailability of poorly absorbed drugs. V. Effect of surfactants on the promoting effect of medium chain glyceride for the rectal absorption of beta-lactam antibiotics in rats and dogs. *J Pharmacobiodyn* 8(8):653-660.
37. Sekine M, Sasahara K, Okada R, Awazu S 1985. Improvement of bioavailability of poorly absorbed drugs. IV. Mechanism of the promoting effect of medium chain glyceride on the rectal absorption of water soluble drugs. *J Pharmacobiodyn* 8(8):645-652.
38. Sekine M, Terashima H, Sasahara K, Nishimura K, Okada R, Awazu S 1985. Improvement of bioavailability of poorly absorbed drugs. II. Effect of medium chain glyceride base on the intestinal absorption of cefmetazole sodium in rats and dogs. *J Pharmacobiodyn* 8(4):286-295.
39. Ueda I, Shimojo F, Kozatani J 1983. Effect of ethyl cellulose in a medium-chain triglyceride on the bioavailability of ceftizoxime. *J Pharm Sci* 72(4):454-458.
40. Unowsky J, Behl CR, Beskid G, Sattler J, Halpern J, Cleeland R 1988. Effect of medium chain glycerides on enteral and rectal absorption of beta-lactam and aminoglycoside antibiotics. *Chemotherapy* 34(4):272-276.
41. Aungst BJ, Saitoh H 1996. Intestinal absorption barriers and transport mechanisms, including secretory transport, for a cyclic peptide, fibrinogen antagonist. *Pharm Res* 13(1):114-119.
42. Takeichi Y, Baba K, Kinouchi Y, Iida Y, Umeno Y, Muranishi S, Nakai Y 1990. Combinative improving effect of increased solubility and the use of absorption enhancers on the rectal absorption of uracil in beagle dogs. *Chem Pharm Bull (Tokyo)* 38(9):2547-2551.
43. Swenson ES, Milisen WB, Curatolo W 1994. Intestinal permeability enhancement: efficacy, acute local toxicity, and reversibility. *Pharm Res* 11(8):1132-1142.
44. Aungst BJ, Saitoh H, Burcham DL, Huang S-M, Mousa SA, Hussain MA 1996. Enhancement of the intestinal absorption of peptides and non-peptides. *J Controlled Release* 41(1,2, Fifth International Symposium on Delivery and Targeting of Pesticides, Proteins and Genes, 1995):19-31.
45. Curatolo W, Ochoa R. 1994. Safety assessment of intestinal permeability enhancers. In deBoer AG, editor *Drug Delivery*, Harwood Publishers. p 367-389.

46. Swenson ES, Milisen WB, Curatolo W 1994. Intestinal permeability enhancement: structure-activity and structure-toxicity relationships for nonylphenoxyethoxyethylene surfactant permeability enhancers. *Pharm Res* 11(10):1501-1504.
47. Stella VJ 1996. SBE7-b-CD, a new, novel and safe polyanionic β -cyclodextrin derivative: characterization and biomedical applications. *Proceedings of the International Symposium on Cyclodextrins, 8th, Budapest, Mar. 31-Apr. 2, 1996.* 471-476.
48. Stella VJ, Rajewski RA 1997. Cyclodextrins: their future in drug formulation and delivery. *Pharm res* 14(5):556-567.
49. Stella VJ, Uekama K, Irie T, Rao VM, Zannou EA, Rajewski RA, Shiraishi S, Okimoto K 1999. The use of (SBE)7M- β -CD (captisol) as a solubilizing and osmotic agent for controlled and complete oral delivery of poorly water soluble drugs. *Proceedings of the International Symposium on Cyclodextrins, 9th, Santiago de Comostela, Spain, May 31-June 3, 1998.* 459-462.
50. Tsutsumi K, Li SK, Ghanem AH, Ho NF, Higuchi WI 2003. A systematic examination of the in vitro Ussing chamber and the in situ single-pass perfusion model systems in rat ileum permeation of model solutes. *J Pharm Sci* 92(2):344-359.
51. Winne D 1978. The permeability coefficient of the wall of a villous membrane. *J Math Biol* 6(1):95-108.
52. Oliver RE, Jones AF, Rowland M 1998. What surface of the intestinal epithelium is effectively available to permeating drugs? *J Pharm Sci* 87(5):634-639.
53. Irie T, Uekama K 1997. Pharmaceutical applications of cyclodextrins. III. Toxicological issues and safety evaluation. *J Pharm Sci* 86(2):147-162.
54. Irie T, Uekama K 1999. Cyclodextrins in peptide and protein delivery. *Adv Drug Deliv Rev* 36(1):101-123.
55. Piel G, Piette M, Barillaro V, Castagne D, Evrard B, Delattre L 2007. Study of the relationship between lipid binding properties of cyclodextrins and their effect on the integrity of liposomes. *Int J Pharm* 338(1-2):35-42.
56. Ono N, Hirayama F, Arima H, Uekama K 1999. Determination of stability constant of β -cyclodextrin complexes using the membrane permeation technique and the permeation behavior of drug-competing agent- β -cyclodextrin ternary systems. *Eur J Pharm Sci* 8(2):133-139.

CHAPTER 6

SUMMARY

The increasing number of therapeutic chemical entities that are not currently capable of effective oral delivery due to poor bioavailability in the intestinal tract due to poor solubility and/or poor permeability has fostered the need to develop formulations that can increase the oral bioavailability to acceptable levels. Although the field has recently seen significant progress from the standpoint of practical formulation development, there has been a great need for progress from the standpoint of gaining a quantitative mechanistic understanding of the interplay of key variables involved in the formulation development of poor bioavailability drugs. A primary focus of this dissertation has been to foster a better understanding of the key variables involved in formulations employing cyclodextrin molecules to increase the bioavailability of poorly soluble, highly permeable compounds. An additional focus of this dissertation was to demonstrate the potential benefits of including a cyclodextrin carrier in permeation enhancing formulations to improve the effectiveness and possibly the safety of the enhancer.

A physical model was designed to incorporate the key parameters involved in the transport of highly lipophilic molecules in the presence of cyclodextrin. The physical model accounted for the cyclodextrin and permeant concentrations, the solution pH, the

permeant pKa, the permeant/cyclodextrin binding constant(s), the aqueous boundary layer thickness, the diffusion coefficients of the free and cyclodextrin-bound permeant, and the intrinsic membrane permeability coefficient. Independent or essentially independent experiments were utilized to determine the parameter values involved. Capric acid was used as a model permeant and hydroxypropyl- β -cyclodextrin (HPB) was used as a model cyclodextrin carrier to demonstrate the reliability of the model by comparing experimental and model-predicted permeability coefficients (P_T) for the transport of capric acid across a silicone polymer membrane over a range of 100% ABL-controlled to 100% membrane-controlled conditions. The P_T values predicted by the flat membrane model (FSM) were in good agreement with the experimental values over the entire range of conditions, validating the physical model. Using the FSM, it was demonstrated that for constant free lumen concentrations of capric acid (i.e., saturated solution), the concentration gradient of free capric acid was reduced with increasing concentrations of HPB, resulting in increasing surface free capric acid concentrations and capric acid flux with increasing concentrations of HPB.

As a result of the good agreement of the experimental and model-predicted results of the in vitro silicone polymer membrane transport experiments, the (FSM) was applied to capric acid transport across rat ileum in the presence of HPB using a single pass perfusion technique. As in the silicone polymer membrane transport experiments, the model accurately described capric acid flux over a range of HPB concentrations. The (FSM) was then extended to account for the villus structure of the ileal membrane, and the predicted results were compared to experimental data. As with the FSM, the P_T values determined using the villus model (VM) were in good agreement with

experimental data, and although both models were in good agreement with experimental data, the VM provided additional insight that was not available from the FSM. First, the VM demonstrated that, when HPB was not present in the luminal solution, capric acid was absorbed primarily at the villus tips; in the presence of HPB, capric acid was able to penetrate further into the villus crypts, thus utilizing a greater fraction of the available surface area of the rat ileum. For the 50 mM HPB case, capric acid was able to utilize 4.5 times as much surface area as the capric acid alone system. This increased accessibility due to HPB, combined with the reduced concentration gradient of free capric acid across the ABL, quantitatively demonstrate why HPB is able to increase the bioavailability of highly lipophilic molecules.

The VM also afforded the opportunity to mechanistically examine how the cyclodextrins may be able to improve the performance of membrane permeation enhancers such as capric acid by better presentation of the enhancer at the membrane surface. Three enhancer/cyclodextrin combinations were investigated, and the experimental data were analyzed with the VM. It was demonstrated that cyclodextrin carriers may increase the effective surface area enhanced by the enhancer, resulting in greater overall permeant enhancement for a given concentration of free enhancer at the villus tips.

The implications of these studies and the interpretation of the experimental results using the VM provide significant insight into the optimum characteristics for ideal combinations of permeation enhancers and cyclodextrin carriers for improving the bioavailability of BCS class II and class III compounds. The VM clearly demonstrates and quantitatively predicts that cyclodextrins may 1) increase the flux of highly

lipophilic compounds, 2) increase the fraction of available surface area utilized for absorption/enhancement, 3) increase the enhancer's duration of action, and 4) increase the enhancement factor for a given enhancer concentration at the villus tip. This is the first time, to our knowledge, that the quantitative modeling of cyclodextrin carrier effects and the use of cyclodextrins to more effectively present permeation enhancers to the membrane surface have been demonstrated. The VM provides the means by which ideal permeant/carrier or enhancer/carrier combinations could be determined in formulation development.